CREEP AND SHRINKAGE OF A HIGH STRENGTH CONCRETE MIXTURE

by

Bradley D. Townsend

Thesis presented to the faculty of the

Virginia Polytechnic Institute and State University

In partial fulfillment of the requirements for the degree of

Master of Science

in

Civil Engineering

Committee:

Richard E. Weyers, Chair

Thomas E. Cousins

Carin L. Roberts-Wollmann

May 8, 2003

Blacksburg, VA

Keywords: creep, shrinkage, high strength concrete, prediction models

CREEP AND SHRINKAGE OF A HIGH STRENGTH CONCRETE MIXTURE

by

Bradley D. Townsend

ABSTRACT

In addition to immediate elastic deformations, concrete undergoes time-dependent deformations that must be considered in design. Creep is defined as the time-dependent deformation resulting from a sustained stress. Shrinkage deformation is the time-dependent strain that occurs in the absence of an applied load. The total strain of a concrete specimen is the sum of elastic, creep, and shrinkage strains.

Several test beams for the Pinner's Point Bridge have been produced by Bayshore Concrete Products Corp., in Cape Charles, VA. These beams feature high strength concrete mix designs with specified 28-day compressive strengths of 55.2 MPa (8,000 psi) and 69.0 MPa (10,000 psi). These test beams were equipped with thermocouples to track interior concrete temperatures, and vibrating wire gages placed at the center of prestressing to record changes in strain.

Laboratory creep and shrinkage testing was conducted on specimens prepared with identical materials and similar mixture proportions to those used at Bayshore. The temperature profile from the test beams during steam curing was used to produce match-cured specimens for laboratory testing. Two match cure batches were produced, along with two standard cure batches. Creep specimens from each batch were placed in the creep room and loaded to 30 percent of their after-cure compressive strength. The creep room had a temperature of 23.0 ± 1.7 °C (73.4 ± 3 ºF) and relative humidity of 50 ± 4 %. Companion shrinkage specimens were also placed in the creep room. Measurements were taken on the creep and shrinkage specimens using a Whittemore gage. Four cylinders were also equipped with embedded vibrating wire gages (VWGs) so that the interior and exterior strains could be compared. The Whittemore and VWG elastic and creep strains were similar, while the VWGs recorded significantly less shrinkage.

The measured creep and shrinkage strains were compared to seven different models to determine which model was the most accurate. The models considered were ACI 209, ACI 209 modified by Huo, CEB Model Code 90, AASHTO-LRFD, Gardner GL2000, Tadros, and Bazant B3. The ACI 209 modified by Huo was most accurate in predicting time-dependent strains.

ACKNOWLEDGEMENTS

I would like to thank the Lord for His grace and provision. He has sustained me and given me hope and a purpose for my life.

I thank Dr. Richard Weyers for allowing me to work on this project, and for providing a great deal of guidance and assistance along the way. I also appreciate the help received from Dr. Cousins and Dr. Roberts-Wollmann as members of my research committee.

I thanks the Virginia Transportation Research Council for funding this project.

I am indebted to Ed Vincent and Chris Waldron for their long hours spent helping to prepare the test specimens. I learned a great deal from Ed about concrete research as he helped me get started.

I am grateful for the opportunity to learn from the faculty of the Structural Engineering and Materials Department. I have enjoyed my coursework and have tremendous respect for each professor.

I thank my family for their unwavering love and support. My parents Doug and Angie Townsend have always been available and have encouraged me. My sister Barbara and brother Donald have brought me great joy and laughter.

I appreciate my friends Shannon Sarracino, Sean Brooks, Chuck Ponton, Dion Minter, George Wood, Josh Via, Scott Adams, Jeremiah Hambrick, and Brian Wray. Their accountability and friendship have strengthened me over the years.

TABLE OF CONTENTS

LIST OF FIGURES

LIST OF TABLES

CHAPTER 1: INTRODUCTION

The use of high strength concrete (HSC) has been steadily increasing, and today it is a very popular construction material. Concrete having a 28-day compressive strength of at least 41.4 MPa (6000 psi) is normally considered high strength.[3] High compressive strengths are achieved by using a low water-to-cementitious materials ratio, requiring the use of water-reducing admixtures to provide adequate workability. High strength concrete offers significant economic advantages over conventional normal strength concrete (NSC) because more slender members can be designed, resulting in reduced material and transportation costs. As structural components become more slender, deflection becomes a more crucial issue, making long-term creep and shrinkage deformations especially important in HSC structures.

All concrete structures undergo time-dependent deformations known as creep and shrinkage. Creep is defined as the deformation over time of a viscoelastic material, in excess of initial elastic strain, that results when a sustained stress is applied. Shrinkage is also a time-dependent deformation, but it occurs in the absence of any applied load. Therefore, the total strain of a concrete specimen at any time is the sum of its initial elastic strain, creep strain, and shrinkage strain.

Creep of concrete may be separated into two components: basic creep and drying creep. Basic creep occurs in a sealed condition, without any exchange of water between the concrete and its surroundings. Drying creep involves water movement to the surrounding environment. The creep experienced by the innermost region of a large concrete member is predominantly basic creep, since very little water is lost to the outside environment.

Shrinkage consists of three different mechanisms, known as drying shrinkage, autogenous shrinkage, and carbonation. Drying shrinkage occurs when excess water not consumed during hydration diffuses into the surrounding environment, resulting in a net volume loss. Autogenous shrinkage is the water loss due to continued hydration of the cement. Carbonation shrinkage is the process by which CO_2 in the atmosphere reacts with $Ca(OH)_2$ in the cement paste, in the presence of moisture.

CHAPTER 2: PURPOSE AND SCOPE

The main purpose of this study is to observe the time-dependent deformation of a high strength concrete mixture used in prestressed bridge girders for the Pinner's Point Bridge. This project consists of creep and shrinkage testing under laboratory conditions. In a related project, several test beams at Bayshore Concrete Products Corporation were instrumented in order to study prestress losses. Results from this study may be compared to the time-dependent deformations measured in the field.

Another objective is to compare observed creep and shrinkage deformations with seven current prediction models and determine which model most accurately predicts creep and shrinkage strains for this mixture.

The materials and mixture proportions used in producing laboratory specimens matched those used in the field. The test variables were specimen size and curing method. Accelerated curing was used for two batches, using a match cure system to replicate the time-temperature profile of the test beams during steam curing. The other two batches were given a standard seven-day moist cure.

CHAPTER 3: METHODS AND MATERIALS

3.1 Introduction

Each procedure involved in this creep and shrinkage study was performed in accordance with the appropriate ASTM specification, with the exception of the thermal coefficient test. ASTM does not provide a specification for this type of test. The concrete mixing procedure is presented in section 3.2, and the test materials are discussed in section 3.3. Section 3.4 outlines the standard and accelerated curing methods, and sections 3.5 through 3.9 cover the creep, shrinkage, strength, modulus and thermal coefficient testing procedures. The test matrix for this study is presented in Table 1.

Curing Method	Batches	Age at Loading	Specimens/Batch
Standard	HSC8-1A HSC8-2A	7 days	8 Compressive Strength 4 Tensile Strength 1 Modulus 3 Shrinkage 3 Creep 3 Shrinkage Prisms
Accelerated	HSC8-3A HSC8-4A	1 day	5 Compressive Strength 2 Tensile Strength 1 Modulus 4 Shrinkage Cylinders 4 Creep Cylinders

Table 1 HSC Test Matrix

3.2 Mixing

Batch mixing was conducted in accordance with ASTM C192.[15] Mixture proportions were determined based on the 55.2 MPa (8000 psi) mix design used in the test beams at Bayshore. These proportions are presented in Table 2. For some of the batches, additional HRWR was added in order to achieve the desired slump. The actual batch weights used to fabricate the laboratory specimens are presented in Appendix B. Tables 3 and 4 present the laboratory fresh concrete properties for the accelerated cure and standard cure batches, respectively. Table 3 also includes the prestressed beam fresh concrete properties and VDOT specifications.

Materials	SSD weights, kg/m^3 (lb/yd^3)
Portland Cement	303 (510)
Slag Cement	202 (340)
Course Aggregate	1157 (1950)
Fine Aggregate	586 (988)
Water	149 (252)
AEA (Daravair)	580 ml/m^3 (15 oz/yd^3)
WR (Hycol)	1044 ml/m^3 (27 oz/yd^3)
HRWR (Adva)	6764 ml/m^3 (175 oz/yd^3)
Cl or Accel (DCI)	19.8 L/m^3 (4.0 gal/yd^3)

Table 2 Bayshore Mixture Proportions

Properties	HSC8-1A	HSC8-2A	Bayshore	VDOT Specs.
Slump, mm (in.)	152 (6)	152 (6)	203 (8)	0-178 (0-7)
Air Content, %	5.6	4.4	6.2	3-6
Temperature, °C (°F)	24.4 (76)	25.6 (78)	25.0 (77)	4.4-32.2 (40-90)
Unit Weight, kg/m^3 (pcf)	2468 (154)	2484 (155)	----	----
Yield	1.02	1.03	----	----
w/cm ratio	0.30	0.30	~ 0.33 *	< 0.4
Curing Method	Match Cure	Match Cure	Steam	N/A

*See Section 5.2 for explanation

Table 3 Accelerated Cure Laboratory and Beam Fresh Concrete Properties

Properties	HSC8-3A	HSC8-4A
Slump, mm (in.)	216 (8.5)	114 (4.5)
Air Content, %	3.5	3.5
Temperature, °C (°F)	25.6 (78)	23.9 (75)
Unit Weight, kg/m3 (pcf)	2549 (159)	2549 (159)
Yield	1.05	1.05
w/cm ratio	0.30	0.30

Table 4 Standard Cure Laboratory Fresh Concrete Properties

3.3 Materials

The materials used in producing the laboratory concrete specimens were obtained from Bayshore, in order to match the materials in the test beams.

The coarse aggregate is a #67 crushed stone from Garrisonville, VA, and the fine aggregate is a natural sand from King George County, VA. Aggregate properties are presented in Appendix B.

Cementitious materials consist of Type II Portland Cement, and a ground granulated blast furnace slag, both produced by Blue Circle Cement. The slag is a grade 120.

The admixtures in the mixture included air entrainment (Daravair), water reducer (Hycol), high-range water reducer (Adva), and corrosion inhibitor (DCI). DCI also acts as an accelerator. These admixtures are produced by Grace Construction Products, and more information can be found on their website at www.na.graceconstruction.com.

3.4 Curing

For the two accelerated cure batches, cylindrical specimens were cast in 100 mm x 200 mm (4 in. x 8 in.) molds whose surface temperatures were controlled by the Sure Cure system. A 22-hour heated curing regimen was used to simulate steam curing of the test girders at Bayshore. The temperature profile of the test girders during steam curing was recorded using embedded thermocouples. This profile was entered into the Sure Cure system, so that the test specimens would experience the same curing temperatures as the test girders. The laboratory and field temperature profiles are presented in Appendix E. In order to maintain a moist environment, wet burlap and plastic sheeting were placed over the molds during curing.

The cylindrical standard cure creep and shrinkage specimens were cast in 150 mm x 300 mm (6 in. x 12 in.) steel molds, while the cylindrical strength and modulus specimens were cast in 100 mm x 200 mm (4 in. x 8 in.) plastic molds. Shrinkage prisms were cast in 75 mm x 75 mm x 280 mm (3 in. x 3 in. x 11.25 in.) steel rectangular molds. The test specimens were stored in a moist room for 7 days after casting, in accordance with the standard curing procedure of ASTM C192.[15]

3.5 Creep Testing

Creep testing was performed in accordance with ASTM C512.[19] Because of equipment constraints, there were differences in test procedure between the standard cure and accelerated cure batches.

From each accelerated cure batch, four cylindrical creep and shrinkage specimens were cast. Because the accelerated cure specimens are smaller, four specimens could be stacked in a loading frame, whereas only three standard cure specimens were placed in a frame. The cast in place inserts for attaching gage points could not be used with the Sure Cure cylinder molds. Instead, holes were drilled in the cylinders and the gage points were attached into the holes using a five-minute epoxy. The gage points were spaced 150 mm (6 in.) apart for the accelerated cure specimens.

From each standard cure batch, three cylindrical creep and shrinkage specimens were cast, along with the strength and elastic modulus specimens. Brass inserts were cast into each creep and shrinkage cylinder, so that gage points could be attached after curing. Each cylinder has four gage points, with two on each diametrically opposite side, separated by 200 mm (8 in.).

Test specimens were sulfur-capped immediately after curing, in accordance with ASTM C617.[20] Compressive strength was determined immediately after curing, and the creep, shrinkage, elastic modulus, and remaining strength specimens were placed in the controlled environment of 23.0 ± 1.7 °C (73.4 ± 3 °F) and 50 ± 4 % relative humidity. The creep specimens were stacked in the loading frames and loaded to 30 % of their after cure compressive strength. The applied load was kept constant throughout the test. Within-batch deviations in stress were eliminated since all loaded specimens from a batch were placed in the same loading frame.

Creep and shrinkage measurements were taken on the schedule set forth in ASTM C512,[19] using a Whittemore gage to measure changes in length between the gage points over time. The Whittemore gage reads lengths in increments of 0.0025 mm (0.0001 in.), which equals 17 and 13 microstrain for the accelerated and standard cure specimens, respectively. Measurements were repeated four times on each side of the cylinder, so that each reading is an average of eight measurements.

Strains were calculated by dividing the change in length by the original gage length. In order to calculate creep strain, loaded cylinders were paired with unloaded cylinders by relative magnitudes of deformation. For example, the creep cylinder having the largest total strain was paired with the shrinkage cylinder having the largest shrinkage strain, and so on. Creep strains for each pair were then calculated by subtracting initial elastic strain and companion shrinkage cylinder strain from the total strain.

Vibrating wire gages (VWG) identical to the ones used in the test girders were embedded in the center of two cylindrical creep and shrinkage specimens of accelerated batch 2A. The VWGs are Geokon Model VCE-4200, and have a gage length of 6 in. More detailed information is available on Geokon's website, www.geokon.com. Readings were taken at the same time increments as the Whittemore measurements, and the two were compared in order to observe differences in creep and shrinkage behavior between the center of a concrete specimen and the outer surface

3.6 Shrinkage Testing

In addition to the cylinders for measuring shrinkage, three shrinkage prisms were cast from each standard cure batch and tested in accordance with ASTM C157.[16] Gage points were cast in the ends of each prism. The prisms were kept in the same environment as the creep and shrinkage cylinders, and measured at the same time increments, using a comparator.

3.7 Strength Testing

Compressive and tensile strength tests were performed for each batch. Compressive tests followed ASTM C39,[17] using 100 mm x 200 mm (4 in. x 8 in.) cylinders that were sulfur-capped and stored in the creep room after curing. For the standard cure batches, compressive tests on two specimens were performed at 7, 28, 56, and 90 days after casting. The Sure Cure system limited the number of accelerated cure specimens that could be made, so compressive tests were performed at 1, 7, and 28 days after casting.

Tensile strength for each batch was evaluated using the splitting tensile test of ASTM C496.[18] Two specimens were tested at 7 and 28 days after casting for the standard cure batches and 1 and 28 days after casting for the accelerated cure batches.

3.8 Modulus of Elasticity

Tests were performed one 100 mm x 200 mm (4 in. x 8 in.) cylinder from each batch to determine the modulus of elasticity, following the procedure of ASTM C469.[21] The modulus of elasticity measurements were taken at 7, 28, 56, and 90 days for the standard cure batches, and 1, 28, and 90 days for the accelerated cure batches.

3.9 Thermal Coefficient

The thermal coefficient was measured using two of the accelerated batch 2A shrinkage specimens after the end of creep testing. The specimens were subjected to temperatures ranging from 33 °F to 120 °F (0 °C to 49 °C), for three days at each temperature. Strain Measurements were taken using both the embedded vibrating wire gages and the Whittemore gage. Measurements were taken at ambient conditions before and after thermal testing to ensure that strains were due to temperature differences and not moisture loss or gain.

CHAPTER 4: RESULTS

4.1 Introduction

The following sections present the results of the HSC creep and shrinkage study: Compressive strength and tensile strength measurements are presented in sections 4.2 and 4.3, respectively. Section 4.4 presents elastic modulus measurements, and section 4.5 presents thermal coefficient results. Section 4.6 presents experimental strain measurements and predicted strains from the models. Section 4.7 presents residuals of the prediction models. Section 4.8 presents standard cure shrinkage prism results, and Section 4.9 presents vibrating wire gage measurements.

Batches 1A and 2A were subjected to heated accelerated curing, while batches 3A and 4A were given the standard moist curing regimen.

Whenever possible, experimental results are compared with field measurements obtained from Bayshore Concrete Products. Field compressive strength measurements were performed at Bayshore, while the field modulus of elasticity measurements were performed at Virginia Tech on cylinders obtained from Bayshore. Some results such as compressive strength, modulus of elasticity, and tensile strength are also compared to specified values or ACI and AASHTO design values.

4.2 Compressive Strength

4.2.1 Accelerated Cure

Figure 1 presents the HSC laboratory compressive strength results for accelerated batches 1A and 2A, as well as field results from Bayshore. Each one-day laboratory result represents an average of two measurements, and the others represent single measurements. Each result from Bayshore is an average of three measurements. The specified 28-day compressive strength (f'_c) of 55 Mpa (8000 psi) and release strength (f'_{ci}) of 44 MPa (6400 psi) are presented for comparison.

The one-day compressive strengths for batch 1A and 2A were 68.3 MPa and 68.1 MPa (9910 and 9870 psi), respectively. The seven-day compressive strengths for batch 1A and 2A were 71.0 MPa and 74.1 MPa (10300 and 10740 psi), respectively. The 28-day compressive strengths for batch 1A and 2A were 86.9 MPa and 85.5 MPa (12600 and 12400 psi), respectively. The 90-day compressive strengths for batch 1A and 2A were 82.1 MPa and 83.4 MPa (11900 and 12100 psi), respectively. The Bayshore one-day, seven-day, and 28-day compressive strengths were 45.3 MPa, 50.0 MPa, and 59.0 MPa (6570, 7250, and 8560 psi), respectively

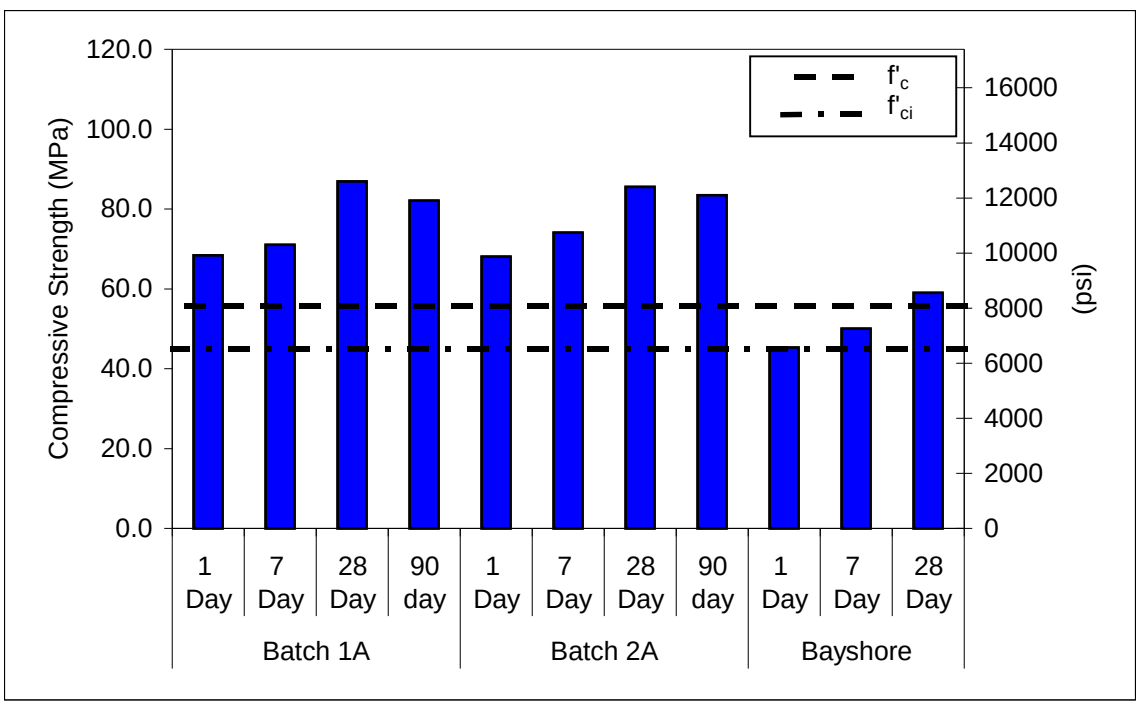

Figure 1 Accelerated Cure Compressive Strengths

4.2.2 Standard Cure

Figure 2 presents the HSC laboratory compressive strength results for standard cure batches 3A and 4A. Each result represents an average of two compressive strength measurements. The specified 28-day compressive strength (f'_c) of 55 Mpa (8000 psi) and release strength (f'_{ci}) of 44 MPa (6400 psi) are presented for comparison.

The seven-day compressive strengths for batch 3A and 4A were 69.0 MPa and 73.1 MPa (10000 and 10600 psi), respectively. The 28-day compressive strengths for batch 3A and 4A were 90.3 MPa and 91.7 MPa (13100 and 13300 psi), respectively. The 56-day compressive strengths for batch 3A and 4A were 95.9 MPa and 97.2 MPa (13900 and 14100 psi), respectively. The 90-day compressive strengths for batch 3A and 4A were 87.6 MPa and 90.5 MPa (12700 and 13100 psi), respectively.

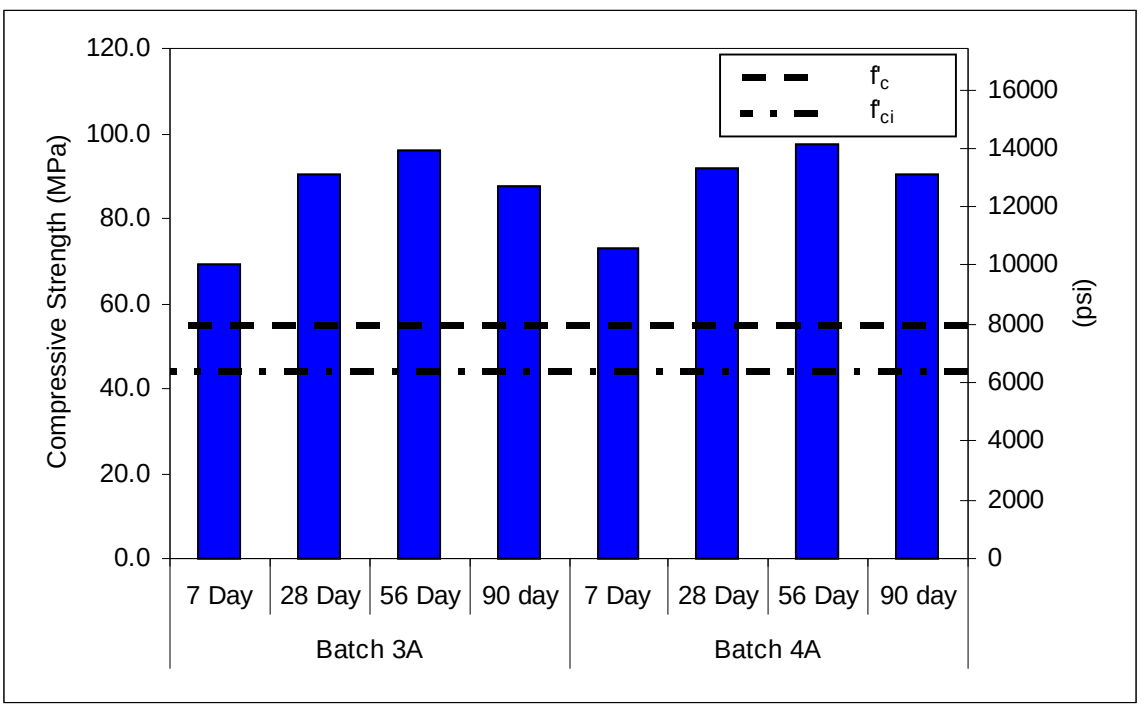

Figure 2 Standard Cure Compressive Strengths

4.3 Tensile Strength

The one-day tensile strengths for batch 1A and 2A were 6.5 MPa and 6.3 MPa (940 and 910 psi), respectively. The seven-day tensile strengths for batch 3A and 4A were 7.3 MPa and 7.2 MPa (1060 and 1040 psi), respectively. The 28-day tensile strengths for batch 1A, 2A, 3A, and 4A were 6.9 MPa, 7.4 MPa, 8.0 MPa, and 7.8 MPa (1000, 1070, 1160, and 1135 psi), respectively. The results for batches 1A and 2A are single measurements. The results for batches 3A and 4A represent averages of two measurements.

Figure 3 presents ratios of the HSC tensile strengths to the square roots of the compressive strengths. The AASHTO design modulus of rupture is 7.5 * SQRT(f'_c).

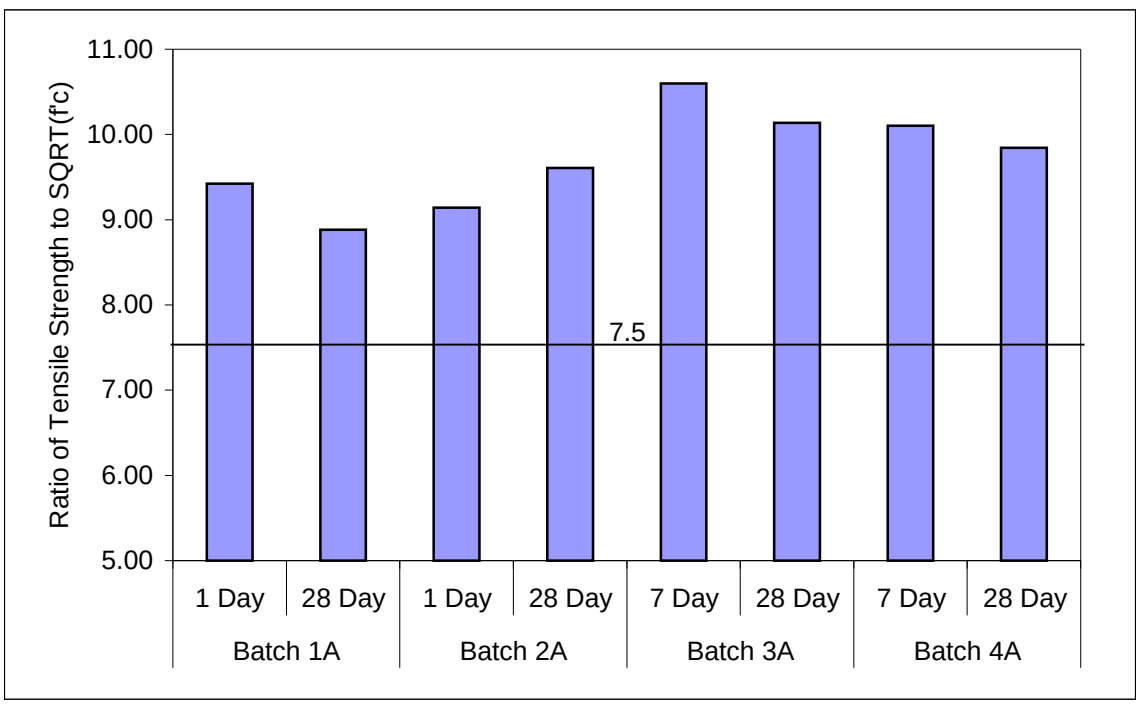

Figure 3 Ratio of Tensile Strength to SQRT(f'c)

4.4 Modulus of Elasticity

4.4.1 Accelerated Cure

Figure 4 presents the HSC modulus of elasticity results for accelerated batches 1A and 2A, along with the results from Bayshore. For the laboratory mixtures, measurements were taken on one specimen per batch at ages of 1, 28, and 90 days. Three Bayshore specimens were tested at 28 days, and the average measurement is presented below. The AASHTO design modulus of elasticity of 39.1 GPa (5650 ksi) is shown for comparison.

The one-day moduli of elasticity for batch 1A and 2A were 44.2 GPa and 44.6 GPa (6400 and 6500 ksi), respectively. The 28-day moduli of elasticity for batch 1A and 2A were both 43.7 GPa (6350 ksi). The Bayshore 28-day modulus of elasticity was 38.9 GPa (5650 ksi). The 90-day moduli of elasticity for batch 1A and 2A were 44.6 GPa and 42.1 GPa (6500 and 6100 ksi), respectively.

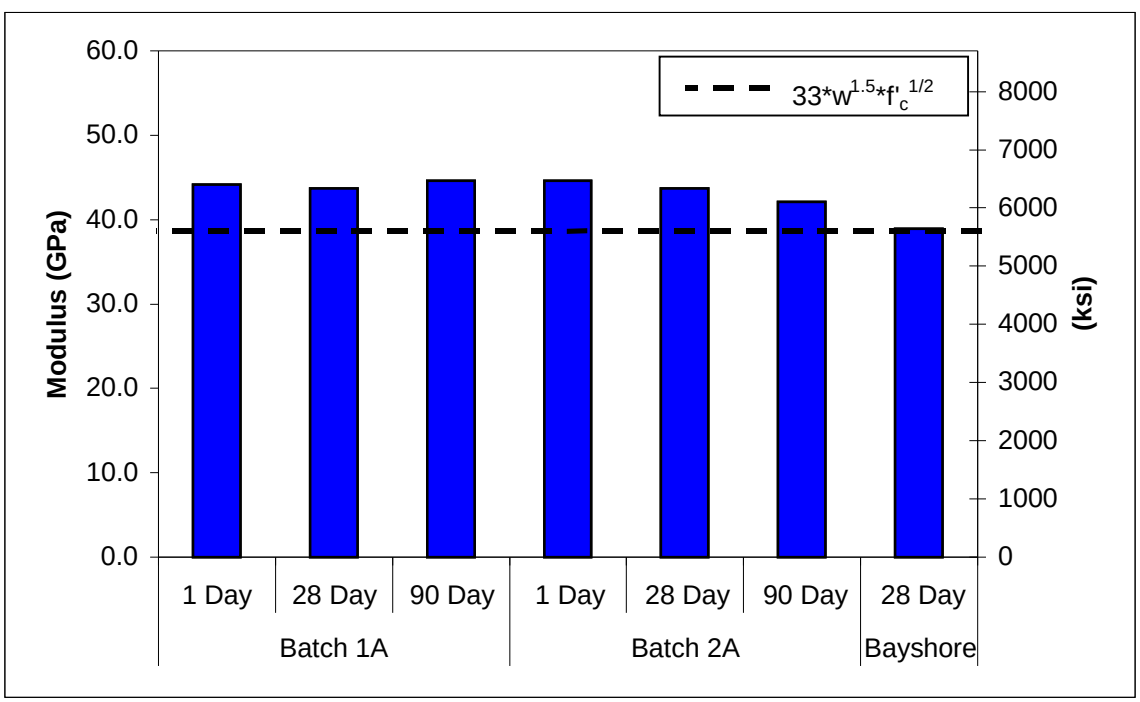

Figure 4 Accelerated Cure Modulus of Elasticity

4.4.2 Standard Cure

Figure 5 presents the HSC modulus of elasticity results for standard cure batches 3A and 4A. Measurements were taken on one specimen per batch at ages of 7, 28, 56, and 90 days. The AASHTO design modulus of elasticity of 39.3 GPa (5700 ksi) is shown for comparison.

The seven-day moduli of elasticity for batch 3A and 4A were 40.6 GPa and 43.0 GPa (5880 and 6240 ksi), respectively. The 28-day moduli of elasticity for batch 3A and 4A were 44.6 GPa and 46.2 GPa (6460 and 6700 ksi), respectively. The 56-day moduli of elasticity for batch 3A and 4A were 45.9 GPa and 45.5 GPa (6650 and 6600 ksi), respectively. The 90-day moduli of elasticity for batch 3A and 4A were 46.9 GPa and 45.7 GPa (6800 and 6600 ksi), respectively.

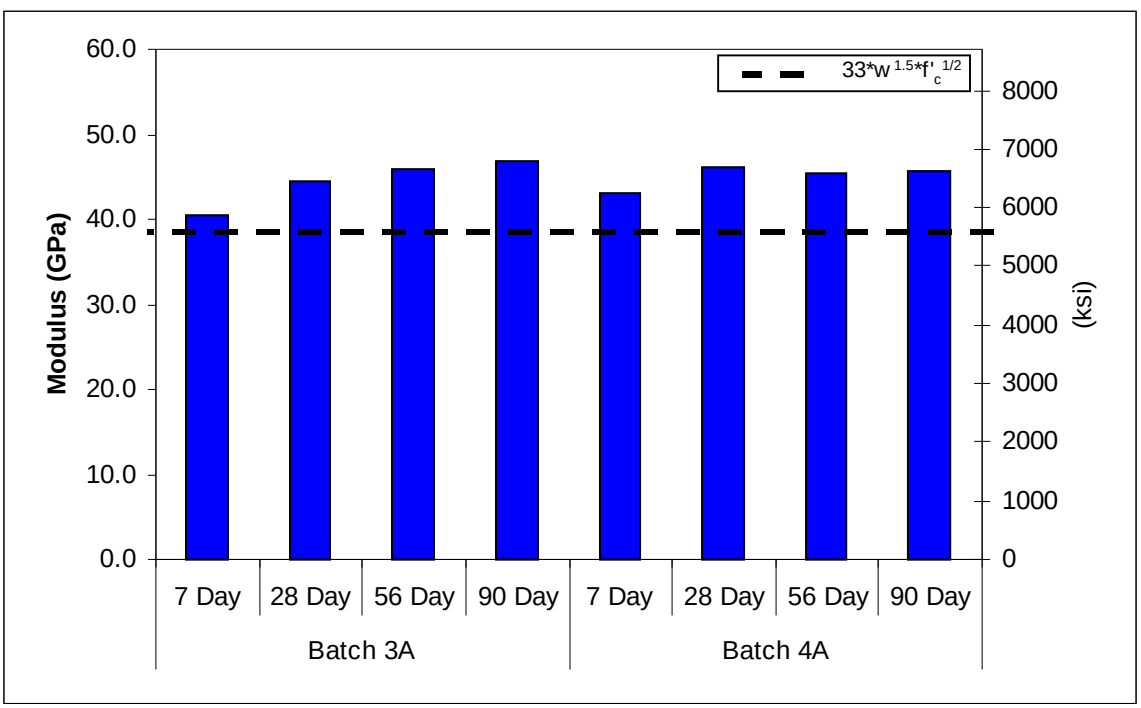

Figure 5 Standard Cure Modulus of Elasticity

4.5 Thermal Coefficient

The coefficient of thermal expansion for the HSC mixture was found to be 8.3 ± 0.7 microstrain per °C (4.6 ± 0.4 microstrain per °F) at a 95% confidence level.

4.6 Experimental and Predicted Strains

Figures 6 through 11 present the HSC experimental total strain, shrinkage, and creep measurements for accelerated cure and standard cure batches. Measurements were taken daily for a week after loading, then weekly thereafter, but some measurements are not shown in the figures for clarity. For the accelerated cure batches, each curve represents an average of four specimens, and for the standard cure batches, each curve represents an average of three specimens. Each creep curve represents an average of four (accelerated cure) or three (standard cure) pairs of loaded and unloaded specimens.

The figures also present 95 percent confidence intervals for each data point. The 95 percent confidence interval is the range in which 95 percent of the population measurements can be expected to fall.

Figures 12 through 25 present the total strain, shrinkage, and creep strains predicted by the models. The predicted strains were calculated using measured compressive strengths and elastic strains. The predicted time-dependent strains were added to the measured initial elastic strains. The following models were considered:

- ACI 209R-92 (ACI 209) [9]
- ACI 209R-92, modified by Huo (ACI 209 Modified) [11]
- Comite Euro-International Du Beton Model Code 1990 (CEB 90) [12]
- AASHTO-LRFD Specification (AASHTO-LRFD) [14]
- Gardner and Lockman's GL2000 Model (GL2000) [10]
- Tadros' Revised AASHTO-LRFD (Tadros) [4]
- Bazant's B3 Model (B3) [13]

The equations for prestress loss due to creep and shrinkage in the AASHTO Standard Specification are based on the ACI 209 model.

4.6.1 Accelerated Cure Experimental Strains

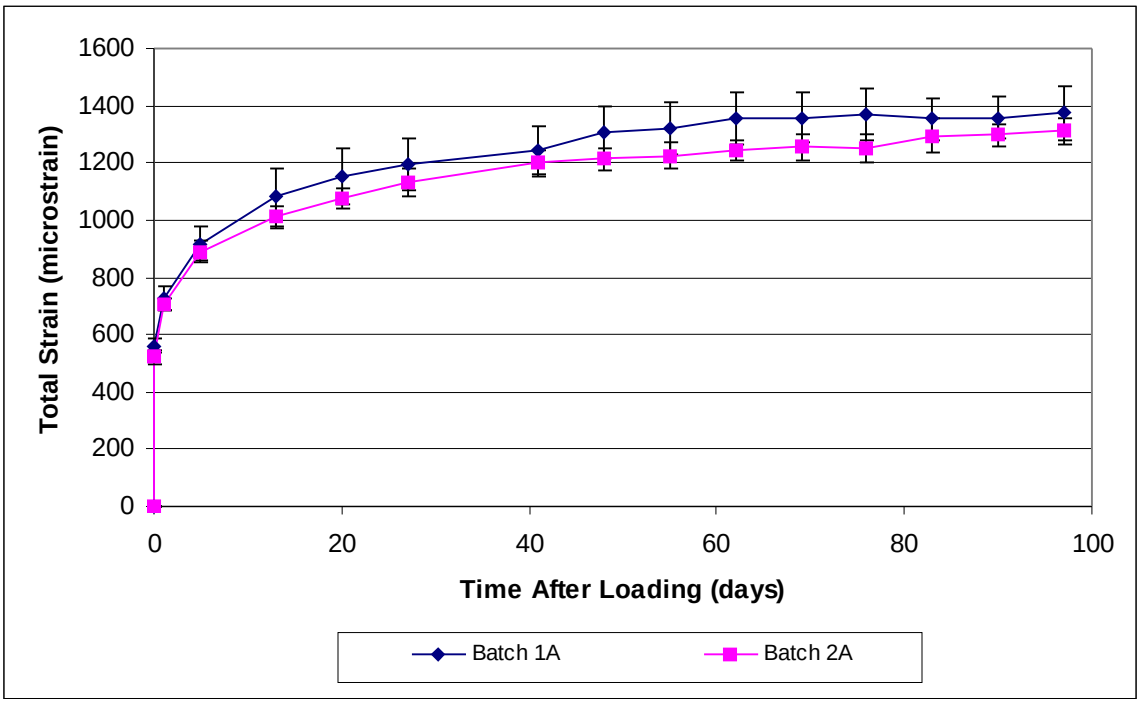

Figure 6 Accelerated Cure Experimental Total Strain

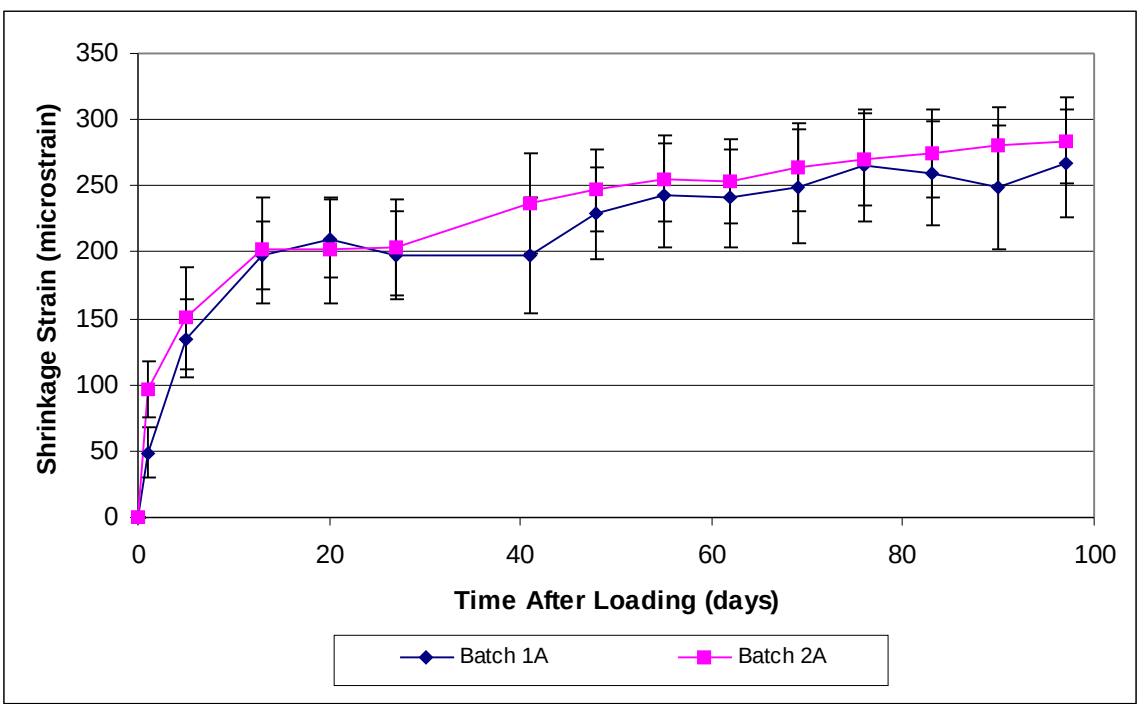

Figure 7 Accelerated Cure Experimental Shrinkage Strain

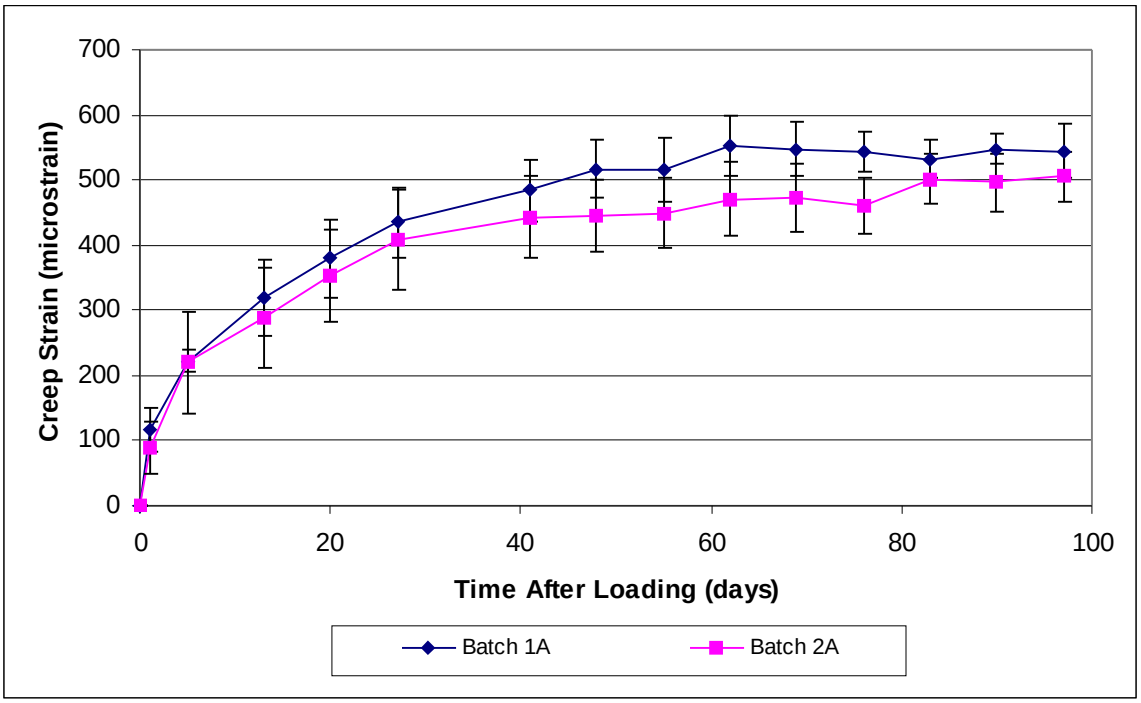

Figure 8 Accelerated Cure Experimental Creep Strain

4.6.2 Standard Cure Experimental Strains

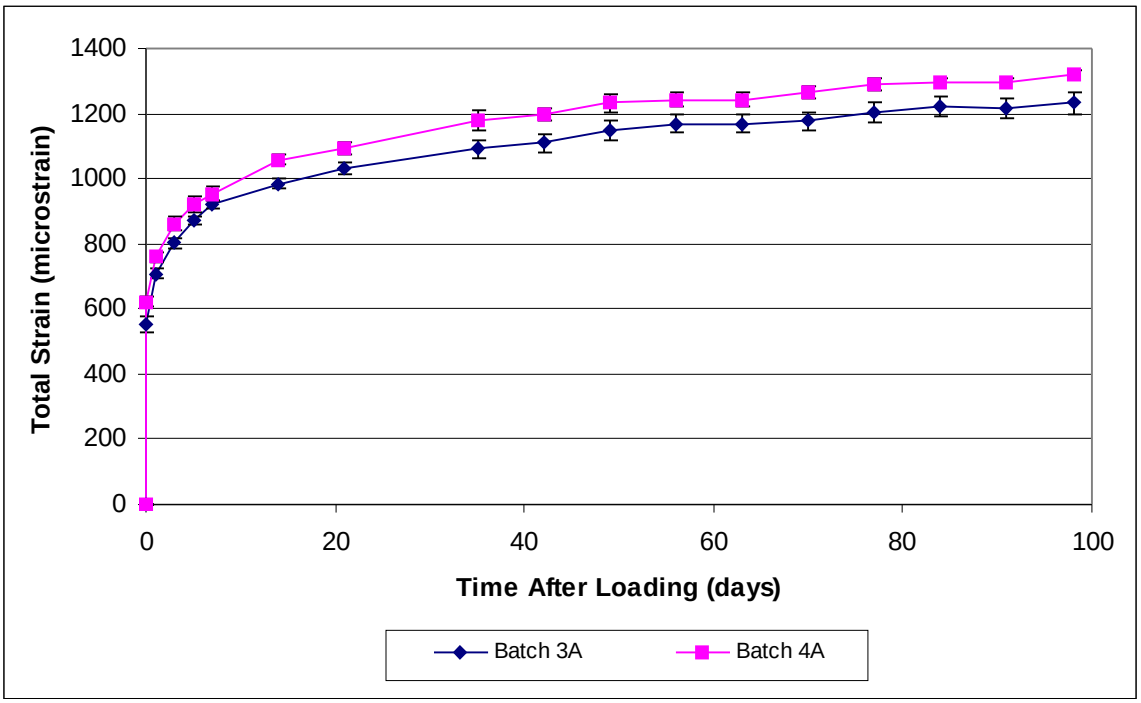

Figure 9 Standard Cure Experimental Total Strain

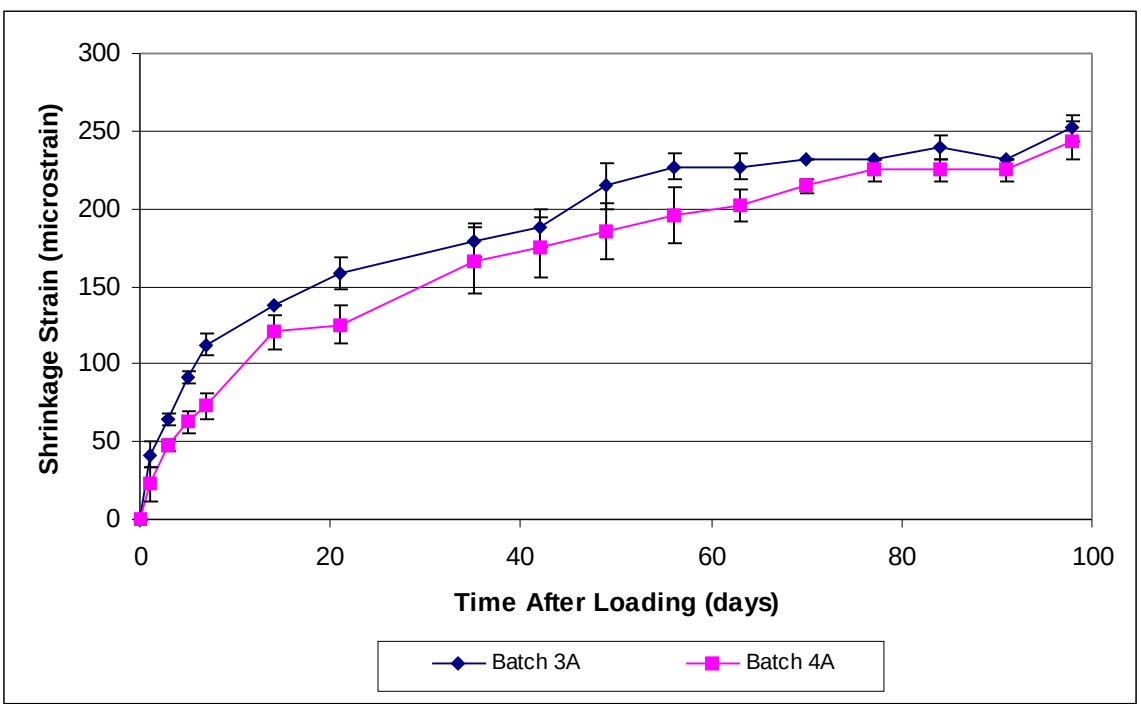

Figure 10 Standard Cure Experimental Shrinkage Strain

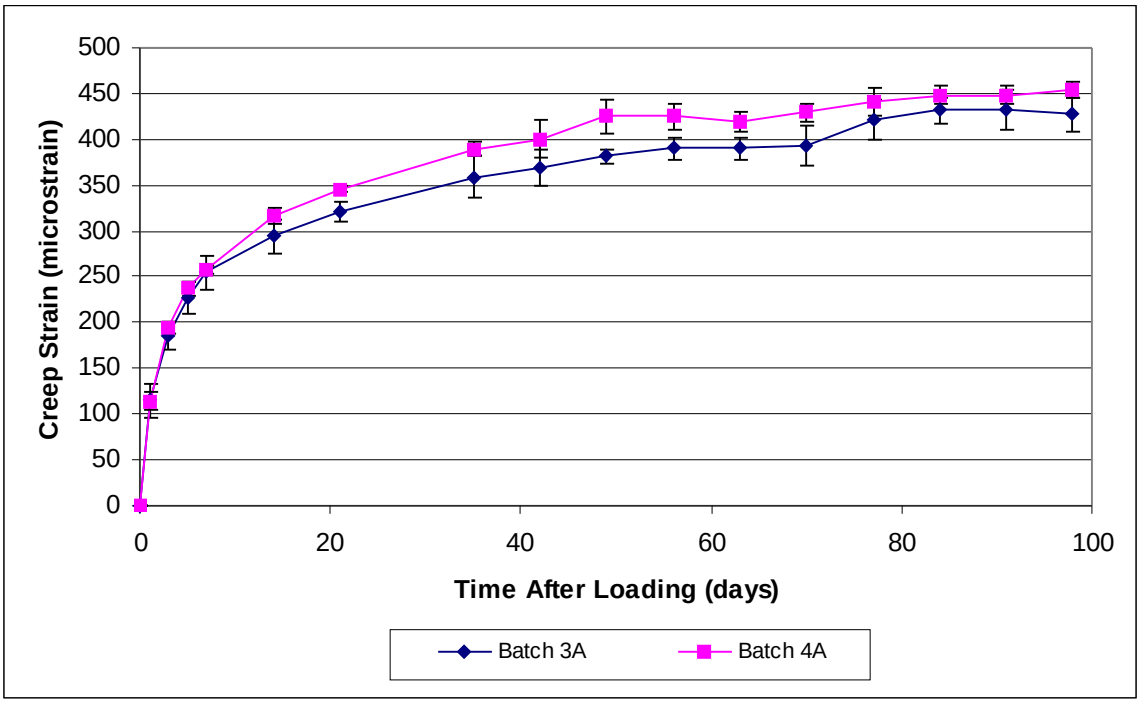

Figure 11 Standard Cure Experimental Creep Strain

4.6.3 Accelerated Cure Predicted Strains

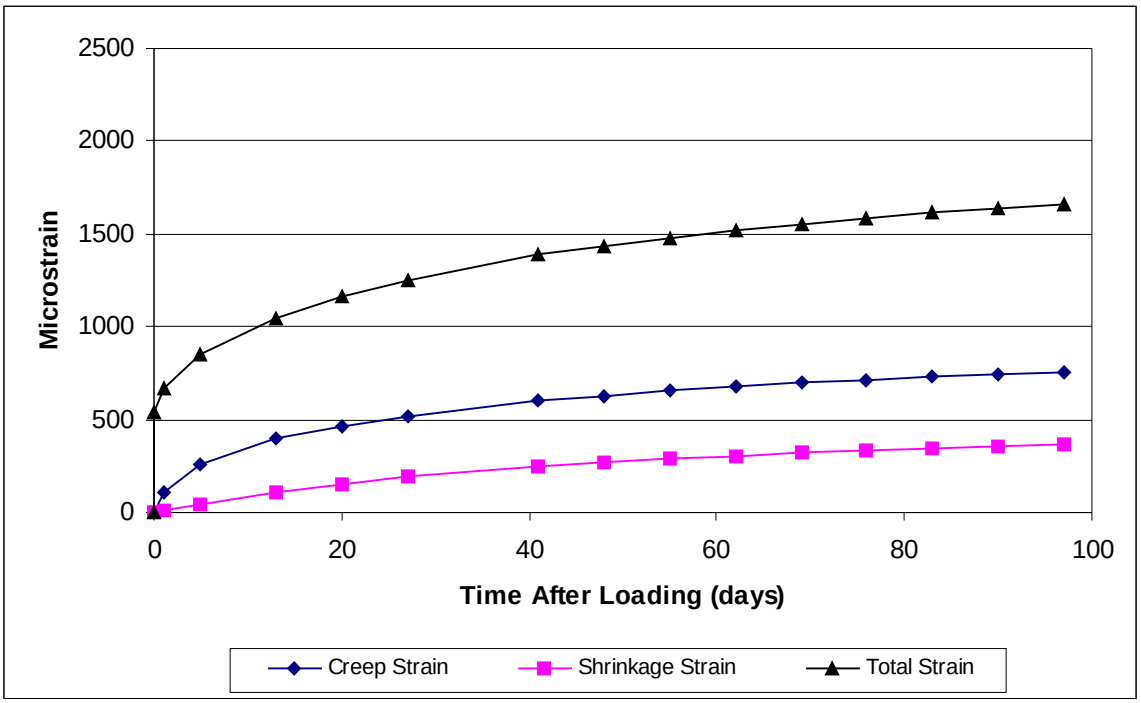

Figure 12 ACI 209 Accelerated Cure Predicted Strains

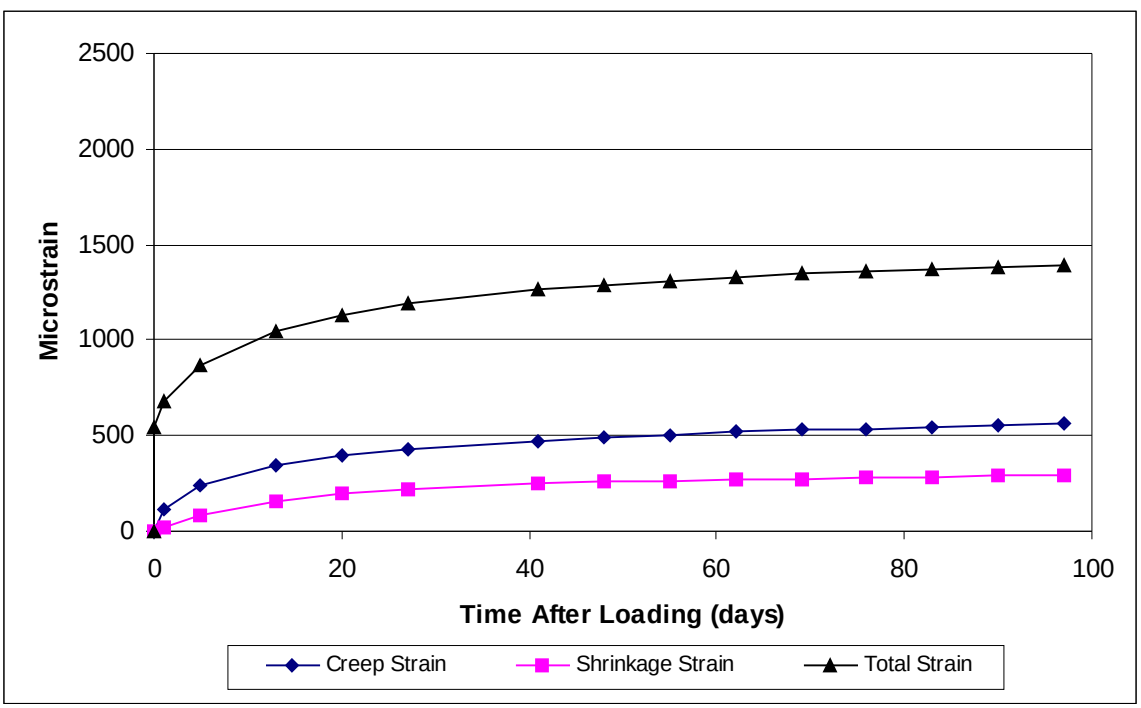

Figure 13 ACI 209 Modified Accelerated Cure Predicted Strains

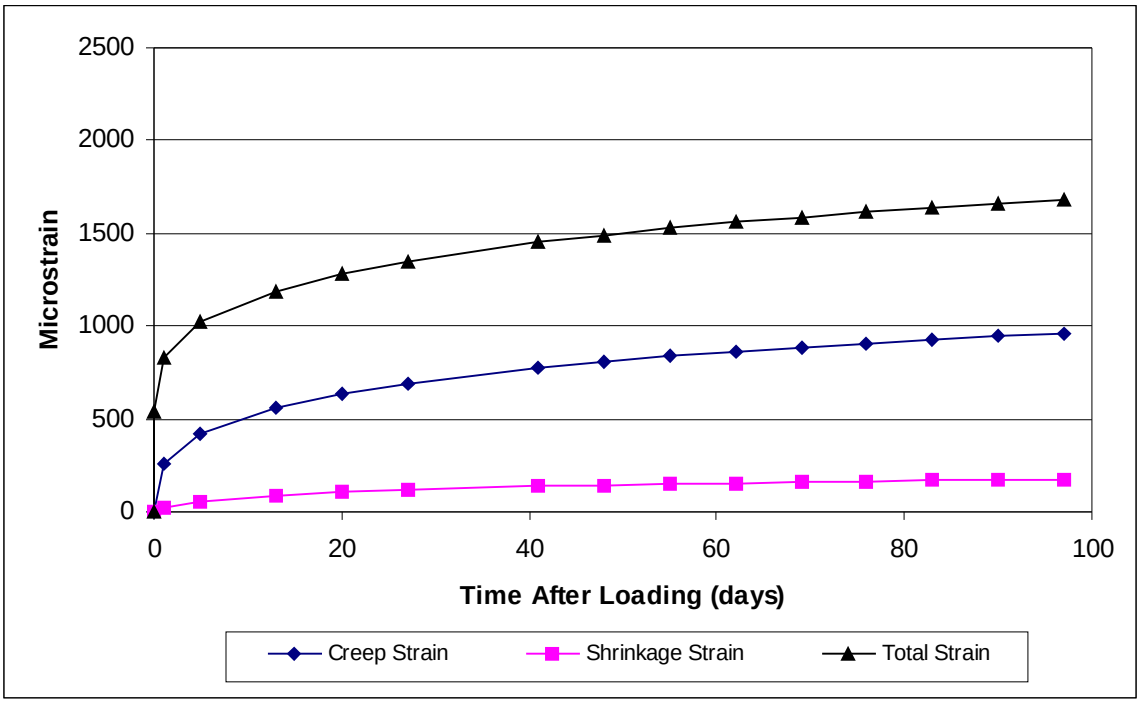

Figure 14 CEB-MC90 Accelerated Cure Predicted Strains

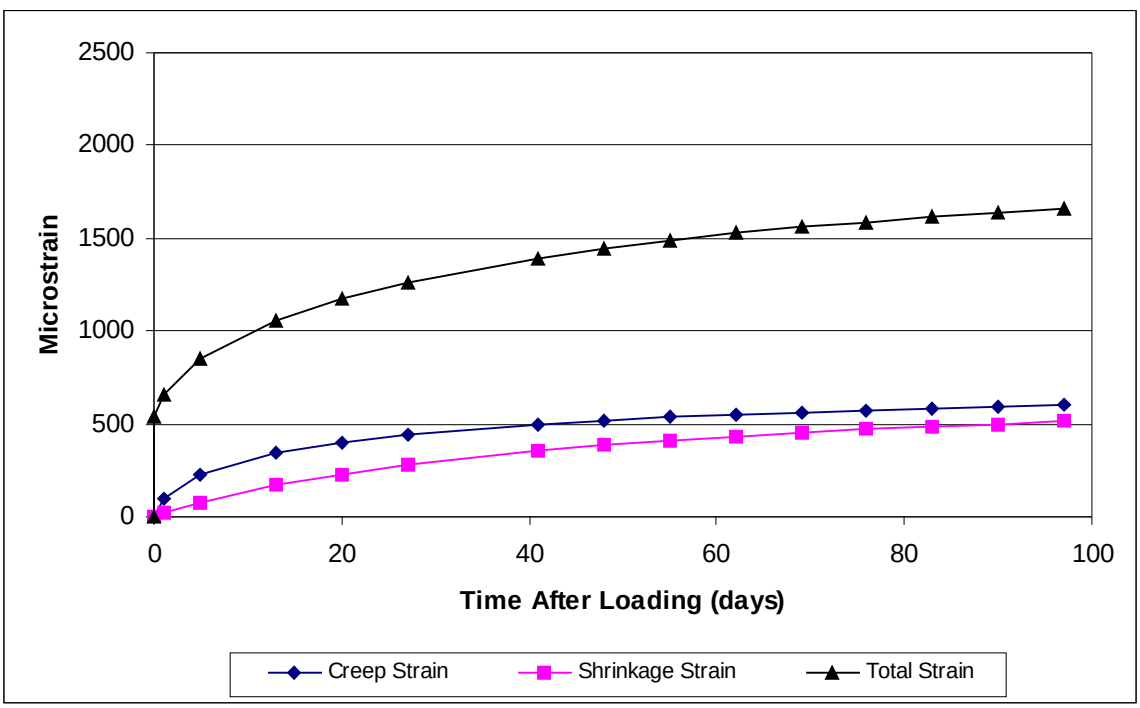

Figure 15 AASHTO-LRFD Accelerated Cure Predicted Strains

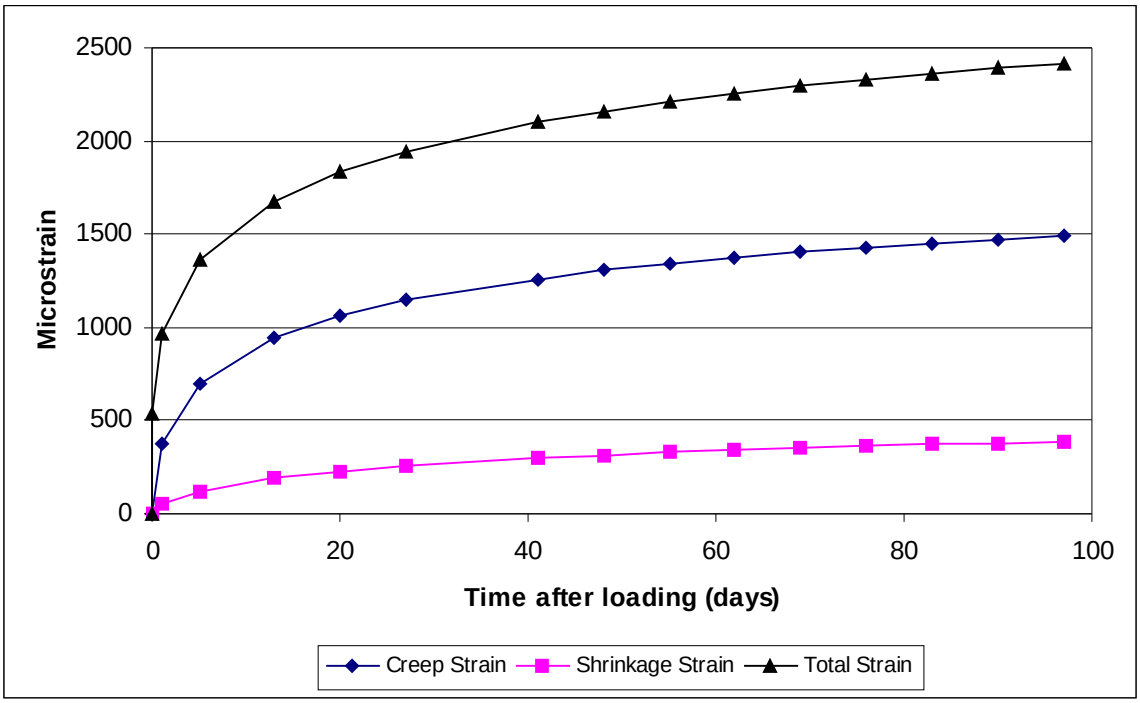

Figure 16 GL2000 Accelerated Cure Predicted Strains

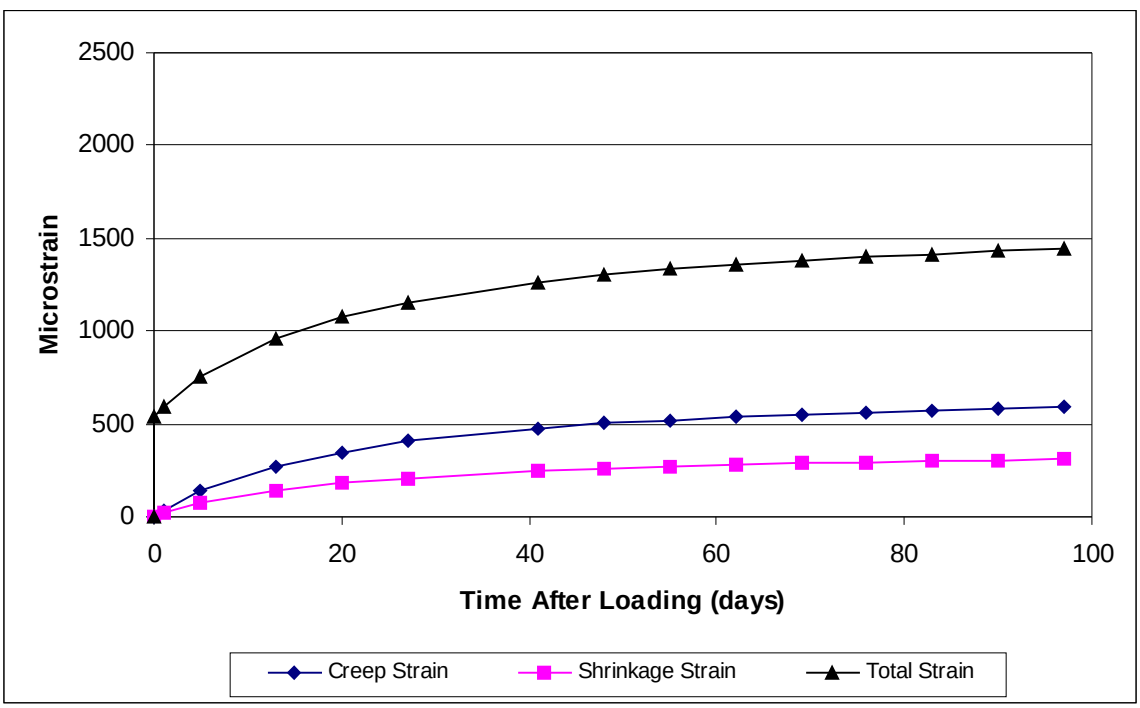

Figure 17 Tadros Accelerated Cure Predicted Strains

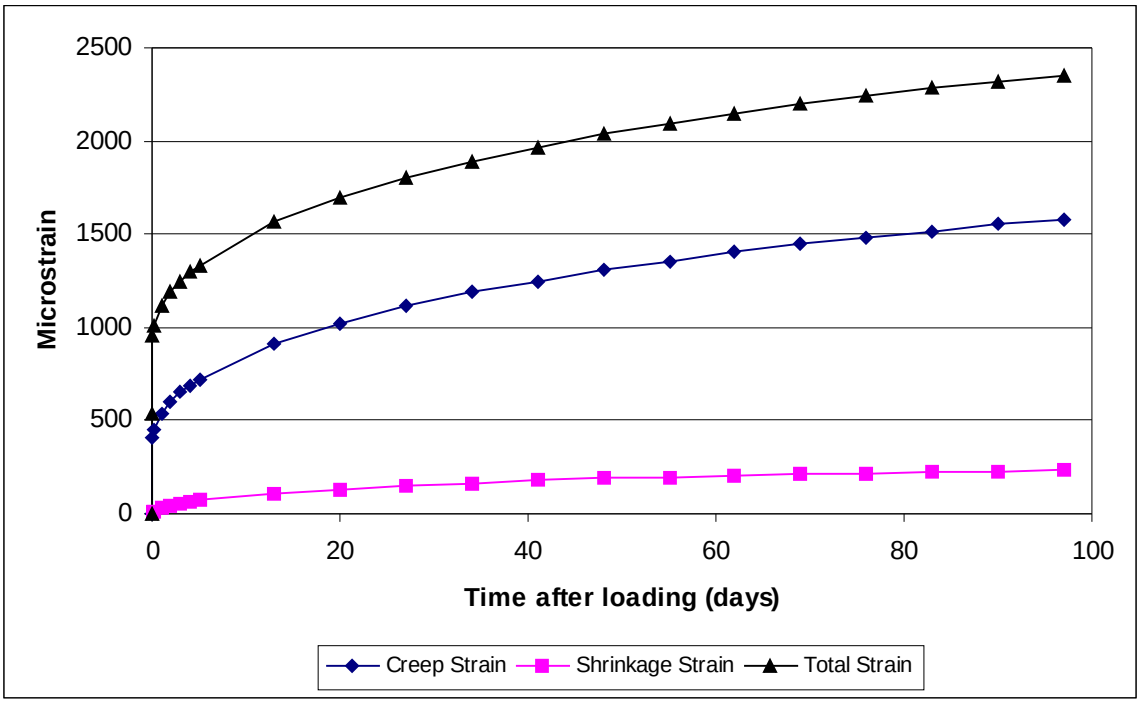

Figure 18 B3 Accelerated Cure Predicted Strains

4.6.4 Standard Cure Predicted Strains

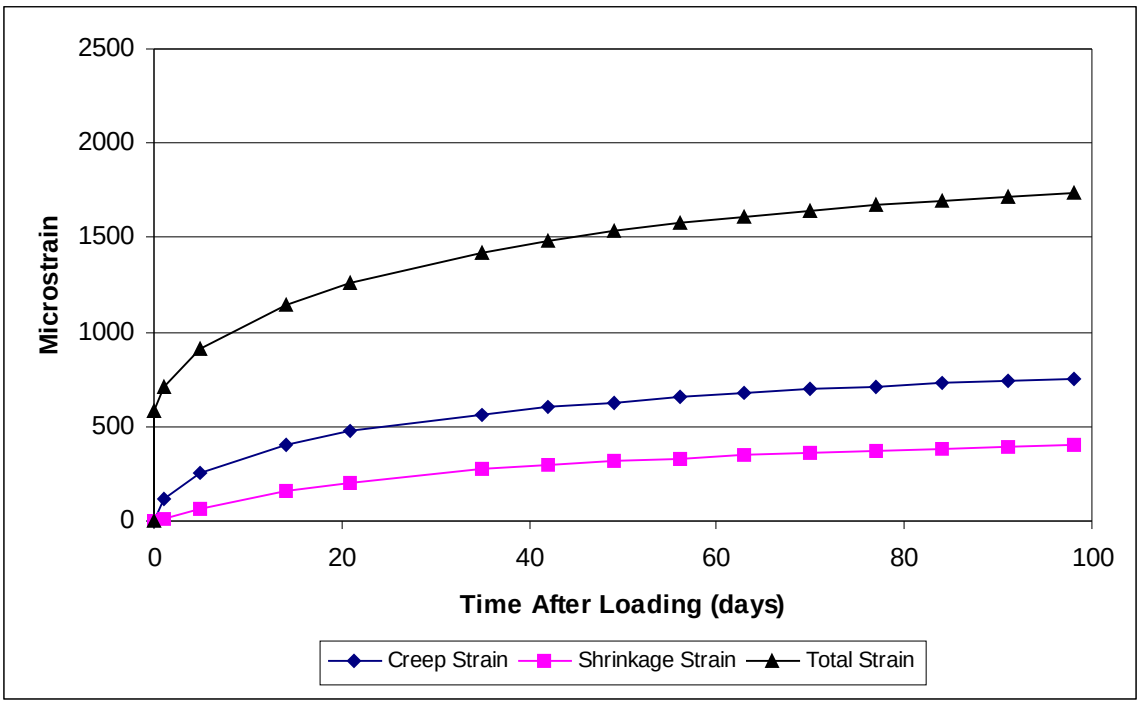

Figure 19 ACI 209 Standard Cure Predicted Strains

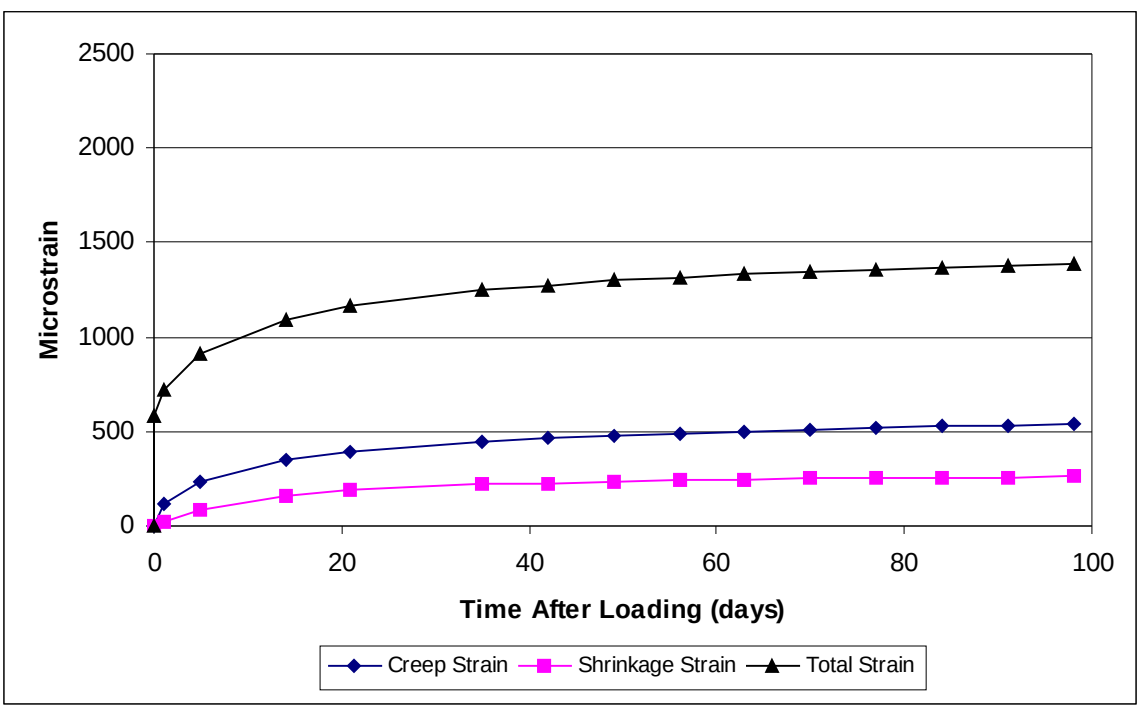

Figure 20 ACI 209 Modified Standard Cure Predicted Strains

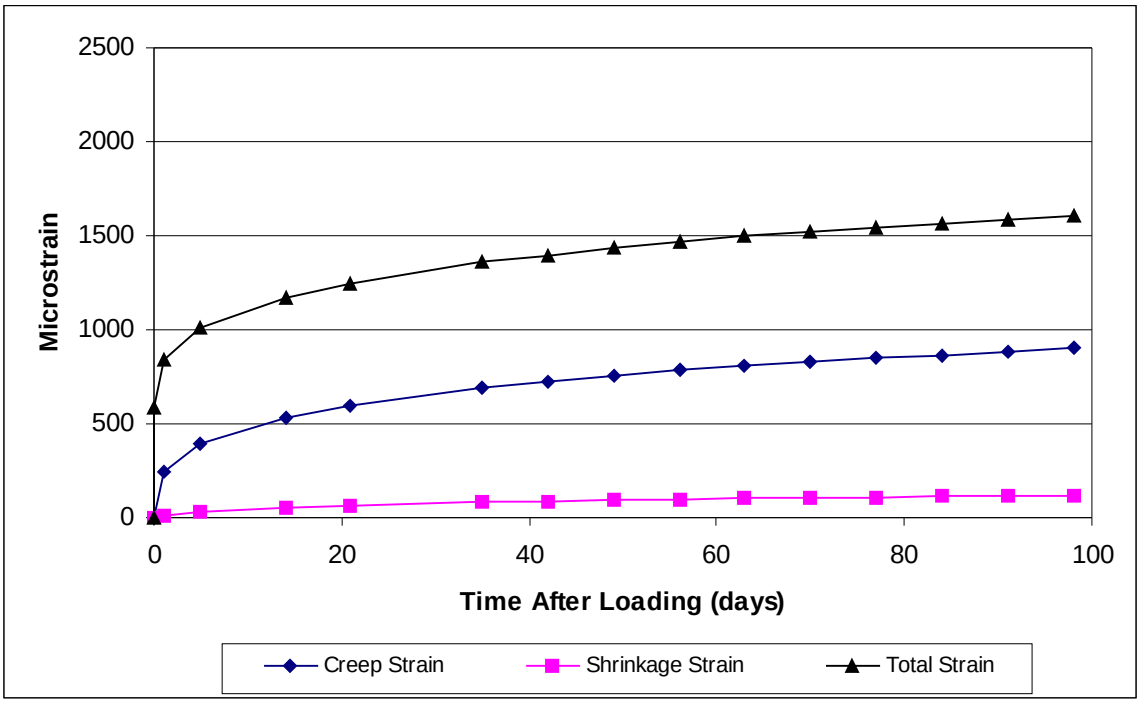

Figure 21 CEB-MC90 Standard Cure Predicted Strains

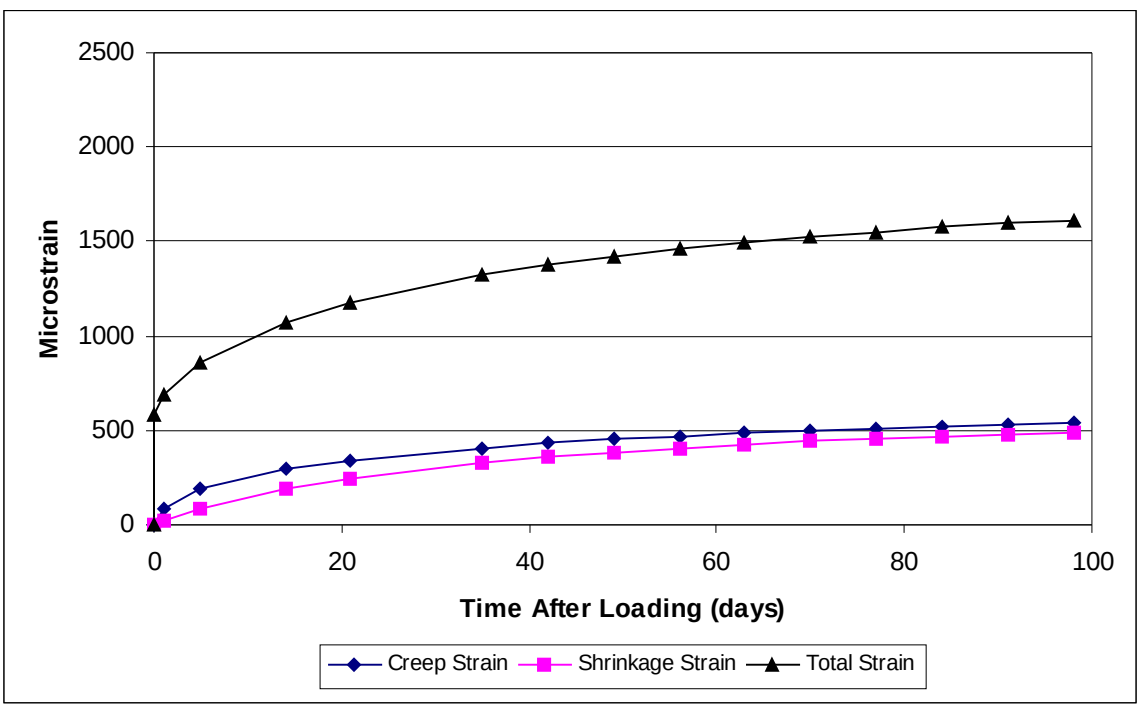

Figure 22 AASHTO-LRFD Standard Cure Predicted Strains

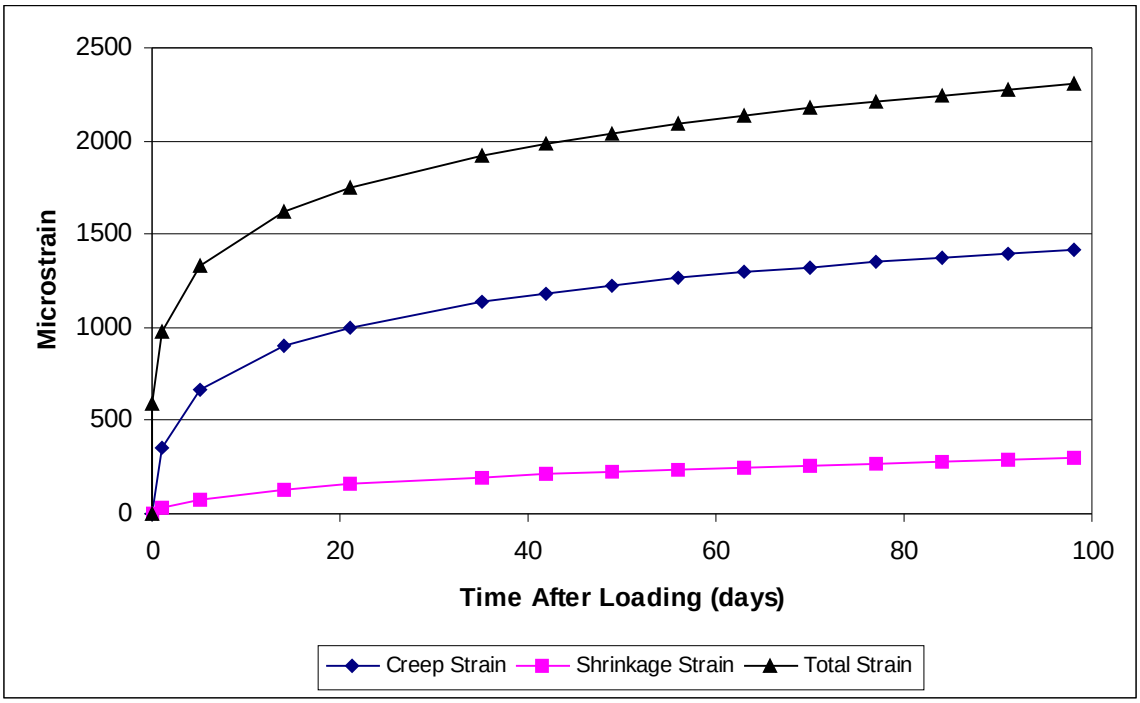

Figure 23 GL2000 Standard Cure Predicted Strains

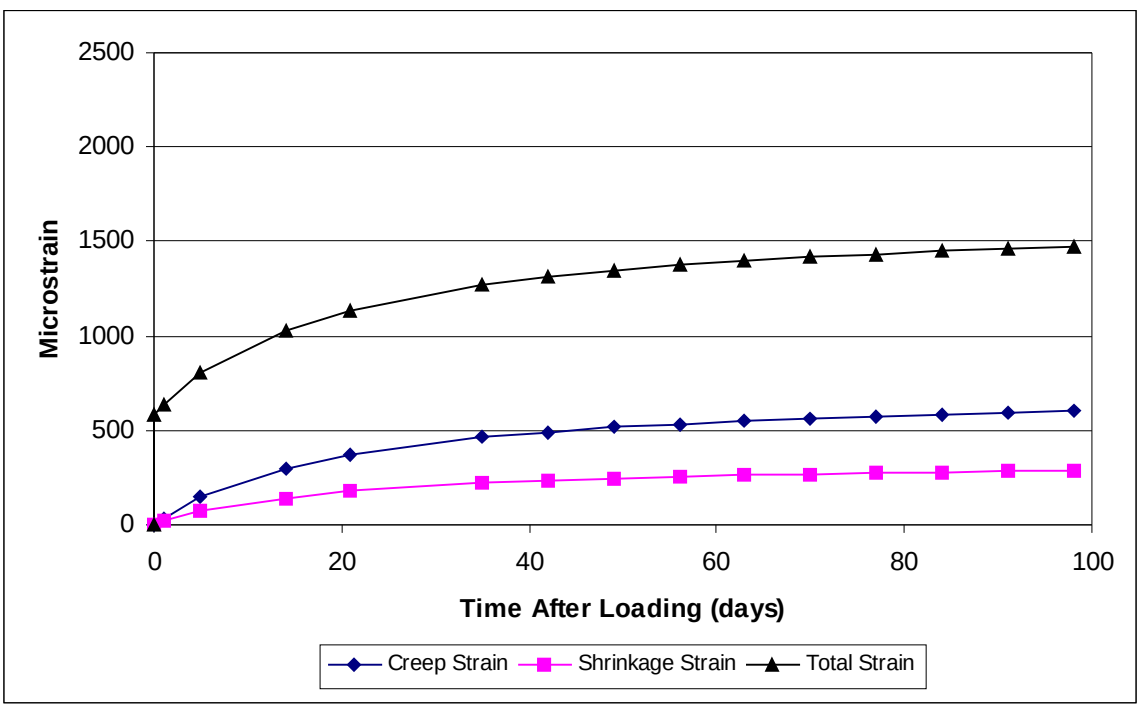

Figure 24 Tadros Standard Cure Predicted Strains

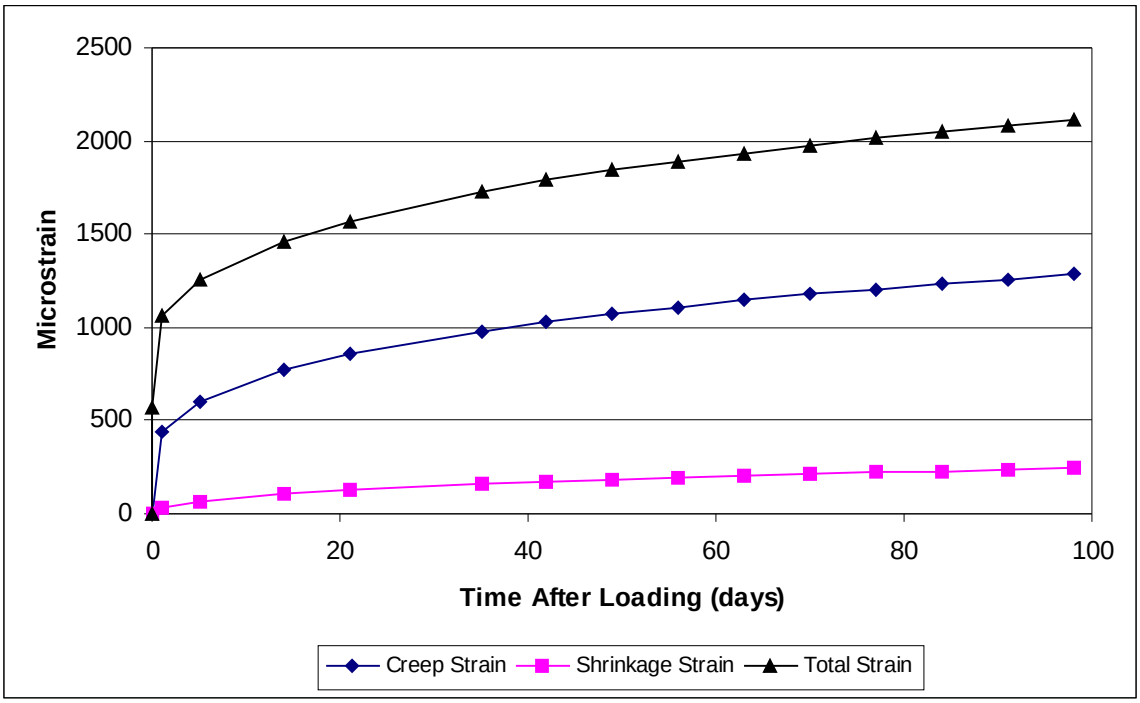

Figure 25 B3 Standard Cure Predicted Strains

4.7 Prediction Model Residuals

Figures 26 through 49 present residuals of the prediction models for accelerated cure and standard cure batches. Accelerated cure total strain, shrinkage, and creep residuals are presented in Sections 4.7.1 through 4.7.3. Standard cure total strain, shrinkage, and creep residuals are presented in Sections 4.7.4 through 4.7.6. A residual is defined as the algebraic difference between a predicted value and an experimental value. A negative residual indicates that a model is under predicting the experimental data, and a positive residual indicates the model is over predicting the experimental data.

As shown in section 4.6, the experimental strains for the two accelerated cure batches were not significantly different, and likewise for the standard cure batches. Therefore, the two batches from each curing method were combined and treated as a single data set for comparison with the models. The accelerated cure and standard cure mean residuals and 95 percent confidence intervals are shown as a function of time for the eight accelerated cure specimens and six standard cure specimens.

4.7.1 Accelerated Cure Total Strain Residuals

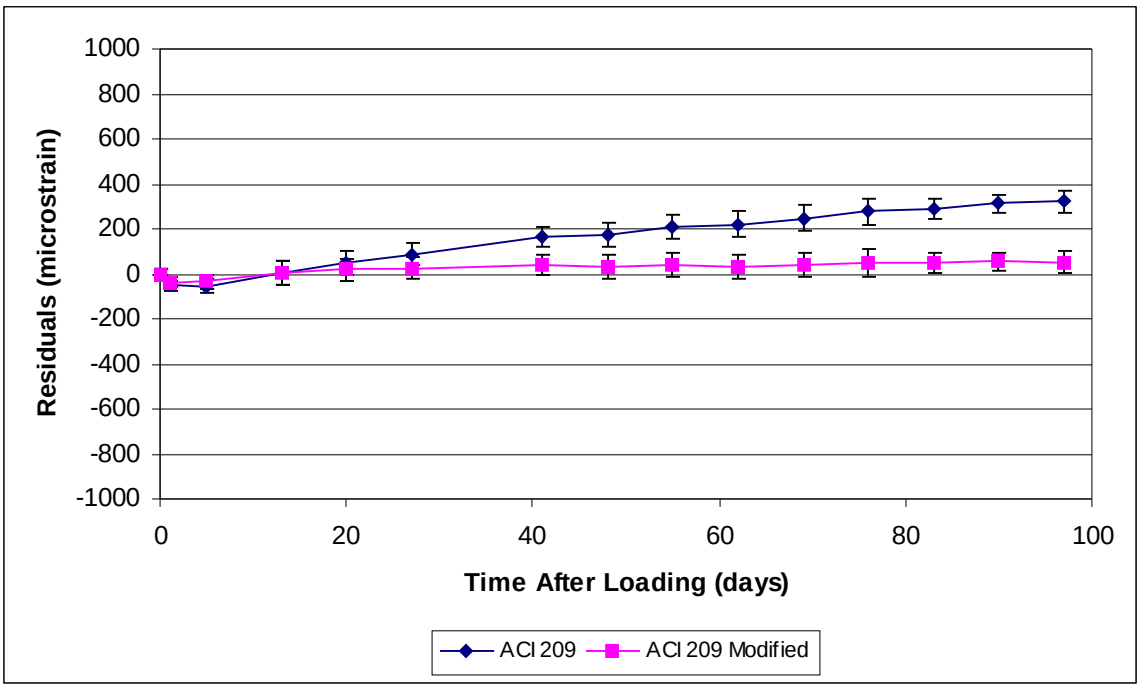

Figure 26 ACI 209 and ACI 209 Modified Accelerated Cure Total Strain Residuals

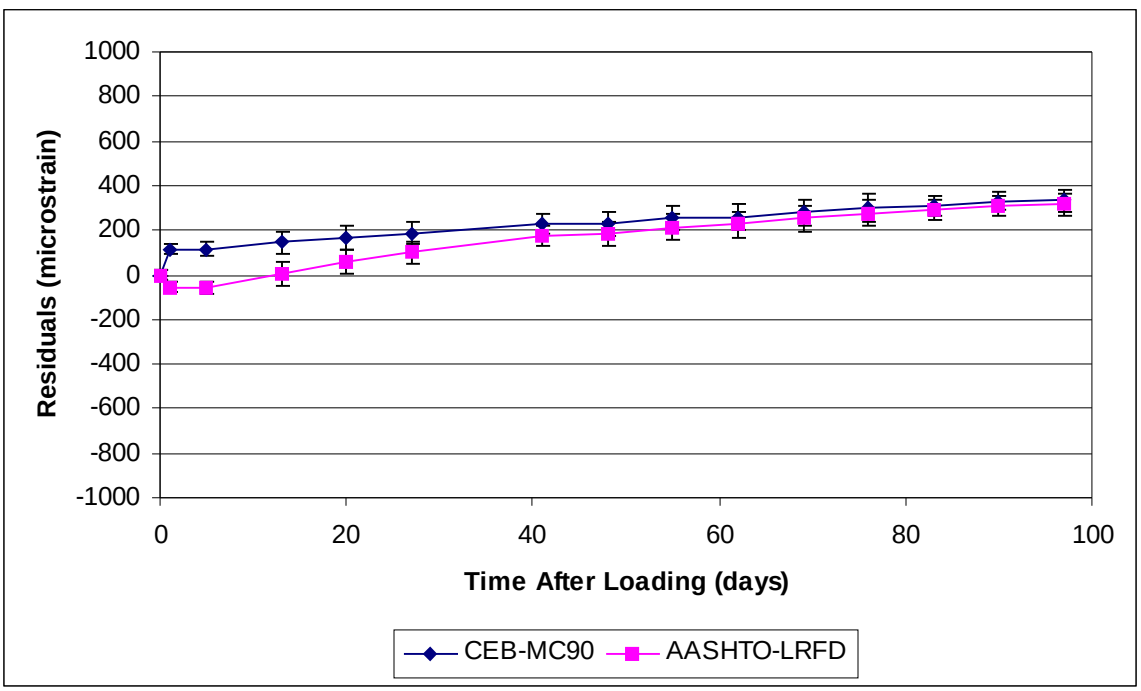

Figure 27 CEB-MC90 and AASHTO-LRFD Accelerated Cure Total Strain Residuals

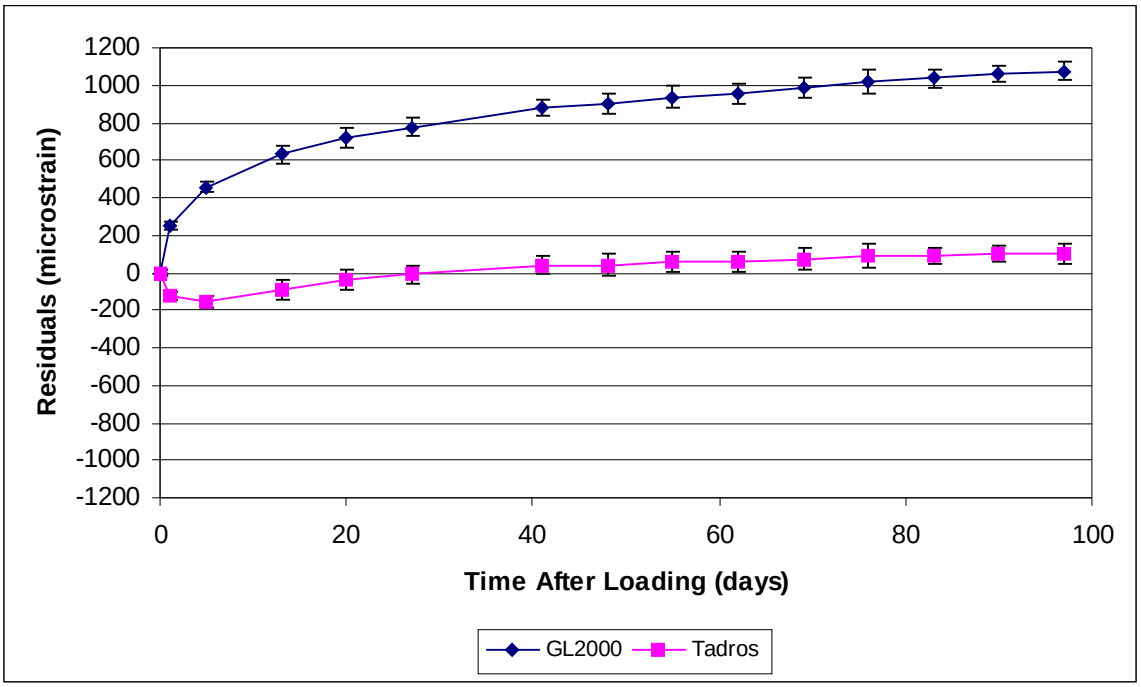

Figure 28 GL2000 and Tadros Accelerated Cure Total Strain Residuals

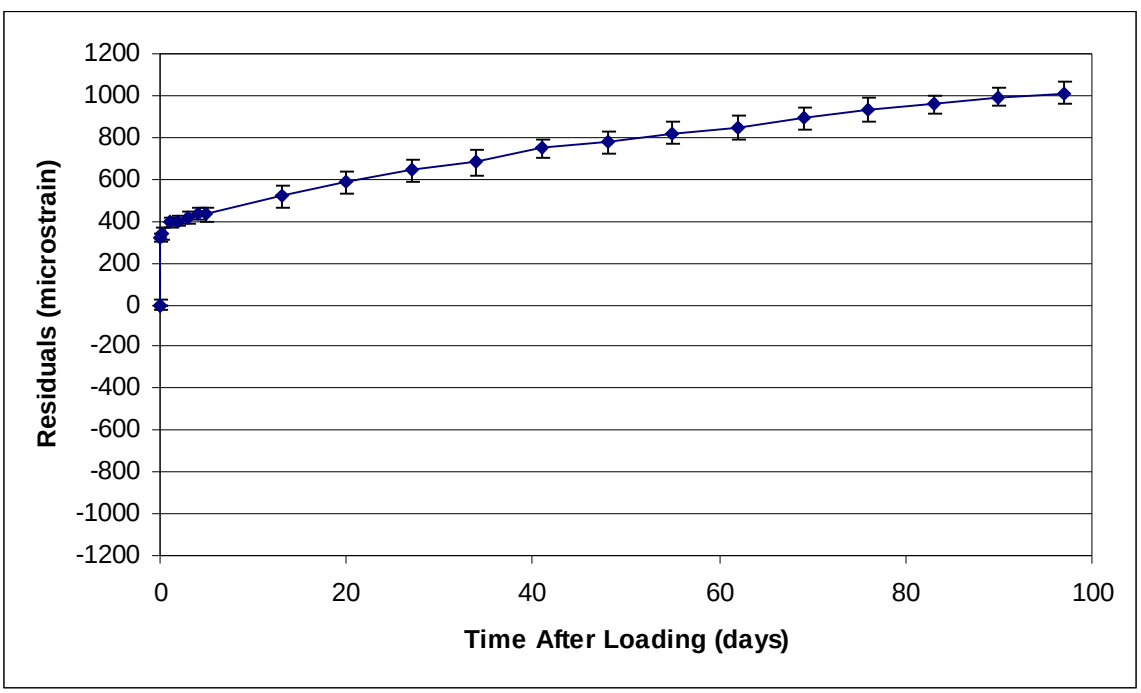

Figure 29 B3 Accelerated Cure Total Strain Residuals

4.7.2 Accelerated Cure Shrinkage Residuals

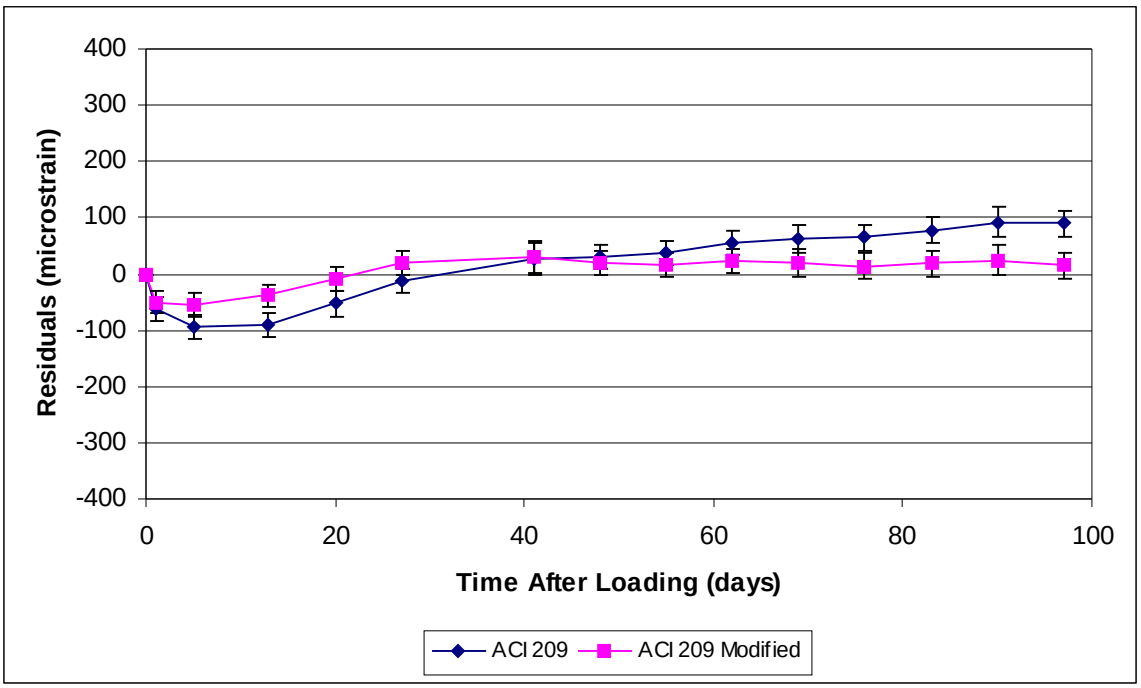

Figure 30 ACI 209 and ACI 209 Modified Accelerated Cure Shrinkage Residuals

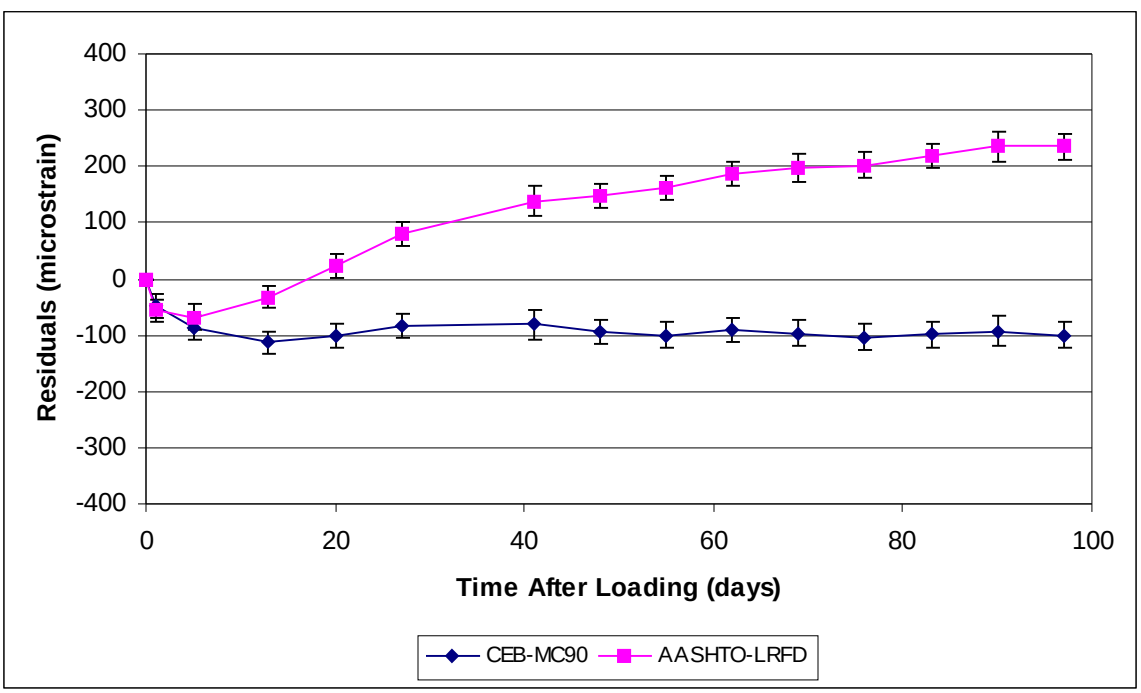

Figure 31 CEB-MC90 and AASHTO-LRFD Accelerated Cure Shrinkage Residuals

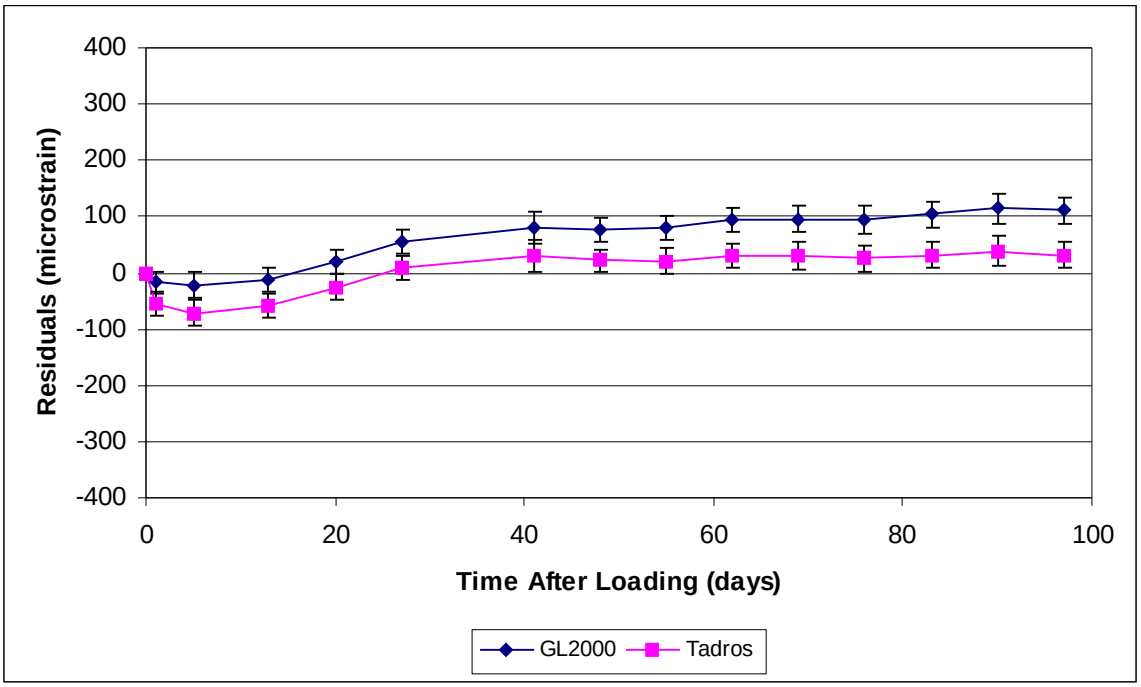

Figure 32 GL2000 and Tadros Accelerated Cure Shrinkage Residuals

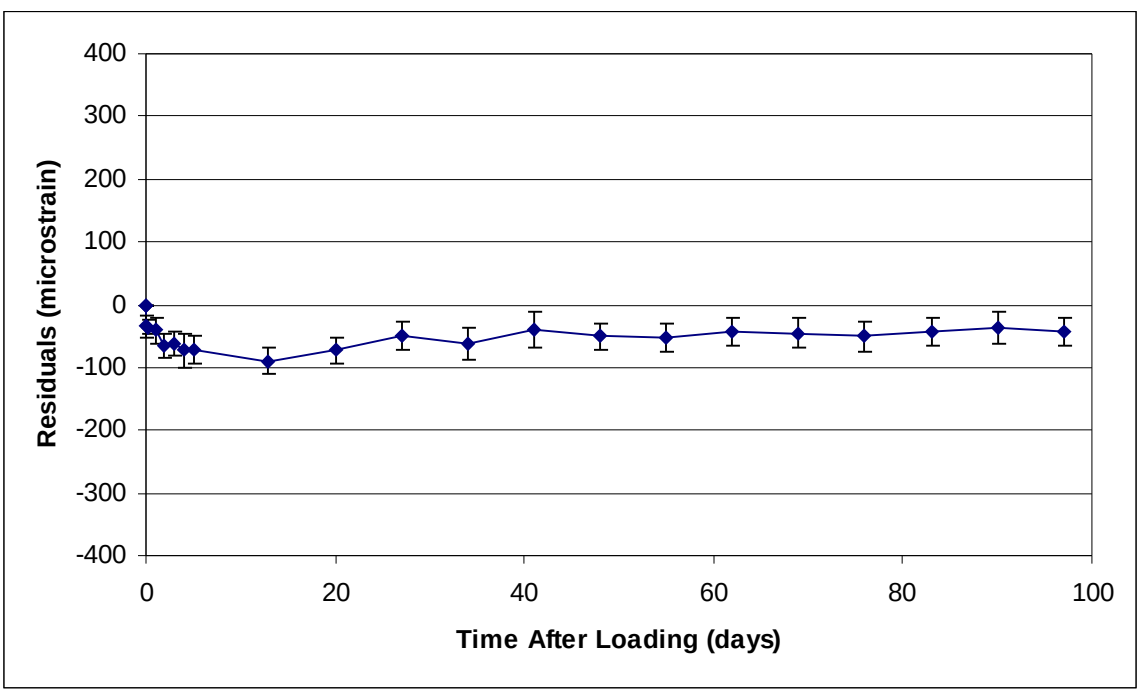

Figure 33 B3 Accelerated Cure Shrinkage Residuals

4.7.3 Accelerated Cure Creep Residuals

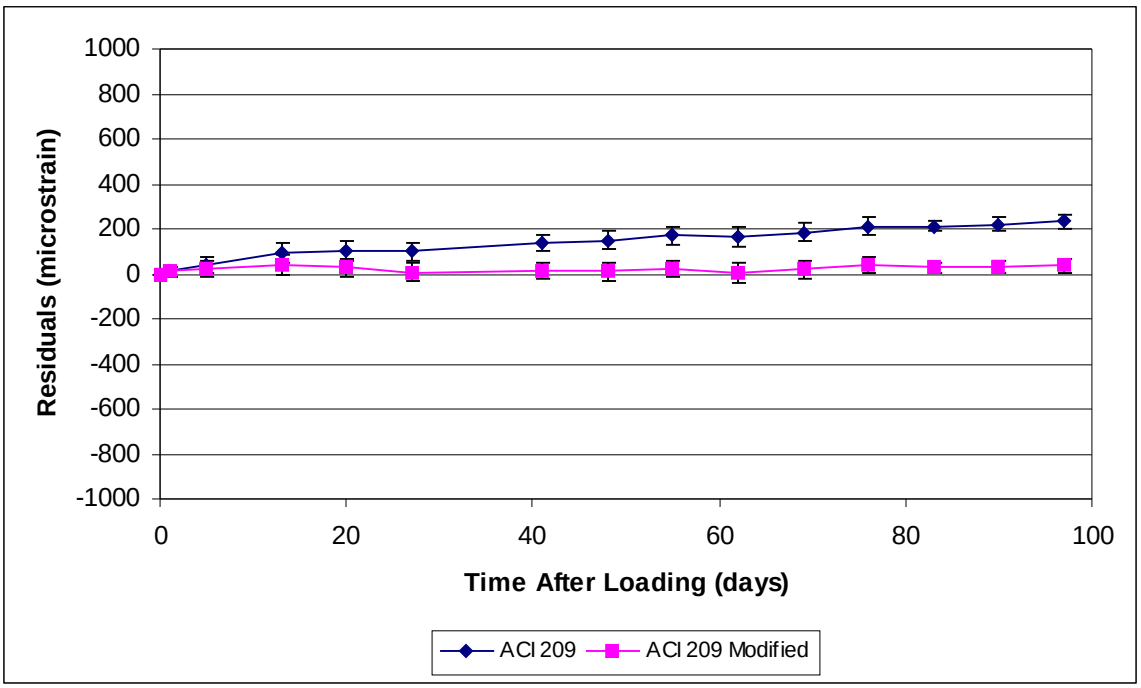

Figure 34 ACI 209 and ACI 209 Modified Accelerated Cure Creep Residuals

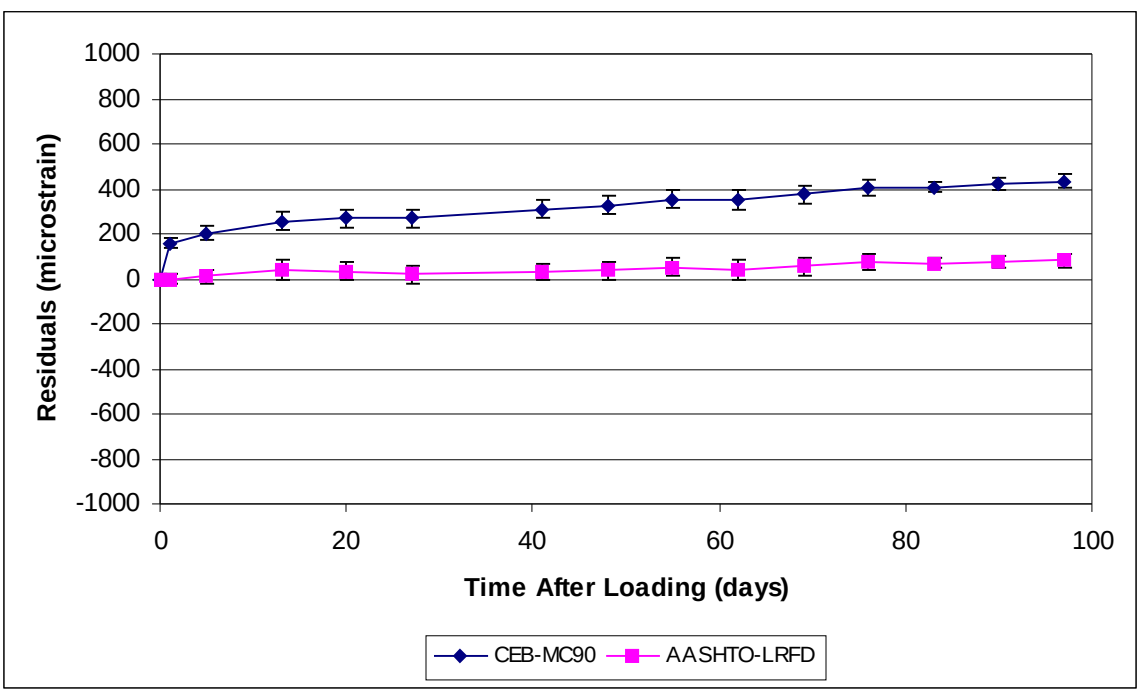

Figure 35 CEB-MC90 and AASHTO-LRFD Accelerated Cure Creep Residuals

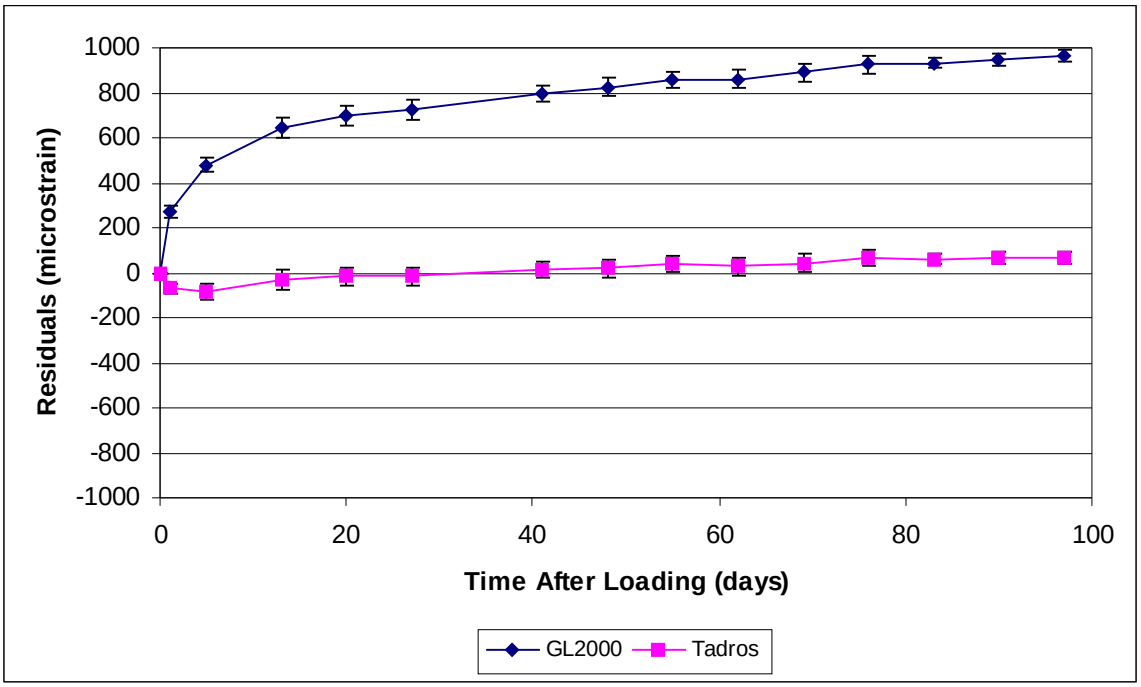

Figure 36 GL2000 and Tadros Accelerated Cure Creep Residuals

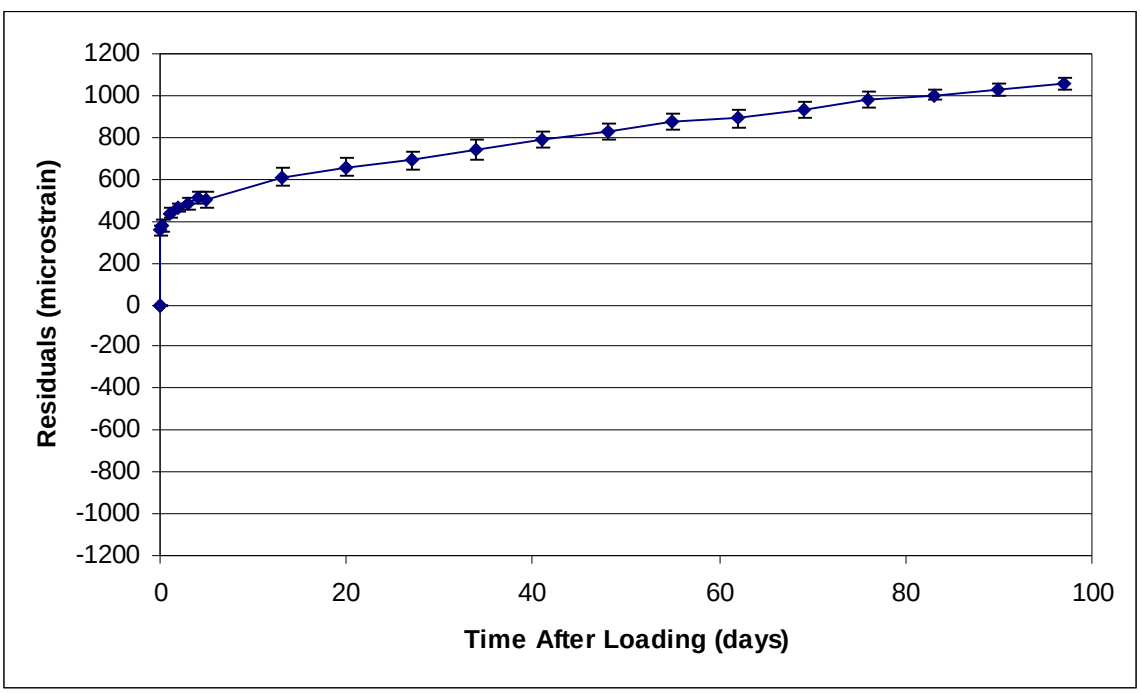

Figure 37 B3 Accelerated Cure Creep Residuals

4.7.4 Standard Cure Total Strain Residuals

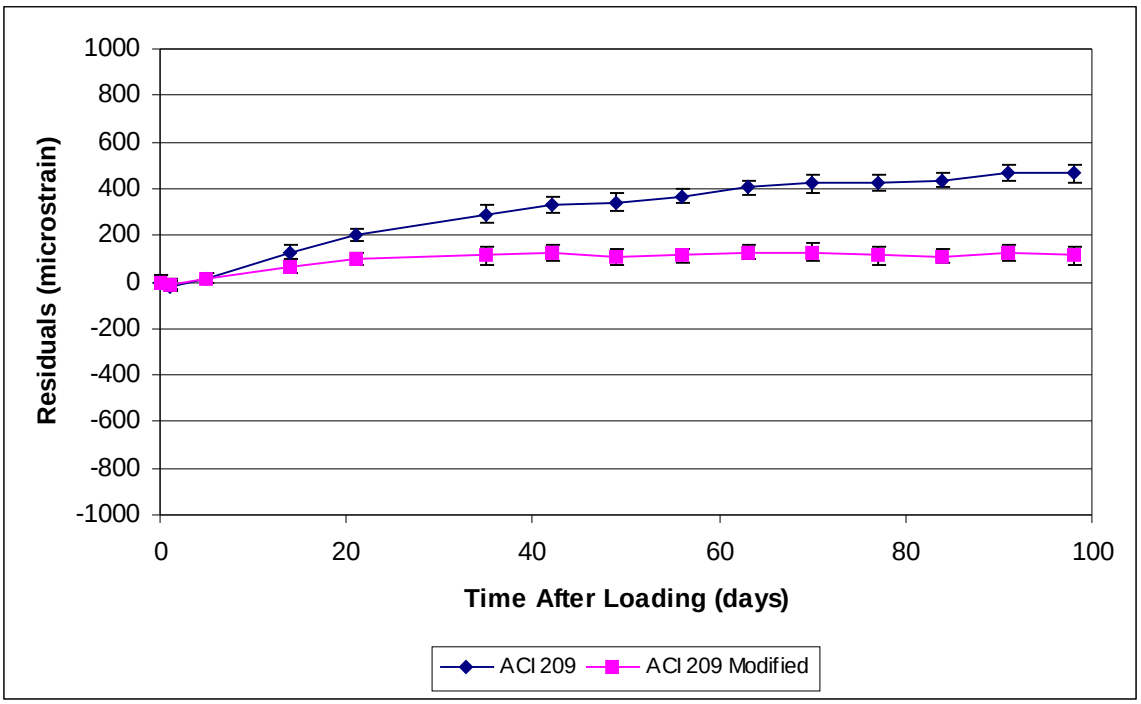

Figure 38 ACI 209 and ACI 209 Modified Standard Cure Total Strain Residuals

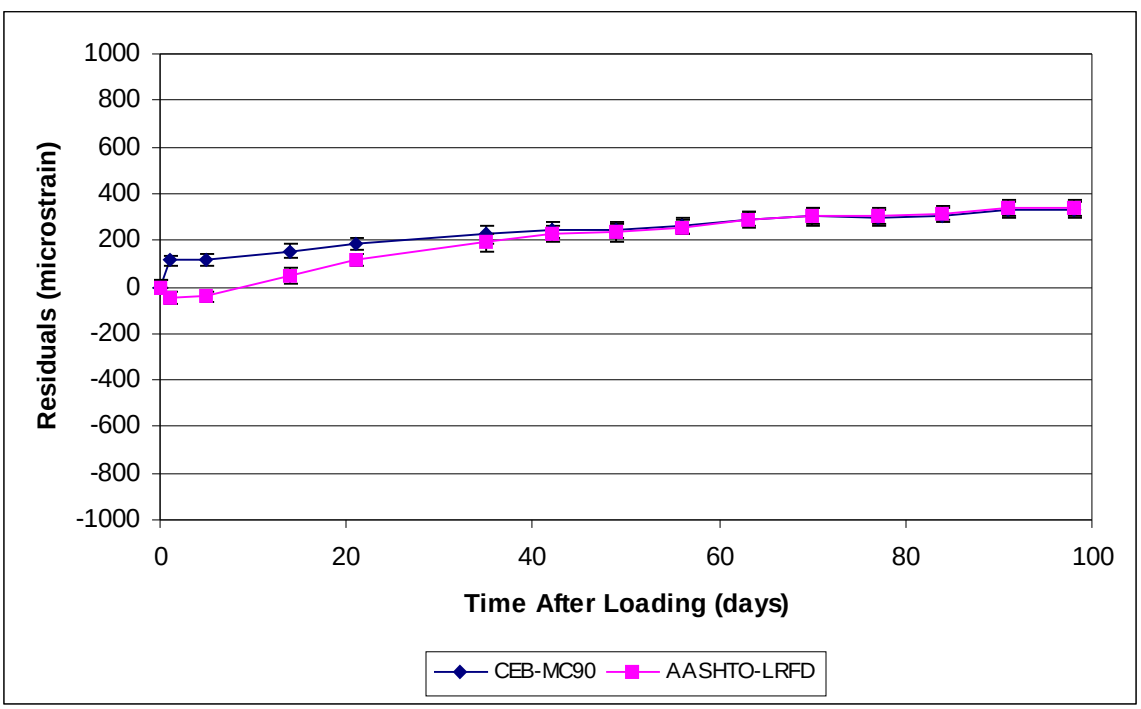

Figure 39 CEB-MC90 and AASHTO-LRFD Standard Cure Total Strain Residuals

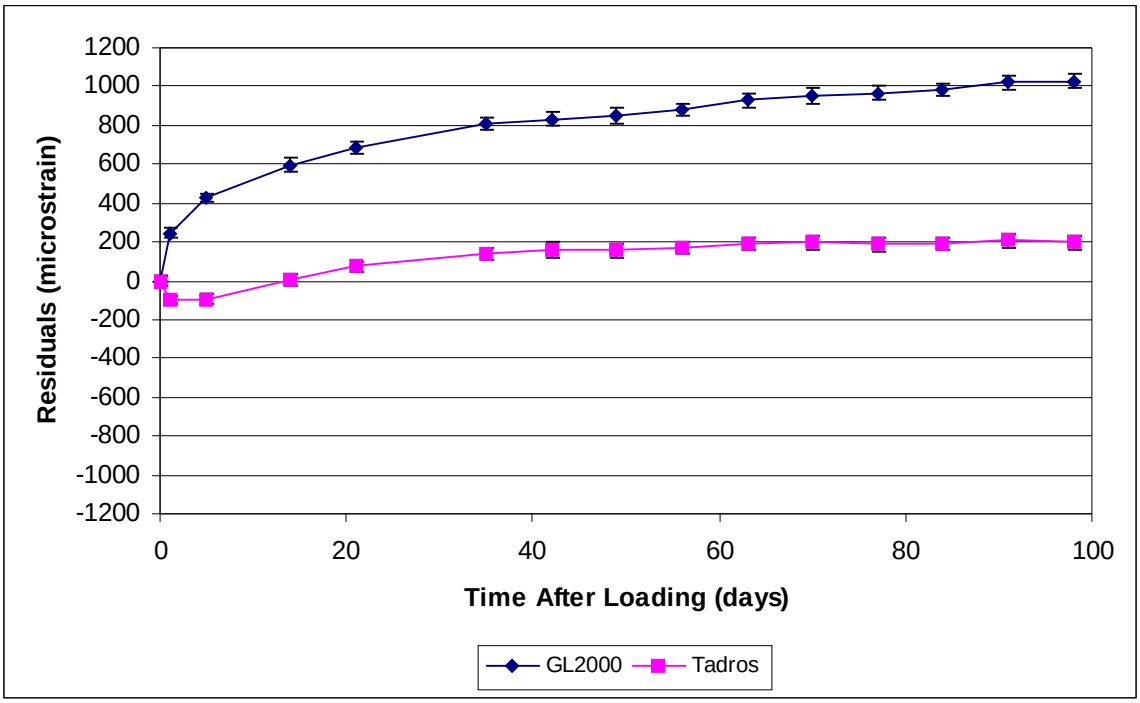

Figure 40 GL2000 and Tadros Standard Cure Total Strain Residuals

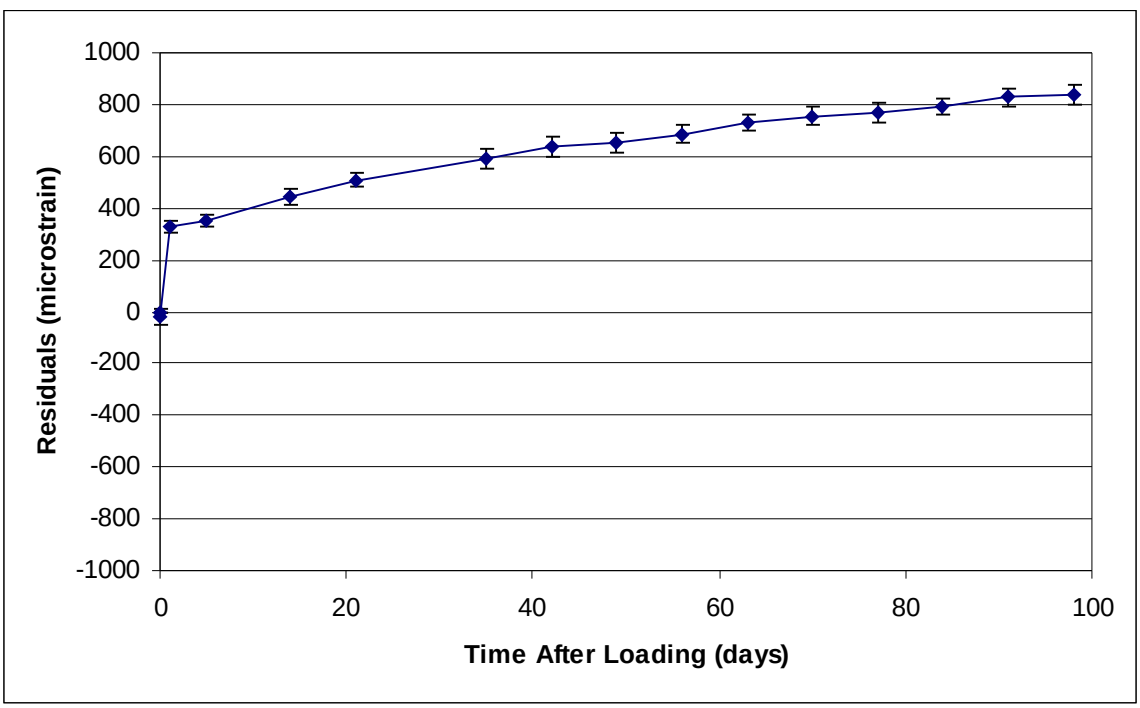

Figure 41 B3 Standard Cure Total Strain Residuals

4.7.5 Standard Cure Shrinkage Residuals

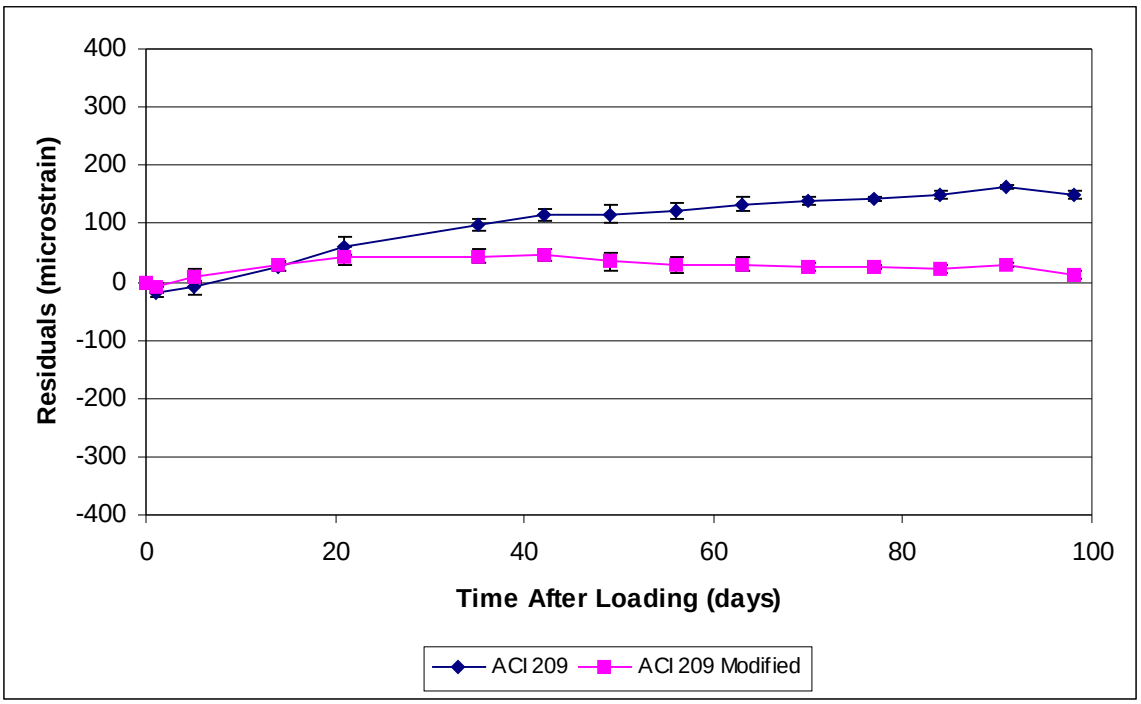

Figure 42 ACI 209 and ACI 209 Modified Standard Cure Shrinkage Residuals

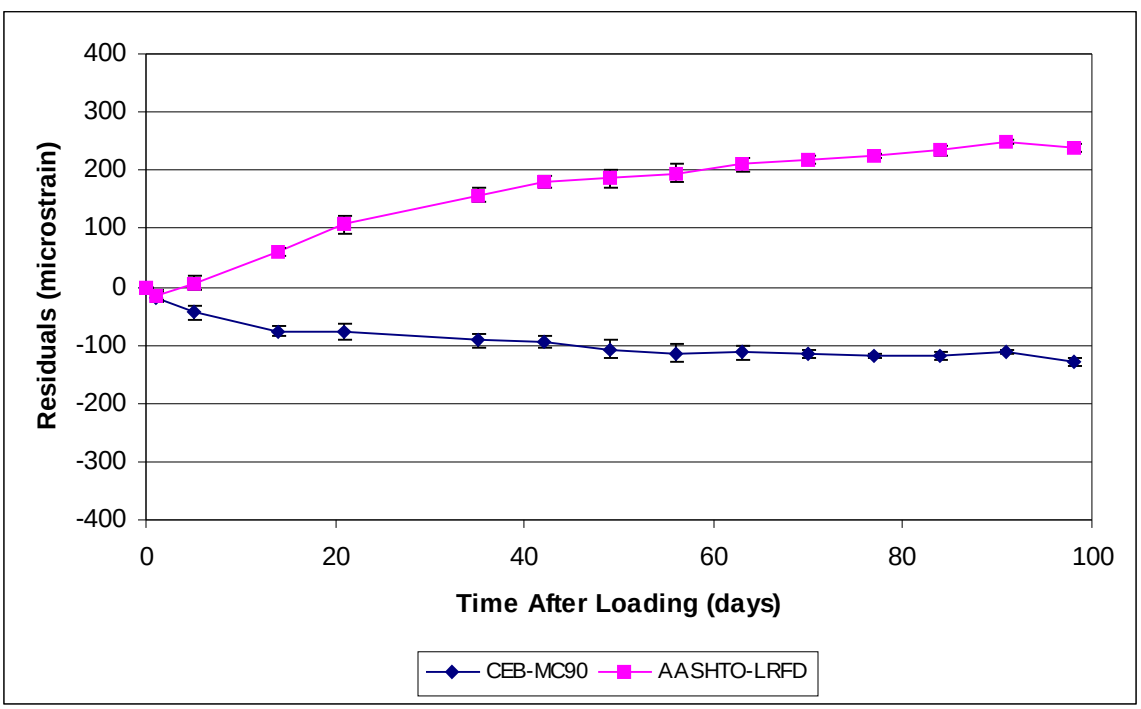

Figure 43 CEB-MC90 and AASHTO-LRFD Standard Cure Shrinkage Residuals

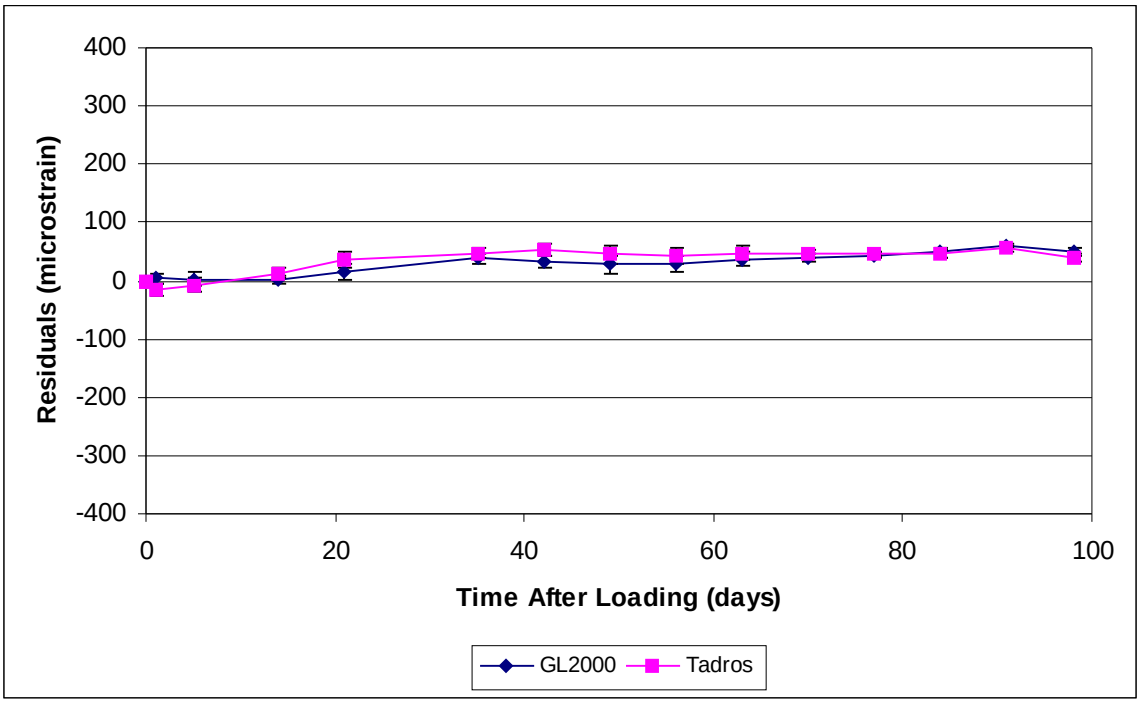

Figure 44 GL2000 and Tadros Standard Cure Shrinkage Residuals

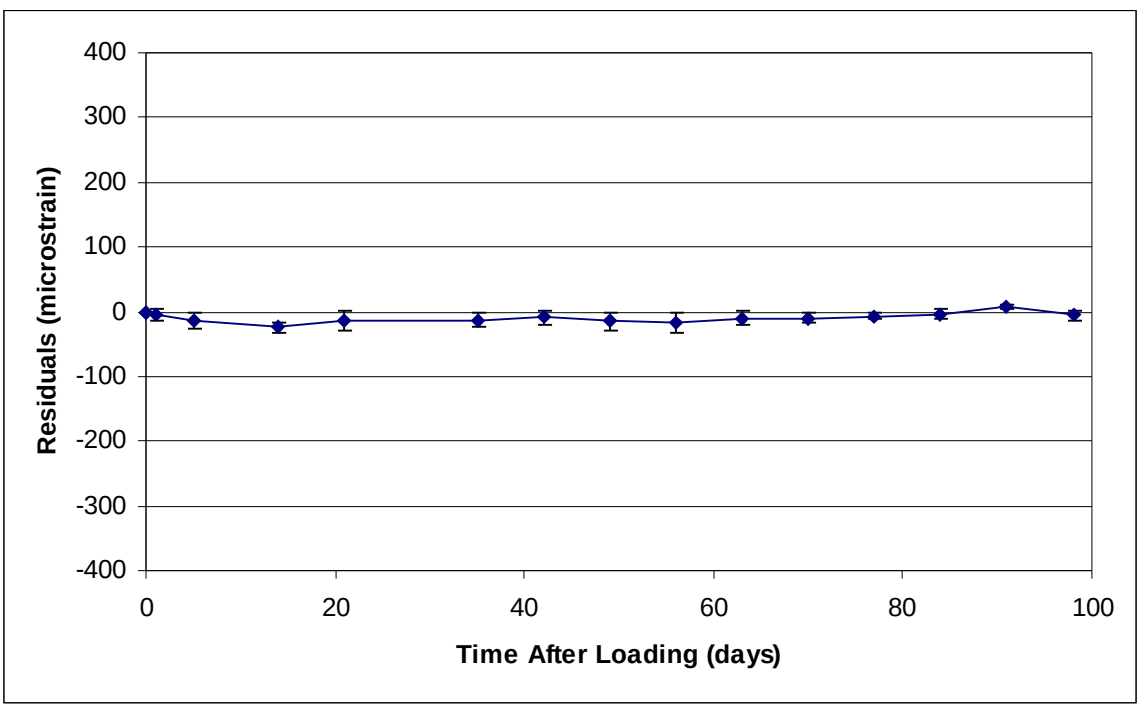

Figure 45 B3 Standard Cure Shrinkage Residuals

4.7.6 Standard Cure Creep Residuals

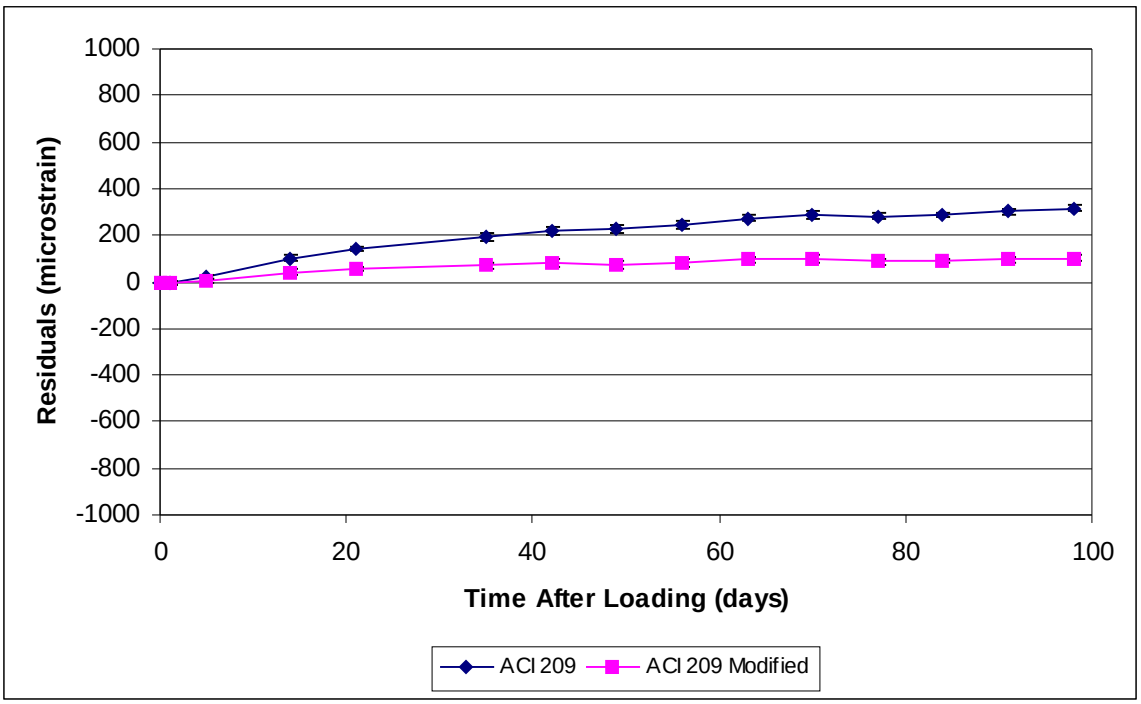

Figure 46 ACI 209 and ACI 209 Modified Standard Cure Creep Residuals

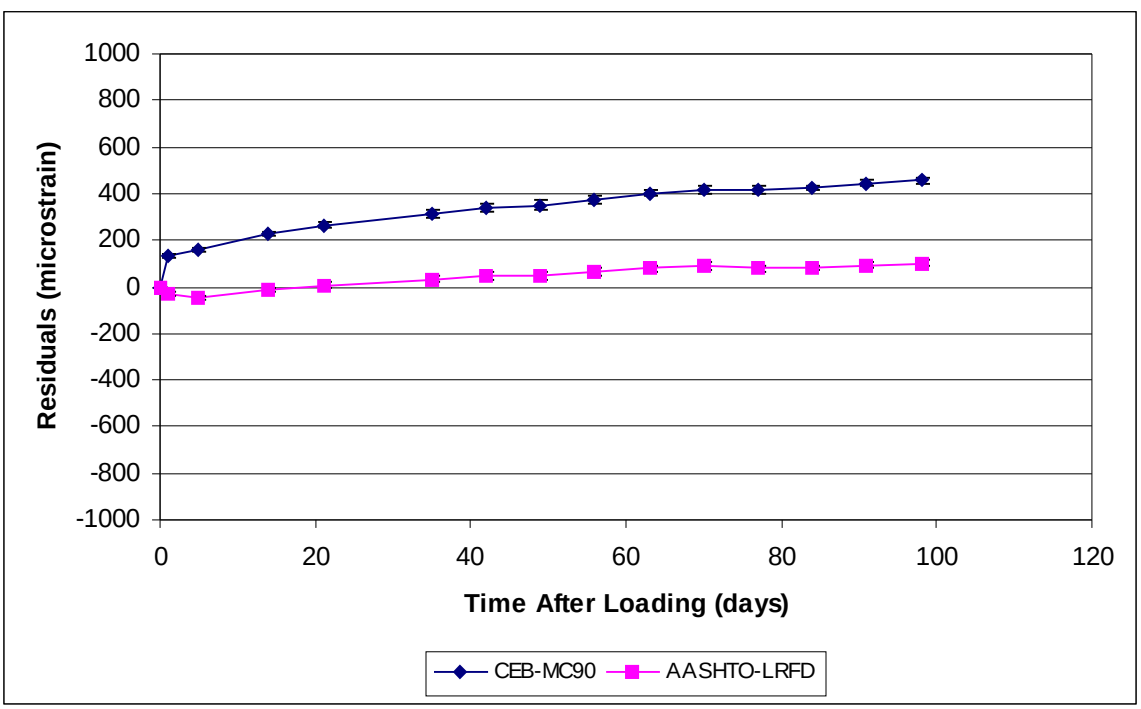

Figure 47 CEB-MC90 and AASHTO-LRFD Standard Cure Creep Residuals

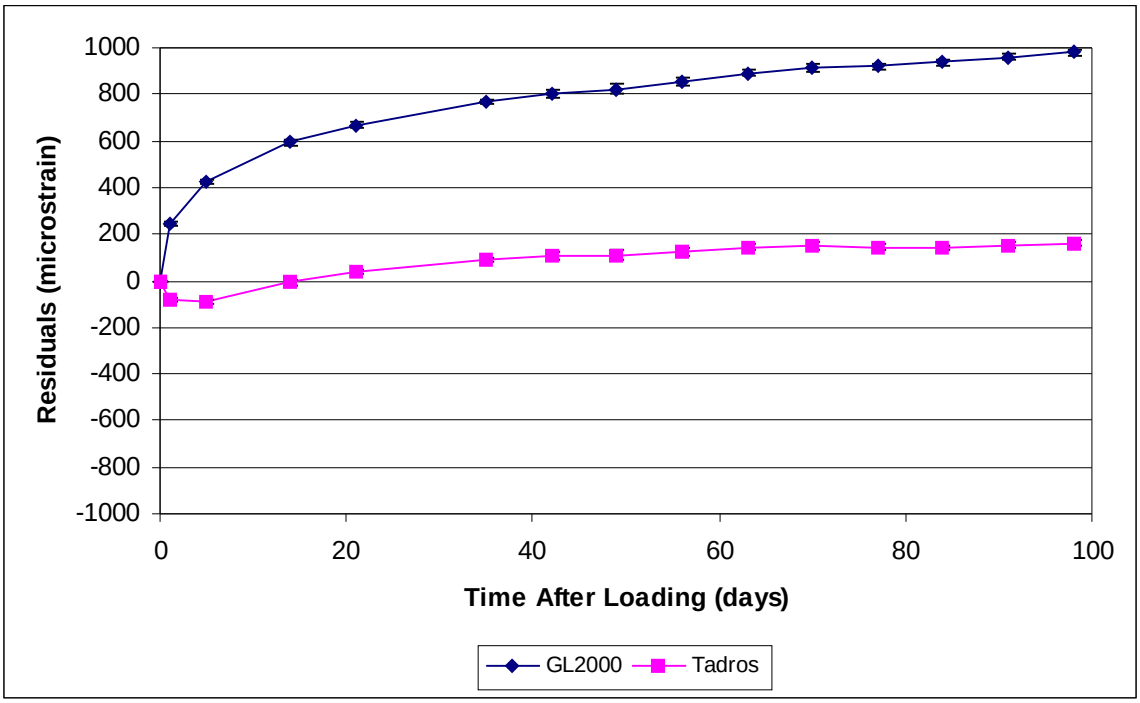

Figure 48 GL2000 and Tadros Standard Cure Creep Residuals

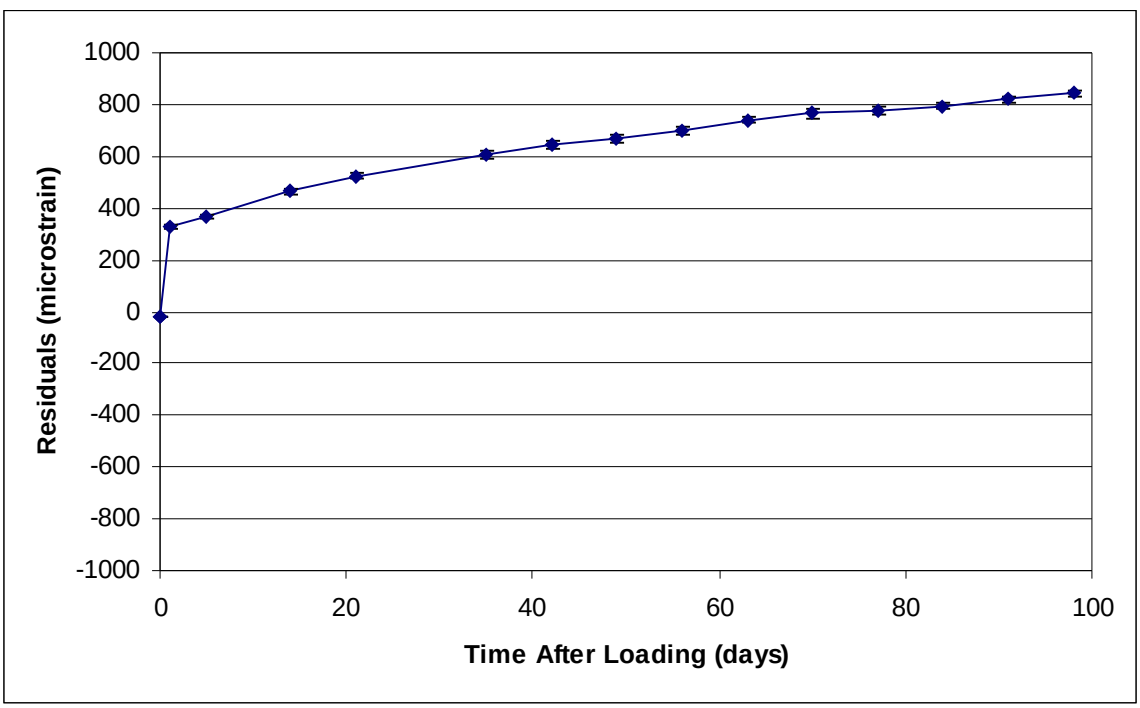

Figure 49 B3 Standard Cure Creep Residuals

4.8 Shrinkage Prisms

Figures 50 through 53 present the results of shrinkage prism testing. The data from standard cure batches 3A and 4A were not significantly different, and thus were combined for comparison purposes. Three prisms were cast from each standard cure batch. The mean and 95% confidence interval of the six prisms are shown, along with the predicted values from the models. Shrinkage prism data is presented in terms of percent length change, which is equal to microstrain x 10^{-4}.

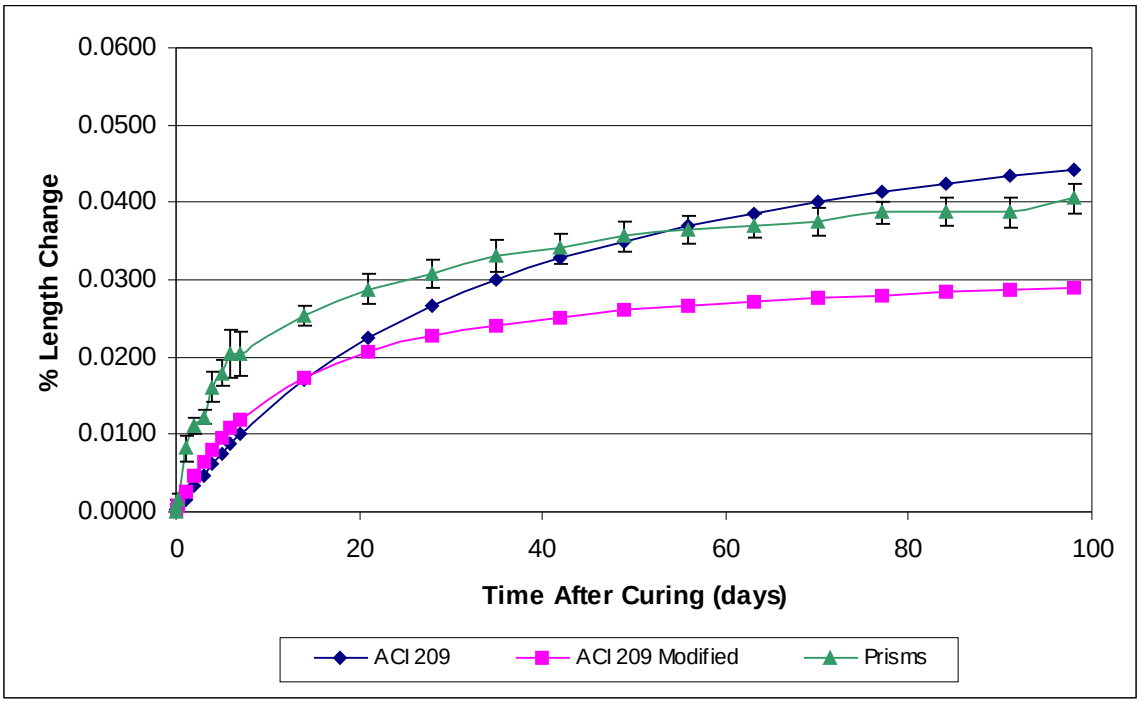

Figure 50 Shrinkage Prism Data with ACI 209 and ACI 209 Modified Models

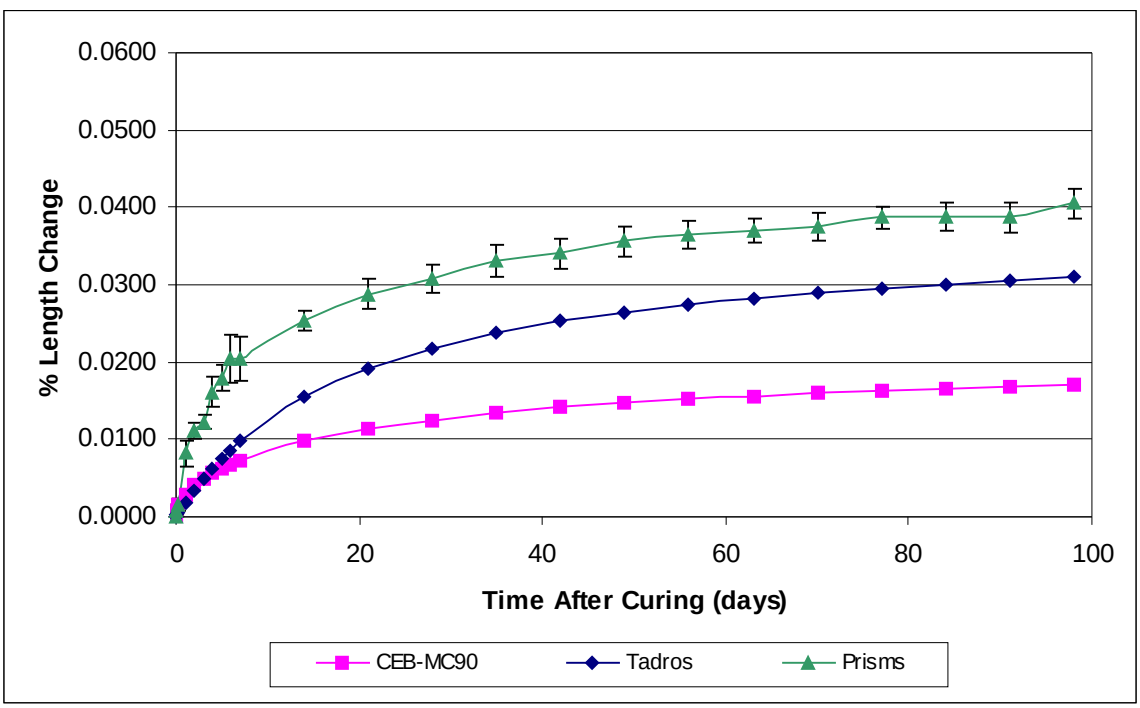

Figure 51 Shrinkage Prism Data with CEB-MC90 and Tadros Models

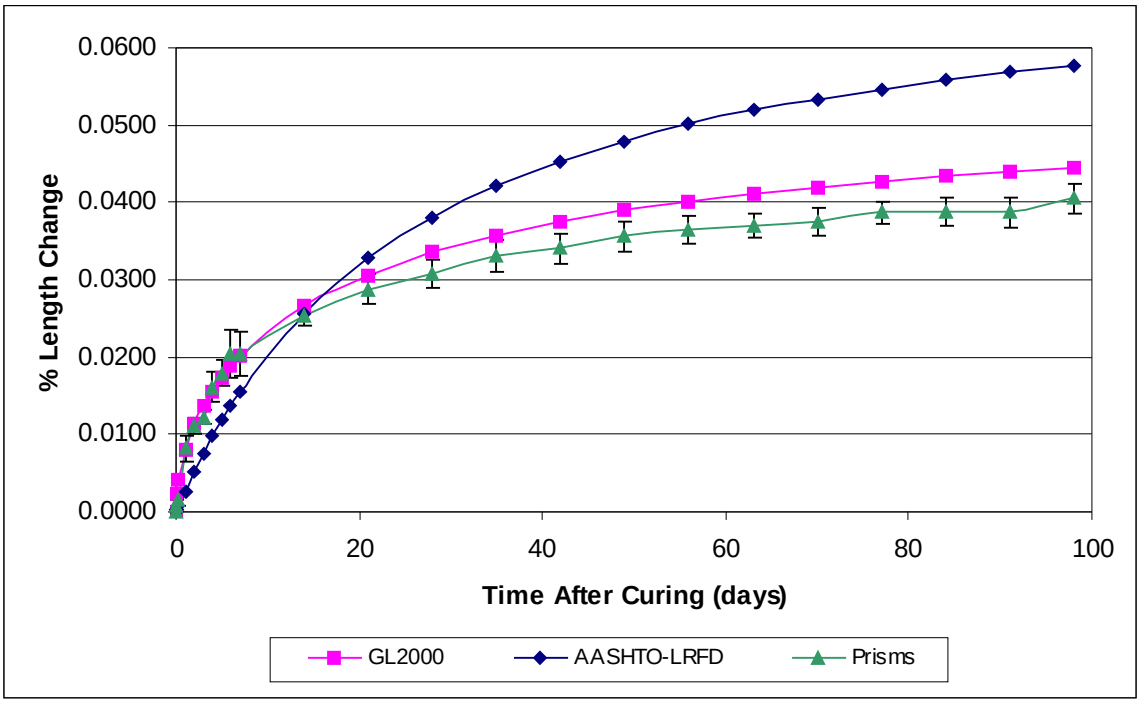

Figure 52 Shrinkage Prism Data with GL2000 and AASHTO-LRFD Models

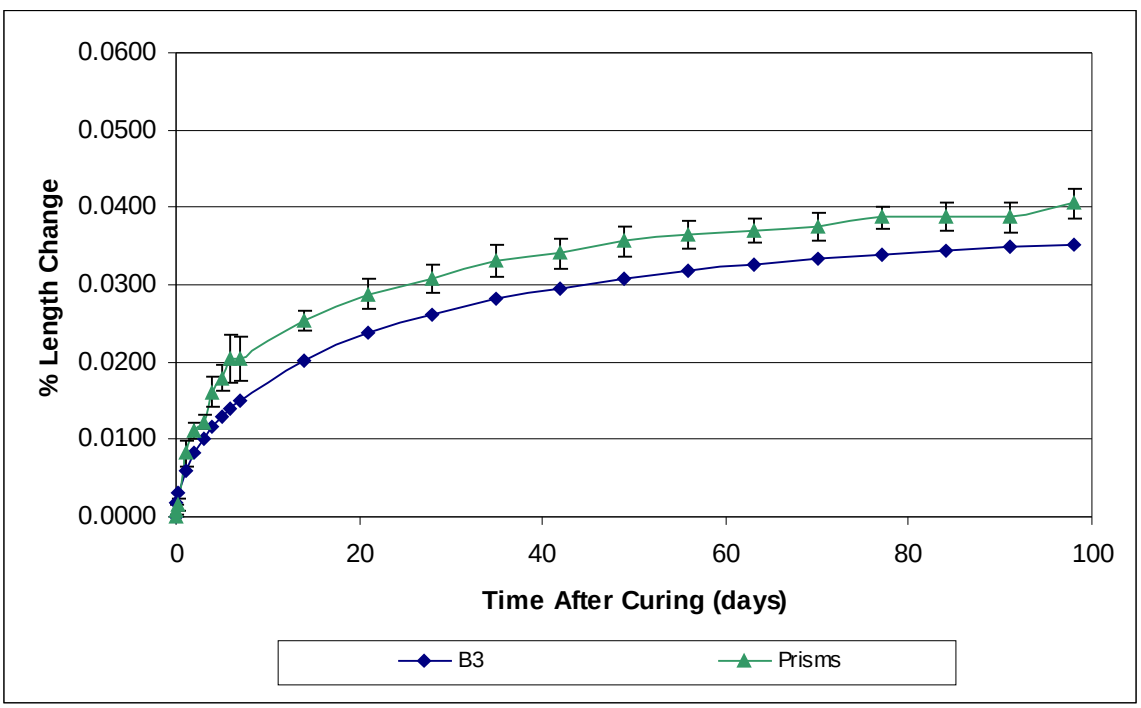

Figure 53 Shrinkage Prism Data with B3 Model

4.9 Vibrating Wire Gages

Figures 54 through 57 present strain measurements of the specimens from accelerated batch 2A that had the embedded vibrating wire gages (VWG). Both the Whittemore gage and VWG measurements are shown. Each Whittemore measurement is an average of measurements taken on two diametrically opposite sides of the cylinder. Cylinders 2A-2 and 2A-4 are loaded creep specimens, while cylinders 2A-6 and 2A-8 are unloaded shrinkage specimens.

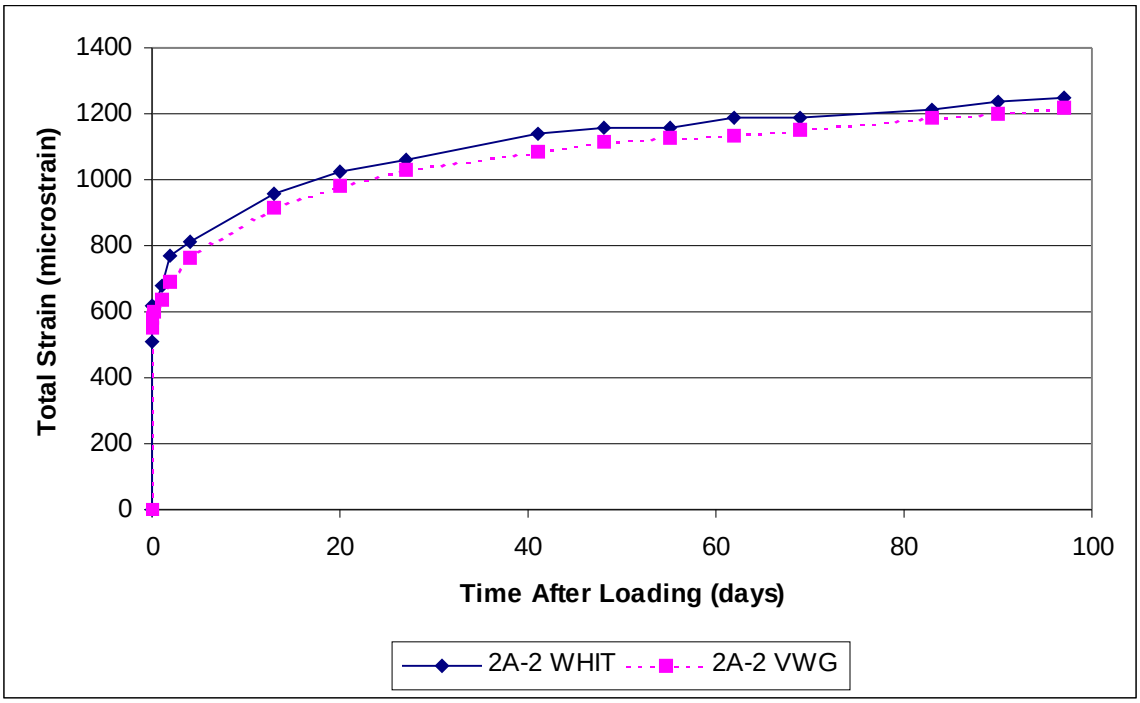

Figure 54 Cylinder 2A-2 Whittemore and VWG Total Strains

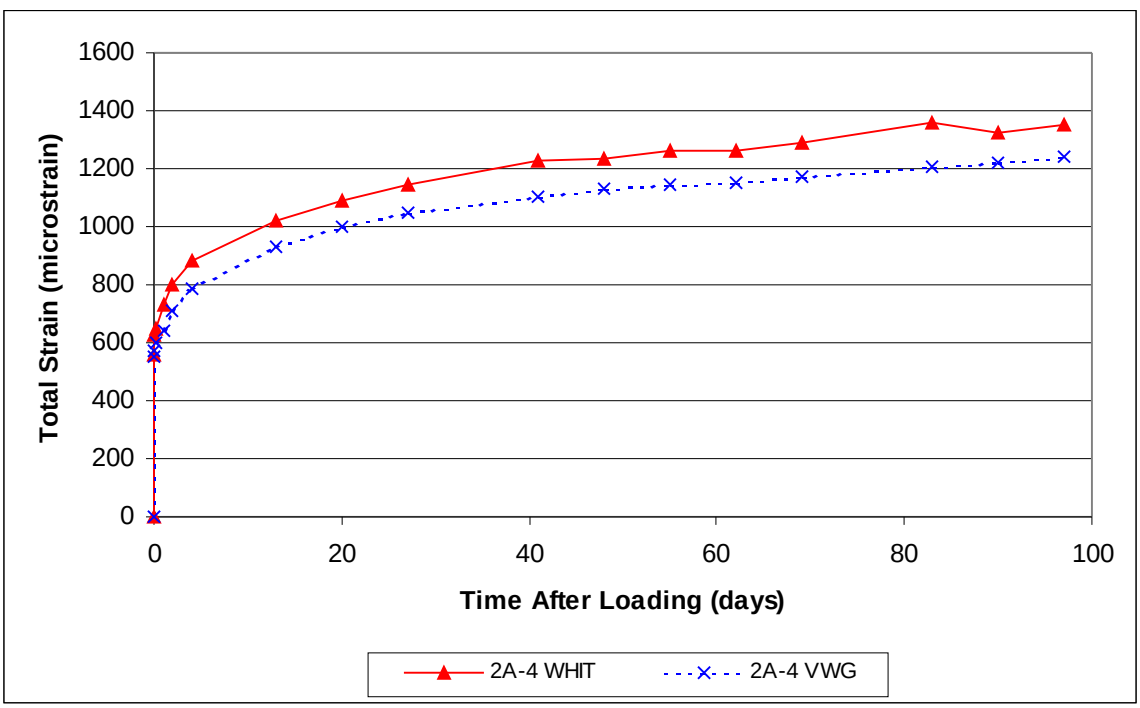

Figure 55 Cylinder 2A-4 Whittemore and VWG Total Strains

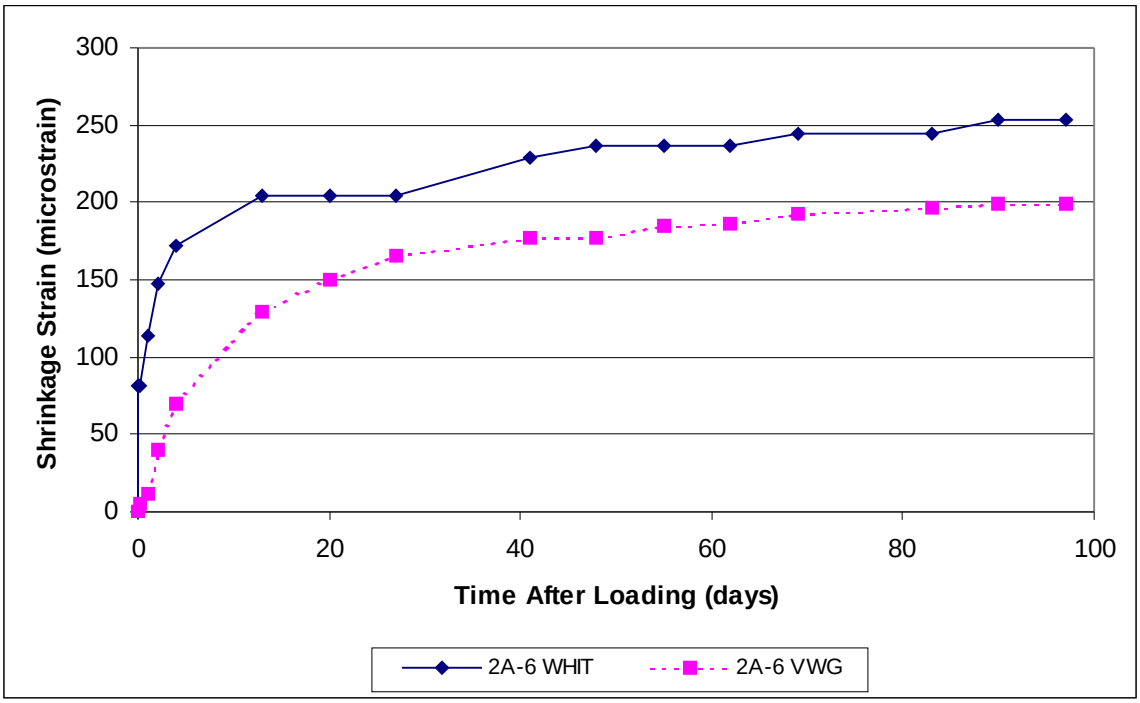

Figure 56 Cylinder 2A-6 Whittemore and VWG Shrinkage Strains

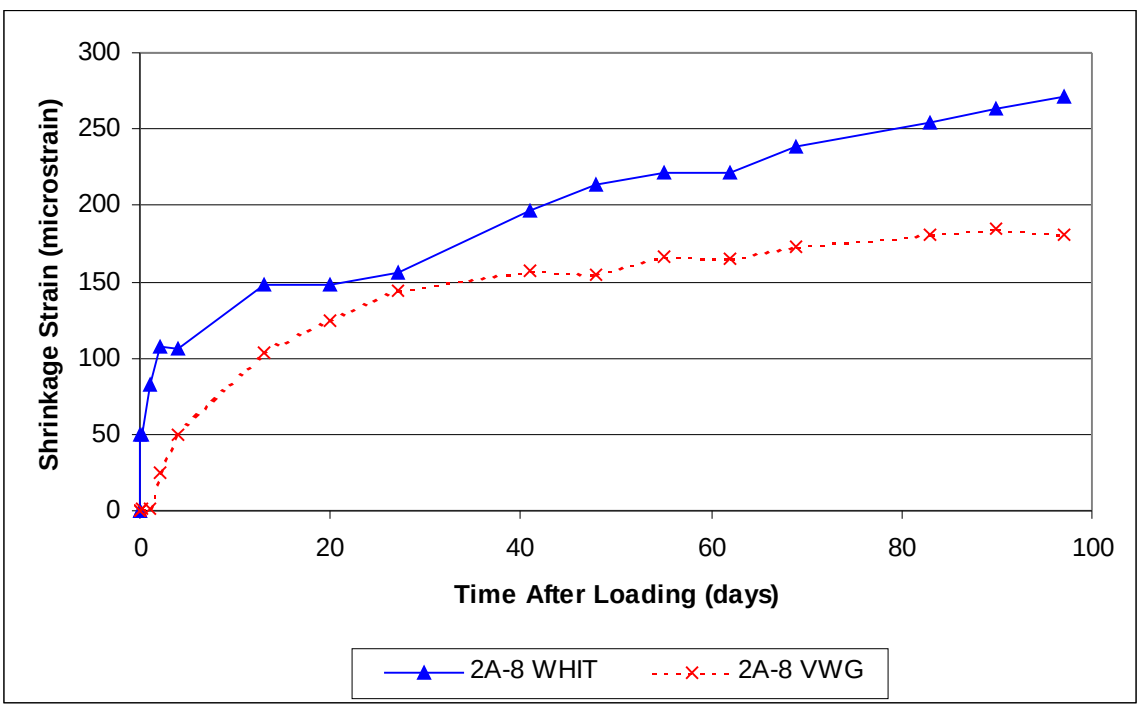

Figure 57 Cylinder 2A-8 Whittemore and VWG Shrinkage Strains

CHAPTER 5: DISCUSSION AND ANALYSIS

5.1 Introduction

This chapter discusses results of the HSC creep and shrinkage study. Compressive strength, tensile strength, modulus of elasticity, and thermal coefficient are discussed in Sections 5.2 through 5.5. Experimental and predicted strains are discussed in Section 5.6. Section 5.7 discusses experimental strain relationships, and Section 5.8 discusses experimental precision. The prediction model residuals, residuals squared analysis, and model rankings are presented in Sections 5.9 through 5.11.

5.2 Compressive Strength

ACI 214 defines laboratory control standards for compressive strength tests ranging from excellent to poor. A between-batch standard deviation of below 1.4 MPa (200 psi) is considered excellent, and above 2.4 MPa (350 psi) is considered poor. The ranges for very good, good, and fair control are in between these values at 1.0 MPa (150 psi) intervals.[7] In general, the compressive strength results for this study met the requirements for acceptable control.

Accelerated cure compressive strength results were presented in Figure 1. The between-batch standard deviation falls in the "excellent" category at 7, 56, and 90 days, and the "fair" category at 28 days.

Standard cure compressive strength results were presented in Figure 2. The between-batch standard deviation at 7 days was 2.7 MPa (400 psi), which indicates poor control. The 28- and 56-day results were in the "excellent" range, and the 90-day results were in the "good" range.

For all four batches, the 90-day compressive strengths were lower than the 56-day strengths. The acceptable laboratory within-batch coefficient of variation from ACI 214 is 5.0 percent.[7] The accelerated cure coefficients of variation between the 56- and 90-day results are under 5.0 percent for each batch, which indicates that the difference is within the expected variability of the compressive strength test. However, the coefficients of variation between the standard cure results at these ages exceed the specified limit. Each standard cure batch had one cylinder

strength at 90 days that was significantly less than the other three cylinders at 56 and 90 days. Neglecting the two outlying results, the within-batch coefficients of variation for standard cure batches 3A and 4A are less than 2.0 percent at 56 and 90 days.

The average seven-day strengths for the two curing methods were similar, but the standard cure batches had significantly higher strength gain with time. This is because the accelerated curing procedure consumes more water and creates a more porous hydrated cement matrix than standard curing. The standard cure specimens contained more excess water after curing, which allowed for continued hydration and thus densification of the cement matrix. The use of accelerated curing allows for rapid initial strength gain, but significantly decreases the potential for continued strength gain after curing.

As seen in Figure 1, the Bayshore compressive strengths were 30 percent lower than the laboratory accelerated cure strengths. This disparity is due in part to differences in the amounts of water in the concrete mixtures. The aggregate for the laboratory mixtures was dried before mixing, whereas the aggregate in Bayshore's mixtures was likely in SSD condition. Aggregate absorption was not accounted for in the laboratory mixtures, resulting in a w/cm ratio of 0.30. The w/cm ratio should have been 0.33 with the aggregate in SSD condition. According to charts found in "High Performance Concrete: Properties and Applications," a decrease in w/cm ratio from 0.33 to 0.30 would cause a compressive strength increase of at most 13.8 MPa (2000 psi), which is half of the observed strength difference.[3] The Bayshore concrete also had a higher air content than the laboratory mixtures (see table 3), but the differences in air content and w/cm ratio do not fully explain the strength differences. A possible explanation is that the Bayshore mixture contained more water than the amount specified in the mix design. The fact that the Bayshore mixture had a higher air content than the laboratory mixtures supports this explanation in that a higher water content increases fluidity and air content of a mixture.

5.3 Tensile Strength

Tensile strength results were presented in section 4.3. The tensile strengths greatly exceeded the AASHTO design values. On average, the end-of-cure tensile strengths equaled 9.8 percent of the end-of-cure compressive strengths. The 28-day tensile strengths equaled 8.5 percent of the 28-day compressive strengths on average. The ratio of tensile strength to compressive strength decreases as the compressive strength increases, which is an expected trend.[2]

5.4 Modulus of Elasticity

Accelerated cure modulus of elasticity results were presented in Figure 4. The AASHTO design modulus is based on the measured unit weight of the laboratory accelerated cure batches and the specified 28-day compressive strength of 55.2 MPa (8000 psi). As expected, the measured modulus results are higher than the AASHTO design value, since the measured compressive strengths are significantly higher than the specified strength. The accelerated cure modulus measurements did not increase with time. In some cases, the measured modulus decreased slightly over time, which suggests that some experimental error was involved.

Figure 58 presents the relationship between modulus of elasticity and compressive strength results for the accelerated cure and Bayshore specimens. With the exception of the 1-day results, the AASHTO design equation over predicts modulus of elasticity.

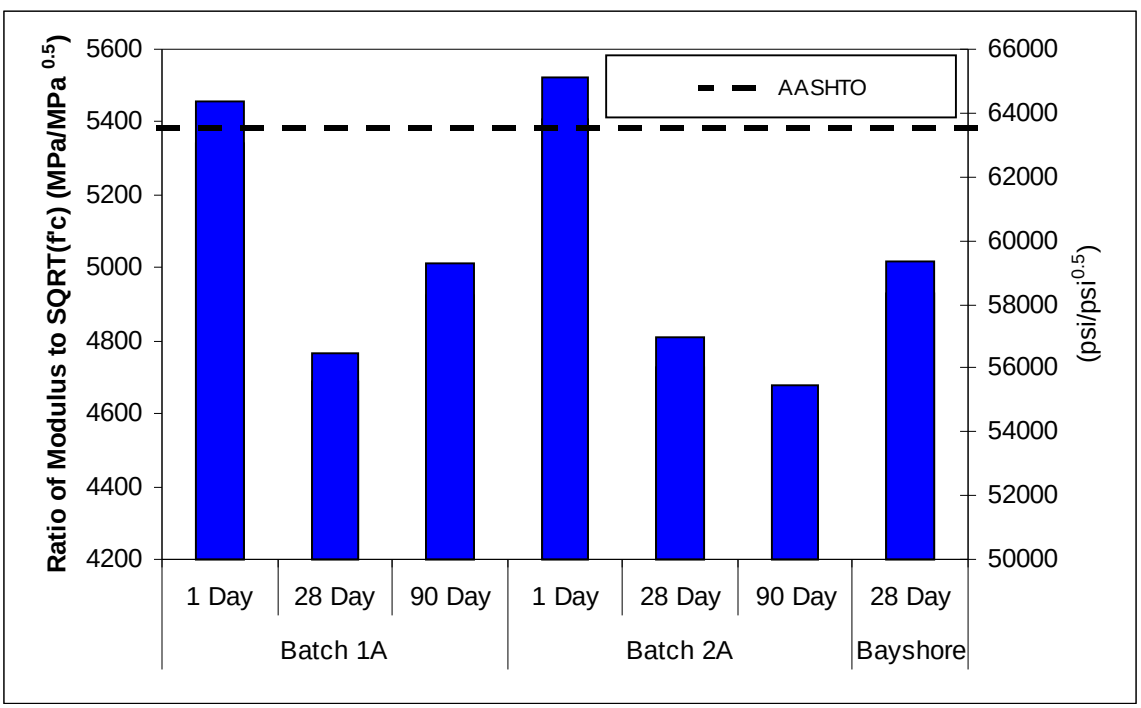

Figure 58 Accelerated Cure Ratio of Elastic Modulus to SQRT(f'_c)

Table 5 presents a comparison of modulus values predicted by three different equations and the measured values for each accelerated cure batch. These values are based on the measured unit weights and 28-day compressive strengths. The ACI 363 equation most accurately predicts modulus of elasticity for this mixture, while the other equations over predict the modulus. The three prediction equations are as follows:

AASHTO-LRFD:[14] $E_c = 33 w_c^{1.5} \sqrt{f'_c}$ (w in pcf, f'$_c$ in psi)

$E_c = 0.043 w_c^{1.5} \sqrt{f'_c}$ (kg/m^3, MPa)

ACI 363[1] Eqn. 5-1: $E_c = (w_c/0.145)^{1.5}(1000 + 1265\sqrt{f'_c})$ (kcf, ksi)

$E_c = (w_c/86)^{1.5}\left(6900 + 3320\sqrt{f'_c}\right)$ (kg/m^3, MPa)

Tadros[4] proposed: $E_c = 33000 K_1 K_2 (0.140 + \frac{f'_c}{1000})^{1.5} \sqrt{f'_c}$ (kcf, ksi)

$E_c = 0.043 k_1 k_2 \left(2240 + \frac{f'_c}{0.431}\right)^{1.5} \sqrt{f'_c}$ (kg/m^3, MPa)

where: K_1 = correction factor for location.

K_2 = correction factor for average, upper-bound, or lower-bound values.

Batch	Experimental	AASHTO-LRFD	ACI 363	Tadros
1A	44.6 (6500)	48.8 (7100)	41.6 (6000)	47.9 (6950)
2A	42.1 (6100)	48.8 (7100)	41.6 (6000)	47.9 (6950)

Table 5 Experimental and Predicted 28-Day Modulus of Elasticity, GPa (ksi)

Standard cure modulus of elasticity results were presented in Figure 5. The AASHTO design modulus was calculated based on the upper limit unit weight of 2484 kg/m^3 (155 pcf) because the equation is not valid for higher unit weights. The actual unit weight of the standard cure mixtures was 2549 kg/m^3 (159 pcf). Unlike the accelerated cure results, the modulus measurements increased significantly from 7 days to 28 days. This reflects continued hydration of the standard cure specimens, as discussed in Section 5.2.

Figure 59 presents the relationship between modulus of elasticity and compressive strength results for the standard cure specimens. The AASHTO design equation over predicts modulus of elasticity at all ages.

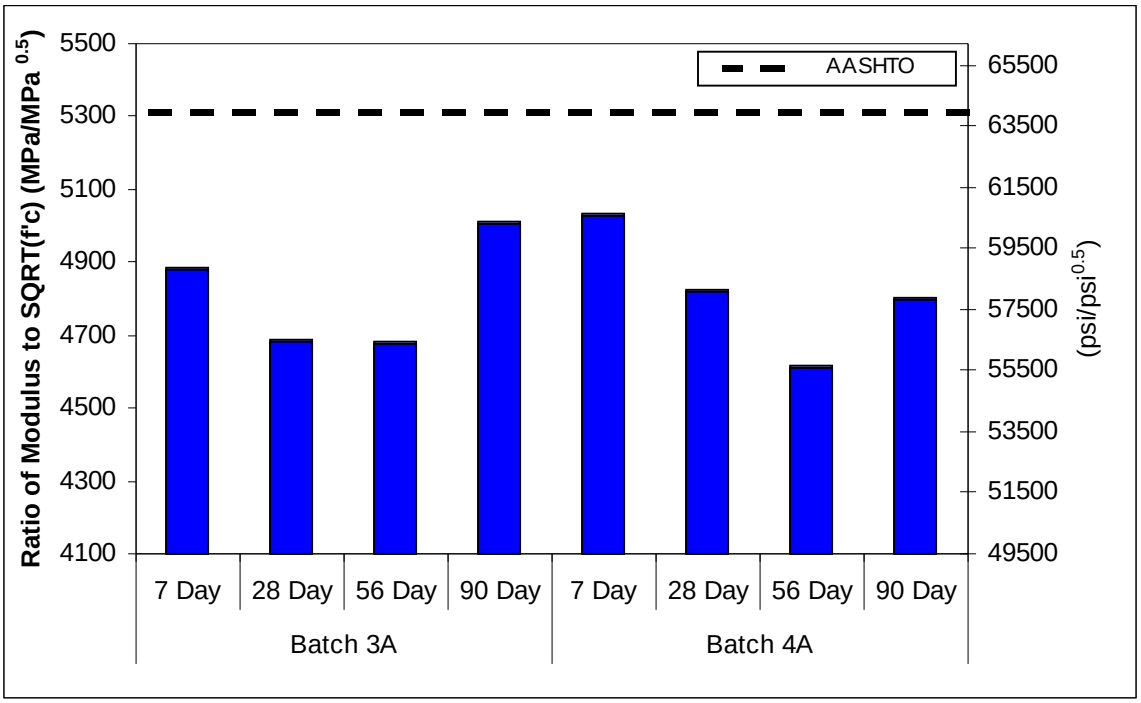

Figure 59 Standard Cure Ratio of Elastic Modulus to SQRT(f'_c)

The Bayshore modulus of elasticity was significantly lower than those of the laboratory accelerated cure batches. This is expected since the Bayshore compressive strengths were lower than the laboratory accelerated cure strengths. The Bayshore modulus was within one percent of the AASHTO design value, and thus is in agreement with the AASHTO design equation.

5.5 Thermal Coefficient

The coefficient of thermal expansion for the HSC mixture was found to be 4.6 ± 0.4 microstrain per °F (8.3 ± 0.7 microstrain per °C) at a 95 percent confidence level. This is within the range of 3.5 to 5 microstrain per °F (6.3 to 9.0 microstrain per °C) given by MacGregor.[2]

5.6 Experimental and Predicted Strains

The experimental total, shrinkage, and creep strain curves were presented in Figures 6 through 11. A noticeable difference is observed between the accelerated cure and standard cure curves in that the standard cure curves have much smaller 95 percent confidence intervals. This indicates that the accelerated cure batches had much more within-batch variation, which is likely a result of the following factors:

- Curing conditions. More variability is inherent with accelerated curing than standard curing. This is corroborated by Vincent's research.[5]
- Gage lengths. The standard cure specimens have a 203 mm (8 in.) gage length, while the accelerated cure gage length is 152 mm (6 in.). Equal length measurement errors result in 33 percent more strain variation for the smaller gage length than for the larger one.
- Learning error. The standard cure batches were tested last, so the standard cure results probably contain less measurement error than the accelerated cure results

Predicted strains from the prediction models were presented in Figures 12 through 25. The GL2000 and B3 models predict the largest creep strain and total strain, while the AASHTO-LRFD model predicts the largest shrinkage strain

5.7 Experimental Strain Relationships

Section 5.7.1 presents the relationship between accelerated cure and standard cure time-dependent strains. Section 5.7.2 presents the relationship between shrinkage strains of standard cure cylindrical specimens and prisms. Section 5.7.3 presents a comparison of field and laboratory data. These relationships are presented using equivalency charts, which plot two data sets that are paired based on time after loading. Section 5.7.4 discusses relationships between strains measured using a Whittemore gage and embedded vibrating wire gages.

5.7.1 Accelerated Cure vs. Standard Cure

Accelerated and standard cure specimens can be expected to behave differently over time because of differences in specimen size, curing method, and compressive strength. Larger specimens generally have less drying creep and shrinkage, especially early on, because it is more difficult for water to move from the center of the specimen to the outside surface. Accelerated curing forms larger hydration products than standard curing. As a result, standard cure specimens have a denser concrete matrix that is more resistant to water movement, thus reducing drying creep and shrinkage. As discussed in Section 5.2, the standard cure specimens had greater compressive strength gain with time than the accelerated cure specimens. As a result, the standard cure creep specimens were loaded to a smaller fraction of their compressive strength at later ages, since the applied stress was kept constant for both curing methods. The following figures do not include any adjustment factors for size or compressive strength. The accelerated cure and standard cure data sets are averages of eight and six specimens, respectively.

The relationship between average accelerated cure and standard cure total strains is presented in Figure 60. The two data sets are nearly equivalent early on, but the accelerated cure strains are higher at later ages.

The relationship between average accelerated cure and standard cure creep strains is presented in Figure 61. The accelerated cure creep strain is significantly higher at later ages. The smaller specimen size resulted in higher drying creep and shrinkage. In addition, the accelerated cure specimens had a less dense cement matrix and less strength gain with time.

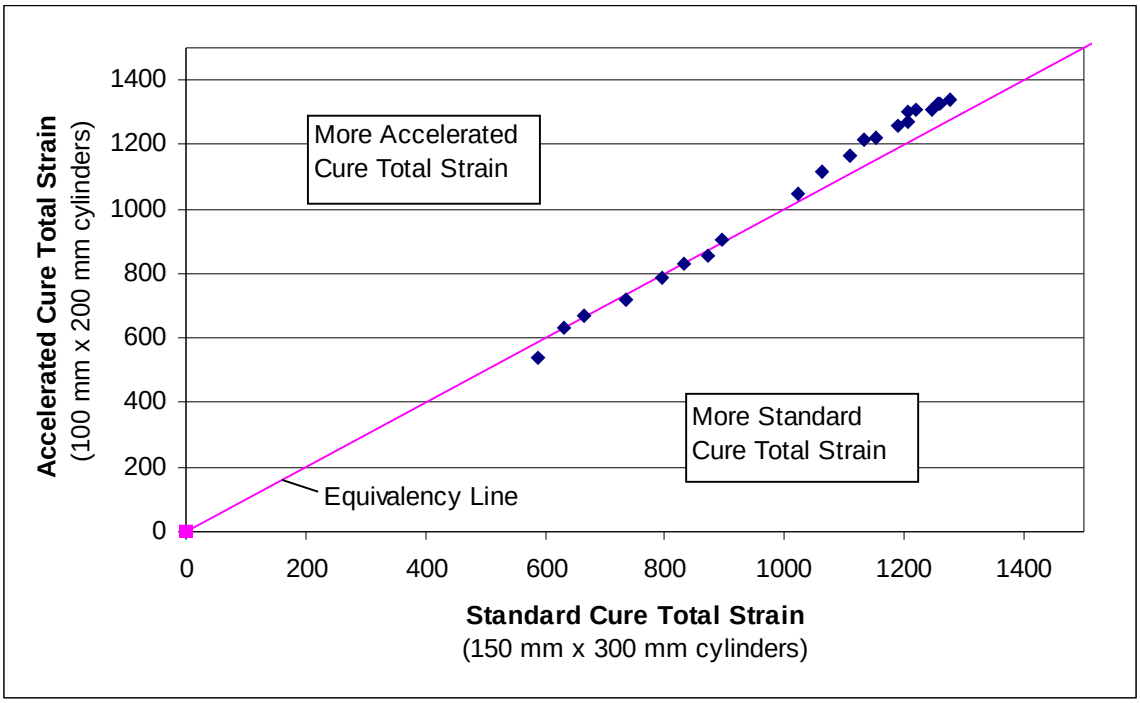

Figure 60 Accelerated Cure vs. Standard Cure Total Strain (microstrain)

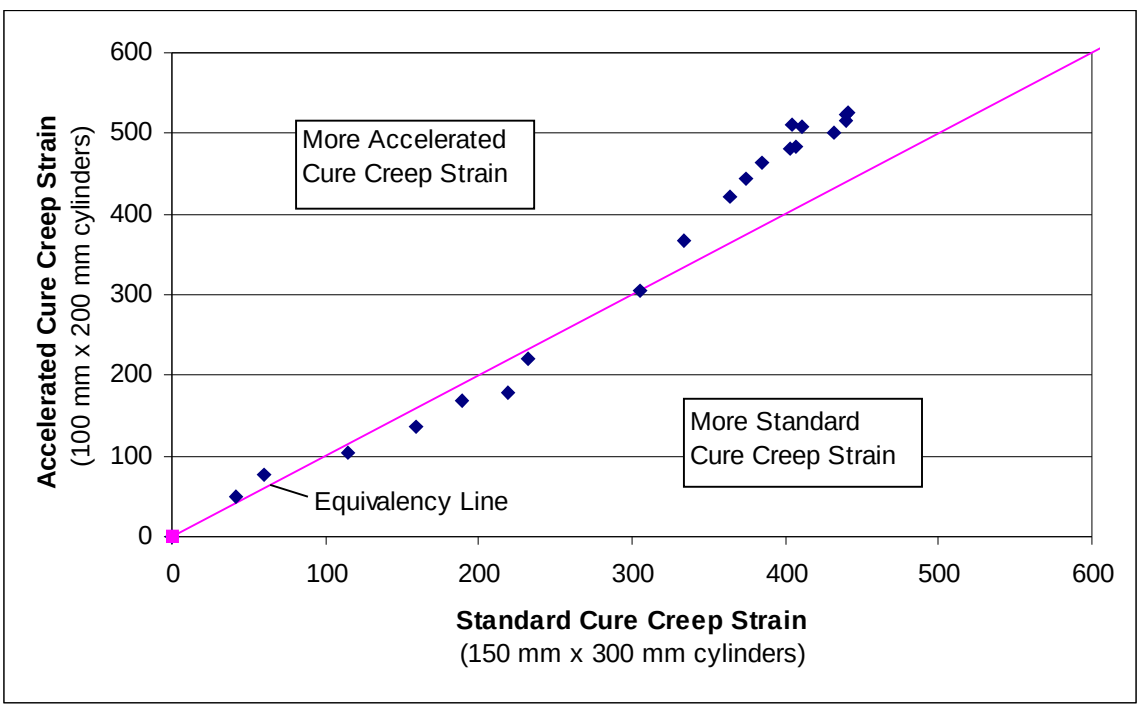

Figure 61 Accelerated Cure vs. Standard Cure Creep (microstrain)

The relationship between average accelerated cure and standard cure shrinkage strains is presented in Figure 62. Shrinkage strain is higher for the accelerated cure specimens due to smaller specimen size and a less dense concrete matrix.

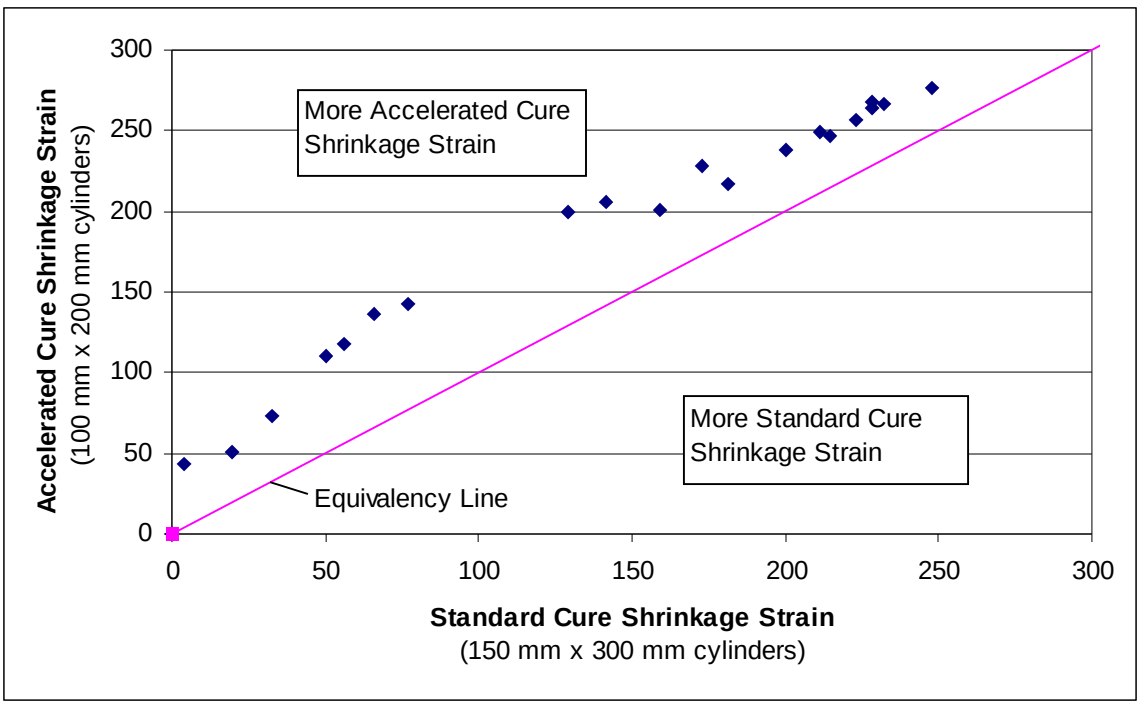

Figure 62 Accelerated Cure vs. Standard Cure Shrinkage (microstrain)

5.7.2 Shrinkage Prisms vs. Cylinders

Figure 63 presents the relationship between shrinkage strains of the 75 mm x 75 mm x 285 mm (3 in. x 3 in. x 11.25 in.) prisms and the 150 mm x 300 mm (6 in. x 12 in.) cylinders. No adjustment was made for specimen size. The prisms had significantly higher shrinkage strains, mainly due to the size difference. The prisms and cylinders had volume-to-exposed surface area ratios of 0.67 and 1.5, respectively.

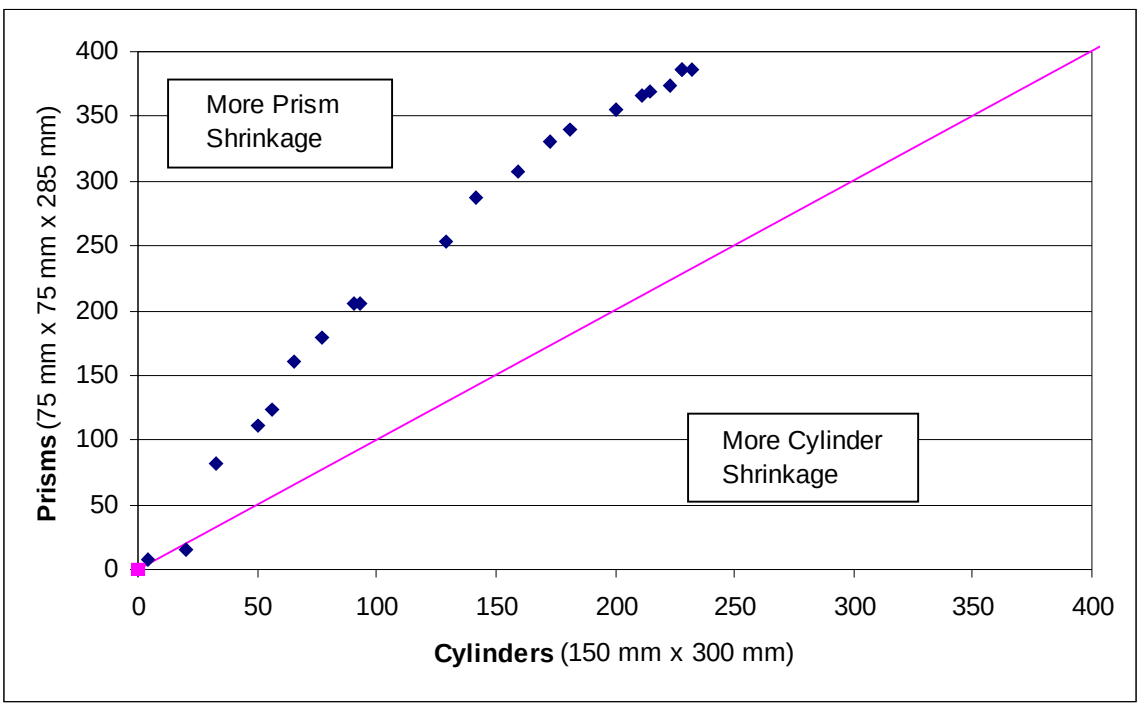

Figure 63 Prism vs. Cylinder Shrinkage Strain (microstrain)

5.7.3 Field vs. Laboratory

Figure 64 presents the relationship between time-dependent strains measured on test girders at Bayshore and those measured in the laboratory. The strain measurements are divided by applied stress, which is not a constant for the two data sets. The field stress is calculated as the initial elastic stress minus estimated prestress losses over time. The field data was obtained from Chris Waldron, and represents the average total strain at the center of prestressing for three test girders. [8] The laboratory data represents the average total strain of eight accelerated cure specimens. The data is not adjusted for parameters such as specimen size, compressive strength, and relative humidity.

The laboratory specimens had significantly higher time-dependent deformations than the test girders. This is to be expected due to the following factors:

- Size effects: The field measurements were taken in the center of a large girder, where drying creep and shrinkage are limited.
- Ambient conditions: The average relative humidity at Bayshore is over 70 percent, compared to the laboratory relative humidity of 50 percent. Relative humidity has a significant effect on drying creep and shrinkage.

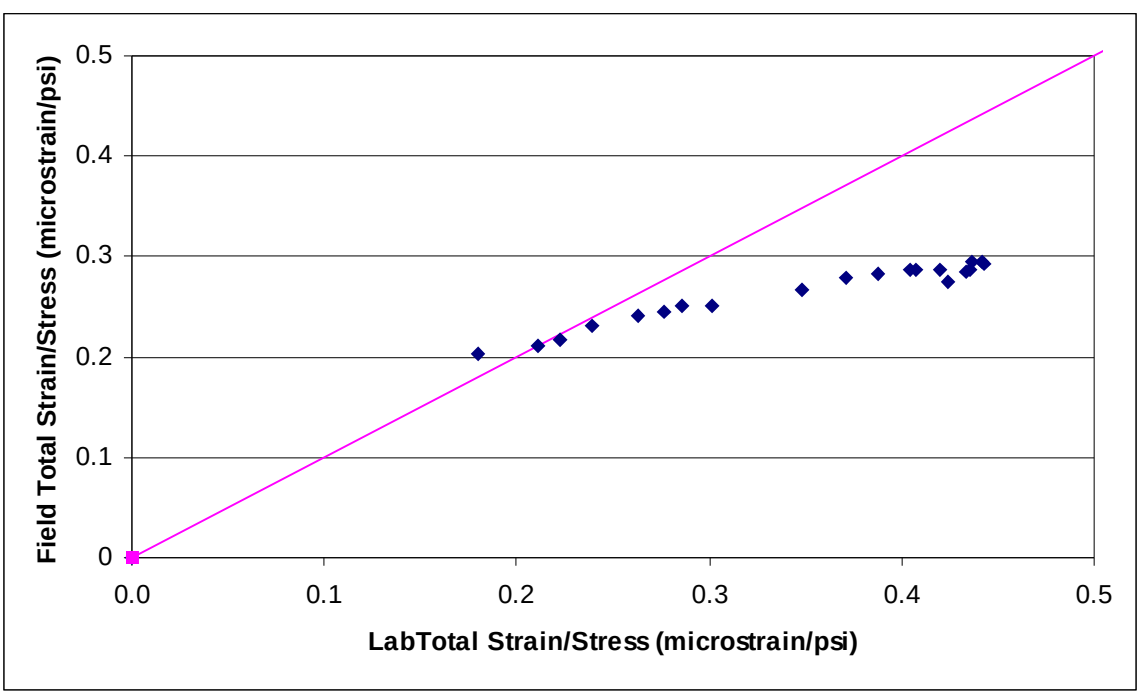

Figure 64 Field vs. Laboratory Accelerated Cure Total Strains

5.7.4 Vibrating Wire Gage vs. Whittemore Gage

Figures 54 through 57 presented strains measured using vibrating wire gages (VWG) and Whittemore gages. For the loaded specimens, there is a general agreement between the strains measured using the two methods, with the VWG strains slightly lower than the Whittemore strains. The unloaded specimens had significantly less VWG strain over time than Whittemore strain. These observations indicate that shrinkage strain is higher at the surface of the specimen than in the middle, but creep and elastic strains are similar at the two locations.

5.8 Experimental Precision

The ASTM Standards include limits on the amount of variability that is acceptable for different types of tests. For creep tests, ASTM specifies required precision in terms of coefficient of variation, which is equal to the standard deviation divided by the mean. According to ASTM C512, the within-batch and between-batch coefficients of variation for creep strains are 4% and 9%, respectively. To obtain the required precisions, these values are multiplied by the appropriate adjustment factors from ASTM C670, which depend on the number of samples being considered. The within-batch adjustment factors for 2, 3, and 4 samples are 2.8, 3.3, and 3.6, respectively.

5.8.1 Accelerated Cure

Table 6 compares the accelerated cure within-batch and between-batch experimental precisions to the required precisions. The within-batch required precision is based on four samples per batch. The experimental precision values represent the creep strains at 63 days after loading. The experimental precisions satisfy the ASTM C512 between-batch requirements, which justifies combining the two accelerated cure batches for comparison with the prediction models.

Table 7 presents experimental precision data at 7, 28, 56, and 63 days after loading. Within-batch (WB) variability decreases with time, which suggests that the measurement consistency improved during the test period. Between-batch (BB) variability increases with time, indicating that the two batches behaved more similarly at early ages than later ages.

Batch	Experimental	Required
1A	8.6%	14.4%
2A	12.3%	14.4%
1A/2A	11.5%	25.2%

Table 6 Accelerated Cure Creep Precision

Time After Loading (days)	Batch 1A Creep				WB Avg	WB Std Dev	WB CV	ASTM Limit CV
	1A-1	1A-2	1A-3	1A-4				
7	236	227	229	198	223	17	7.5%	14.4%
28	447	398	506	388	435	54	12.5%	
56	512	479	588	487	516	50	9.6%	
63	552	519	620	519	553	47	8.6%	

Time After Loading (days)	Batch 2A Creep				WB Avg	WB Std Dev	WB CV	ASTM Limit CV
	2A-1	2A-2	2A-3	2A-4				
7	287	163	289	140	220	79	36.1%	14.4%
28	451	348	495	337	408	77	19.0%	
56	466	408	520	403	449	55	12.3%	
63	508	442	528	403	470	58	12.3%	

Time After Loading (days)	WB Average		BB Avg	BB Std Dev	BB CV	ASTM Limit CV
	1A	2A				
7	223	220	221	2	0.9%	25.2%
28	435	408	421	19	4.5%	
56	516	449	483	47	9.8%	
63	553	470	511	59	11.5%	

Table 7 Accelerated Cure Creep Precision Over Time (microstrain)

5.8.2 Standard Cure

Table 8 presents the standard cure precision results. The within-batch required precision is based on three samples per batch. The experimental precision values represent the creep strains at 63 days after loading. The experimental precisions satisfy the ASTM C512 between-batch requirements, which justifies combining the two accelerated cure batches for comparison with the prediction models.

Table 9 presents experimental precision data at 7, 28, 56, and 63 days after loading. Within-batch variability decreases with time for batch 3A, but slightly increases with time for batch 4A. Between-batch variability increases with time.

Batch	Experimental	Required
3A	2.5%	13.2%
4A	2.4%	13.2%
3A/4A	5.0%	25.2%

Table 8 Standard Cure Creep Precision

Time After Loading (days)	Batch 3A Creep			WB Avg	WB Std Dev	WB CV	ASTM Limit CV
	3A-1	3A-2	3A-3				
7	269	256	238	254	16	6.3%	13.2%
28	376	369	344	363	17	4.6%	
56	401	382	388	390	10	2.6%	
63	401	382	388	390	10	2.6%	

Time After Loading (days)	Batch 4A Creep			WB Avg	WB Std Dev	WB CV	ASTM Limit CV
	3A-1	3A-2	3A-3				
7	263	256	256	258	4	1.5%	13.2%
28	369	368	356	365	7	2.0%	
56	413	424	437	425	12	2.8%	
63	407	424	425	419	10	2.4%	

Time After Loading (days)	WB Average		BB Avg	BB Std Dev	BB CV	ASTM Limit CV
	3A	3A				
7	254	258	256	3	1.1%	25.2%
28	363	365	364	1	0.3%	
56	390	425	408	25	6.1%	
63	390	419	404	20	5.0%	

Table 9 Standard Cure Creep Precision Over Time (microstrain)

5.9 Prediction Model Residuals

Total strain, creep, and shrinkage residuals for each prediction model were presented in Figures 26 through 49. In general, the models over predict time-dependent deformations, suggesting that the models are conservative for HSC mixtures.

Tables 10 and 11 summarize the accelerated cure and standard cure residuals, respectively. The models are identified as over predicting or under predicting. Models that have residuals of zero within the 95% confidence limits are identified with parentheses (). Models with residuals that cannot be distinguished as positive or negative are described as "good."

5.9.1 Accelerated Cure Residuals

The ACI 209 Modified and Tadros models predicted all time-dependent strains within the 95% confidence limits. All of the models were over predicting, except that CEB-MC90 and B3 under-predicted shrinkage strains.

	Total Strain	Creep	Shrinkage
ACI 209	Over predicting	Over predicting	Over predicting
ACI 209 Modified	(Over predicting)	(Over predicting)	(Over predicting)
CEB MC-90	Over predicting	Over predicting	Under predicting
AASHTO-LRFD	Over predicting	(Over predicting)	Over predicting
GL2000	Over predicting	Over predicting	Over predicting
Tadros	(Over predicting)	(Over predicting)	(Over predicting)
B3	Over predicting	Over predicting	Under predicting

Table 10 Accelerated Cure Residuals Summary

5.9.2 Standard Cure Residuals

For the standard cure batches, time-dependent deformations were over predicted in all cases, with the exceptions that the CEB MC-90 and B3 models under predicted shrinkage strain. Because the standard cure variability was less than the accelerated cure variability, it was less likely that the predicted strains would fall in the experimental 95% confidence limits.

	Total Strain	Creep	Shrinkage
ACI 209	Over predicting	Over predicting	Over predicting
ACI 209 Modified	Over predicting	Over predicting	Over predicting
CEB MC-90	Over predicting	Over predicting	Under predicting
AASHTO-LRFD	Over predicting	Over predicting	Over predicting
GL2000	Over predicting	Over predicting	Over predicting
Tadros	Over predicting	Over predicting	Over predicting
B3	Over predicting	Over predicting	(Under predicting)

Table 11 Standard Cure Residuals Summary

5.10 Residuals Squared Analysis

A residuals squared analysis of the total strain, creep, and shrinkage data was performed to determine which prediction model was the most accurate. The following formula illustrates the procedure used to calculate the sum of residuals squared test statistic.

$$\text{Sum of Residuals Squared} = \sum_{t=t_i}^{t_f} \left[(\text{Re}_t)^2 \right]$$

Where: t = time after loading

t_i = initial time considered

t_f = final time considered

Re_t = Residual at time t

For example, if the sum of residuals squared is computed between 0 and 100 days after loading, then $t_i = 0$ and $t_f = 100$. By squaring the residual, this analysis method prevents negative and positive residuals from canceling each other out. The model with the lowest sum of residuals squared is the most accurate predictor.

5.10.1 Accelerated Cure Residuals Squared

Figures 65 through 67 present the sum of residuals squared for accelerated cure total strain, creep, and shrinkage. The values are plotted on a logarithmic scale because of the large range of magnitudes of the test statistic. The orders of prediction accuracy are listed with the best predictor first.

From Figure 65, the order of total strain accuracy is ACI 209 Modified, Tadros, AASHTO-LRFD, ACI 209, CEB-MC90, B3, and GL2000.

From Figure 66, the order of creep strain accuracy is ACI 209 Modified, Tadros, AASHTO-LRFD, ACI 209, CEB-MC90, B3, and GL2000.

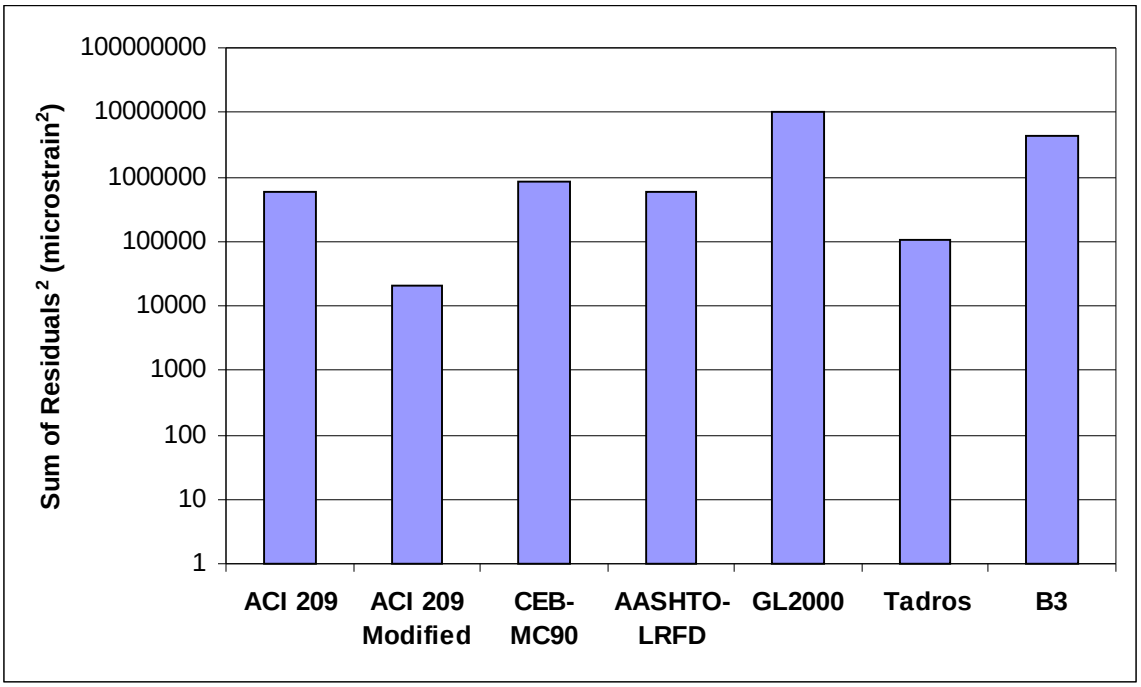

Figure 65 Accelerated Cure Total Strain Sum of Residuals Squared

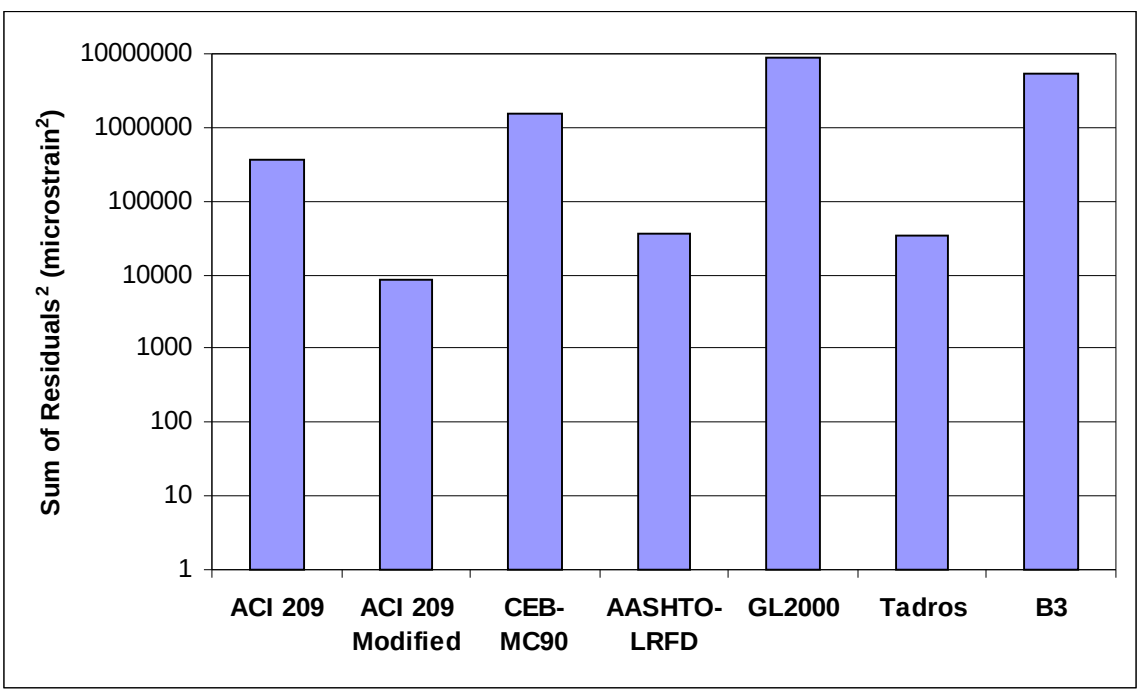

Figure 66 Accelerated Cure Creep Sum of Residuals Squared

From Figure 67, the order of shrinkage strain accuracy is ACI 209 Modified, Tadros, B3, ACI 209, GL2000, CEB-MC90, and AASHTO-LRFD

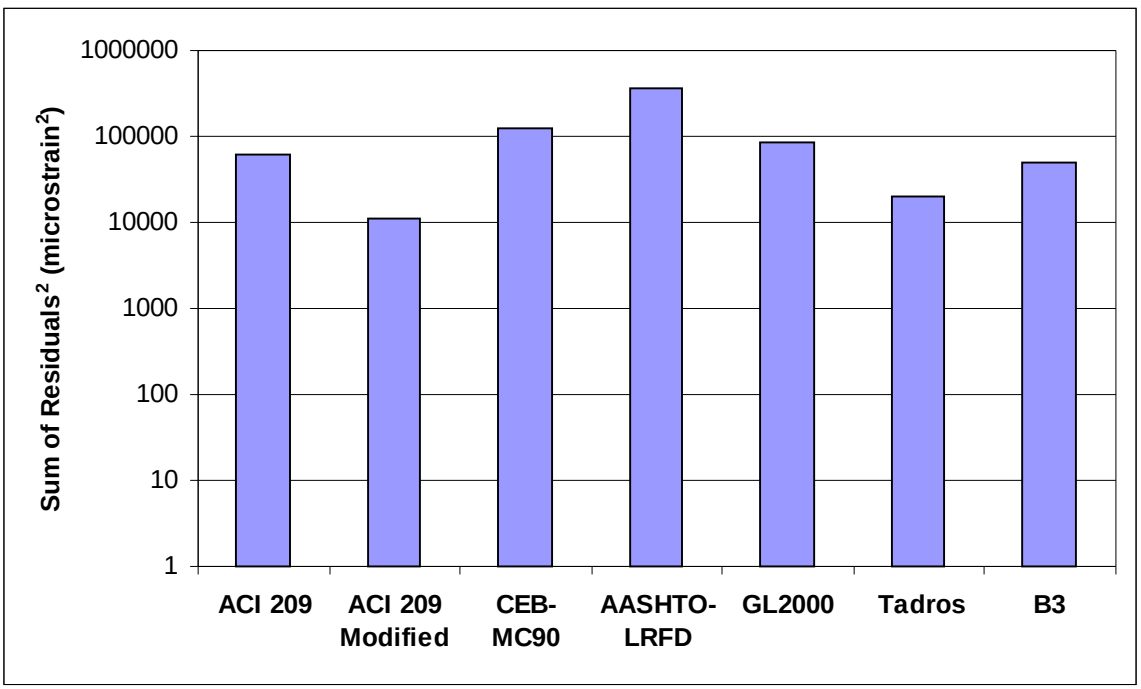

Figure 67 Accelerated Cure Shrinkage Sum of Residuals Squared

5.10.2 Standard Cure Residuals Squared

Figures 68 through 70 present the sum of residuals squared for standard cure total strain, creep, and shrinkage. The values are plotted on a logarithmic scale because of the large range of magnitudes of the test statistic. The orders of prediction accuracy are listed with the best predictor first.

From Figure 68, the order of total strain accuracy is ACI 209 Modified, Tadros, AASHTO-LRFD, CEB-MC90, ACI 209, B3, and GL2000.

From Figure 69, the order of creep strain accuracy is AASHTO-LRFD, ACI 209 Modified, Tadros, ACI 209, CEB-MC90, B3, and GL2000.

From Figure 70, the order of shrinkage strain accuracy is B3, ACI 209 Modified, GL2000, Tadros, CEB-MC90, ACI 209, and AASHTO-LRFD.

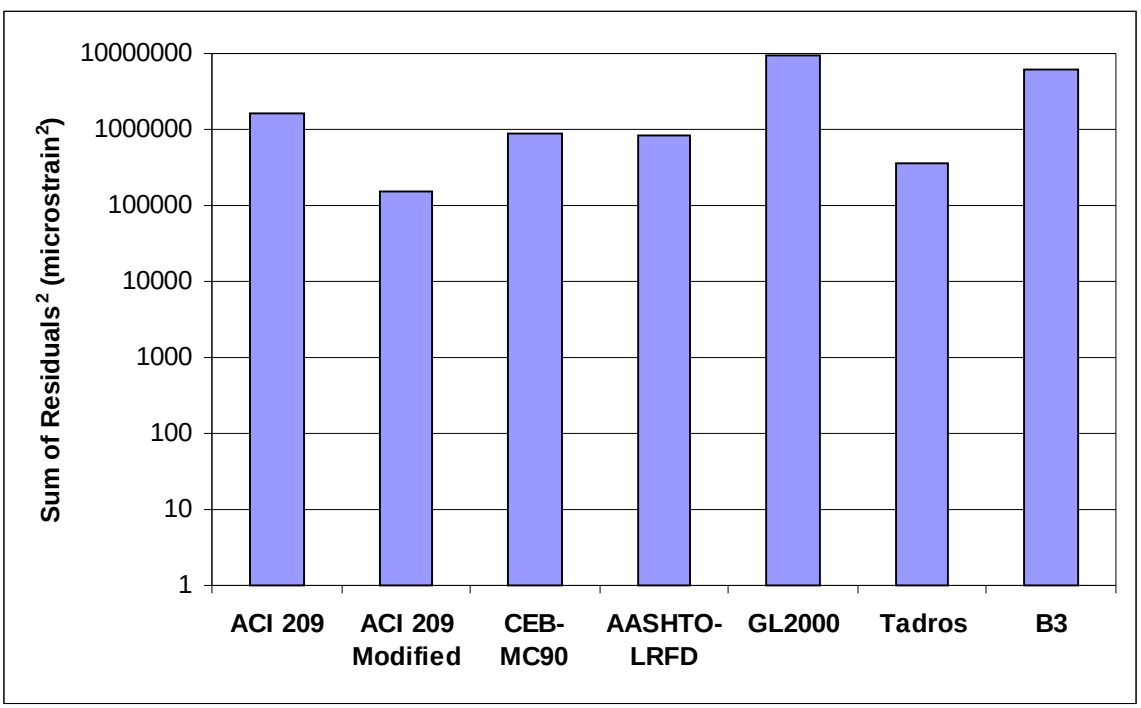

Figure 68 Standard Cure Total Strain Sum of Residuals Squared

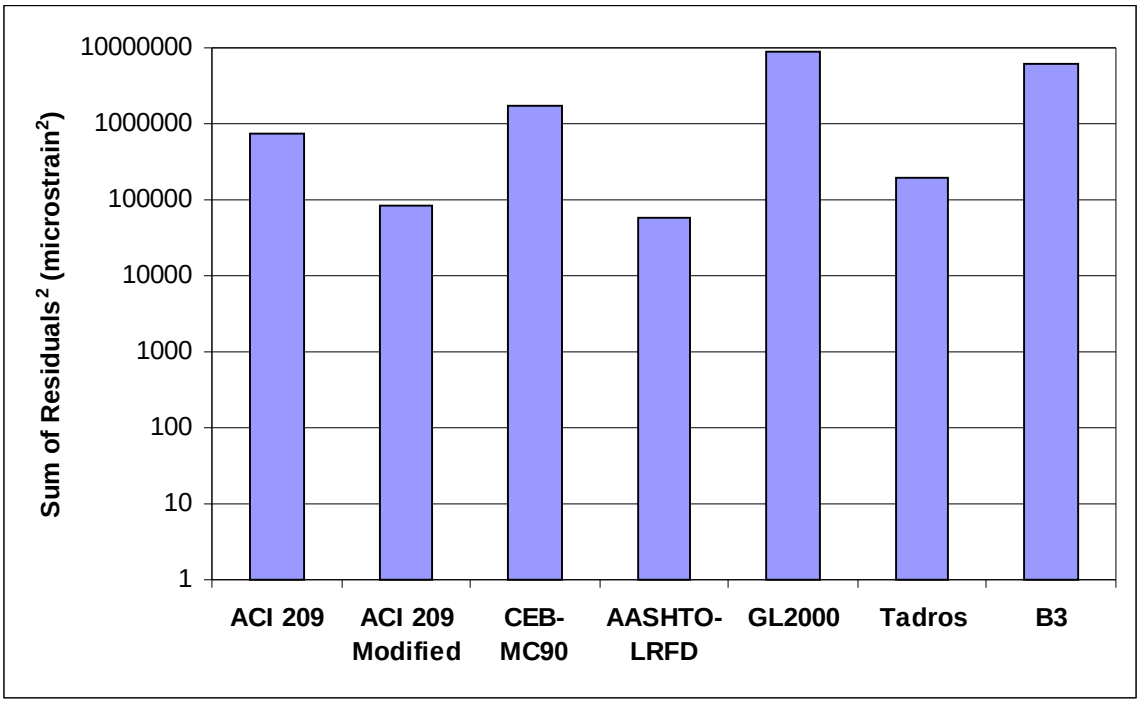

Figure 69 Standard Cure Creep Strain Sum of Residuals Squared

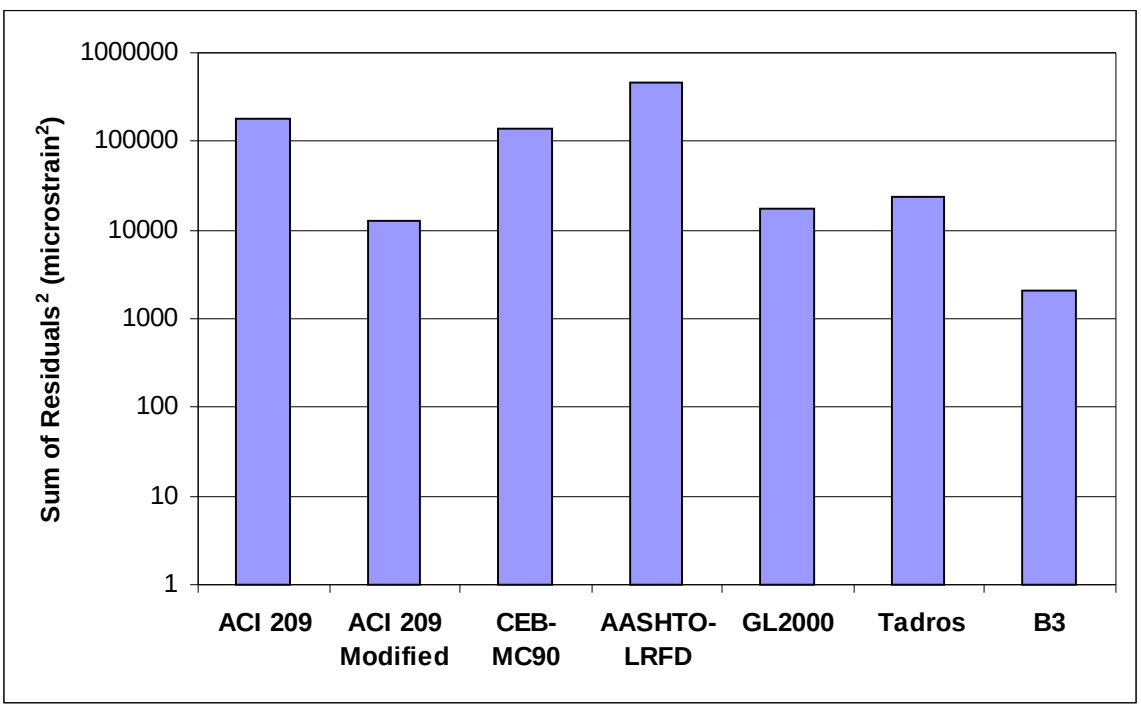

Figure 70 Standard Cure Shrinkage Strain Sum of Residuals Squared

5.10.3 Shrinkage Prisms Residuals Squared

Figure 71 presents the sum of residuals squared for the standard cure shrinkage prisms. The order of prediction accuracy is GL2000, B3, ACI 209, ACI 209 Modified, Tadros, AASHTO-LRFD, and CEB-MC90.

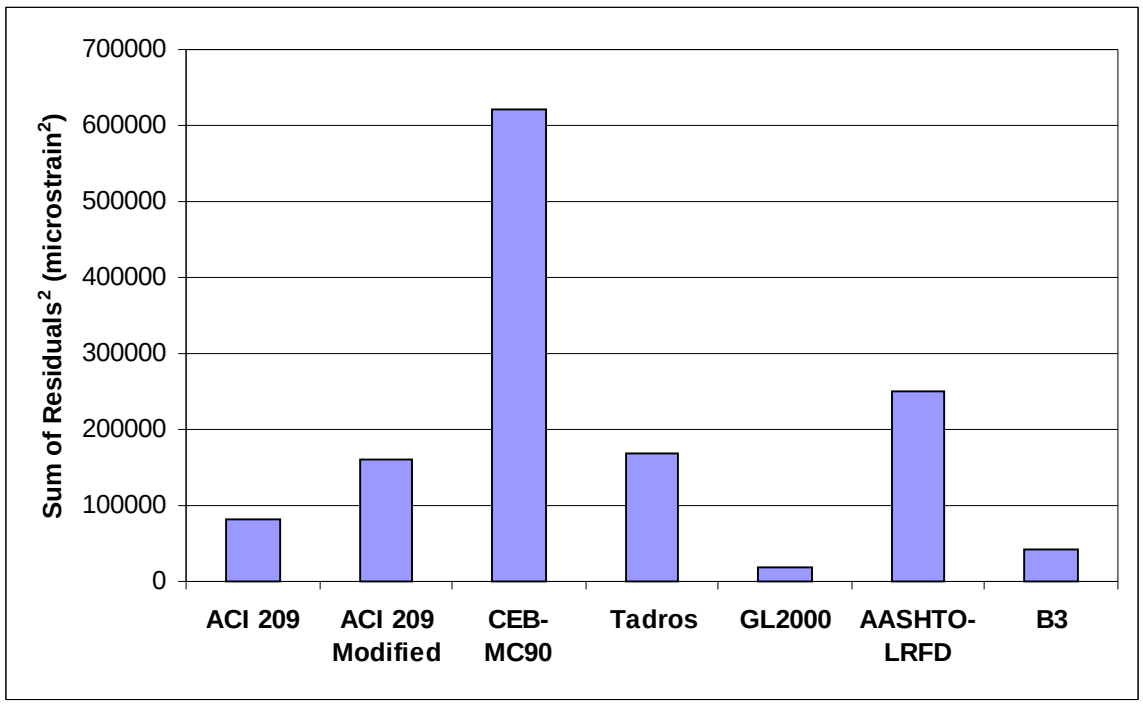

Figure 71 Standard Cure Shrinkage Prisms Sum of Residuals Squared

5.11 Prediction Model Rankings

In this section, the prediction model rankings from the residuals squared analysis are summed to determine the best overall predictor. The accelerated cure and standard cure rankings are determined at 97 and 98 days after loading, respectively.

5.11.1 Accelerated Cure Rankings

Table 12 presents the accelerated cure prediction model rankings. The ACI 209 Modified is the most accurate model for each type of strain.

	Total Strain	Creep	Shrinkage	Sum
ACI 209 Modified	1	1	1	3
Tadros	2	2	2	6
ACI 209	4	4	4	12
AASHTO-LRFD	3	3	7	13
B3	6	6	3	15
CEB MC-90	5	5	6	16
GL2000	7	7	5	19

Table 12 Accelerated Cure Prediction Model Rankings

5.11.2 Standard Cure Rankings

Table 13 presents the standard cure prediction model rankings. The ACI 209 Modified is the best total strain and overall predictor. AASHTO-LRFD was the best predictor of creep strain, and B3 was the best predictor of shrinkage strain.

	Total Strain	Creep	Shrinkage	Sum
ACI 209 Modified	1	2	2	5
Tadros	2	3	4	9
AASHTO-LRFD	3	1	7	11
B3	6	6	1	13
CEB MC-90	4	5	5	14
ACI 209	5	4	6	15
GL2000	7	7	3	17

Table 13 Standard Cure Prediction Model Rankings

5.11.3 Applicability of Prediction Models

Creep and shrinkage behavior depend heavily on the compressive strength of a concrete mixture. High strength concrete has a more dense cement matrix and less free water than normal strength concrete, which are factors that limit the amount of time-dependent water movement within the cement matrix. For a prediction model to accurately predict creep and shrinkage strains for high strength concrete, it should include compressive strength as an important input parameter. Table 14 presents the applicability of each prediction model to high strength concrete.

	f'_c Limit MPa (psi)	Strength Adjustment Factor?	
		Creep	Shrinkage
ACI 209	none	no	no
ACI 209 Modified	none	yes	yes
CEB 90	89.7 (13000)	yes	yes
AASHTO-LRFD	none	yes	no
GL2000	69.0 (10000)	no	yes
Tadros	none	yes	yes
B3	69.0 (10000)	yes	yes

Table 14 Prediction Model Compressive Strength Parameters

In this study, the models that did not include compressive strength as an input parameter greatly over predicted the experimental strains. In some cases, the models considered compressive strength for creep but not shrinkage, and vice versa (AASHTO-LRFD and GL2000).

The Bazant B3 and Gardner GL2000 prediction models are not expected to be accurate for the laboratory mixtures because the laboratory compressive strengths exceed the limits of applicability for each model. B3 considers compressive strength, but this parameter must be modified if the model is to be applied to concretes with compressive strengths of over 69.0 MPa (10000 psi). The GL2000 creep model does not consider compressive strength.

CHAPTER 6: CONCLUSIONS AND RECOMMENDATIONS

Conclusions

For Accelerated Cure Applications

1. The total strain of the HSC accelerated cure mixture loaded to 20.7 MPa (3000 psi) was 1342 ± 49 microstrain at 97 days, at a 95 percent confidence level.

2. ACI 209 Modified by Huo is the most accurate predictor of total, creep, and shrinkage strain for the Bayshore HSC mixture loaded to 20.7 MPa (3000 psi).

3. The accelerated curing technique results in higher variability of time-dependent strains than standard curing.

4. Embedded Vibrating wire gages (VWG) may be used to measure laboratory time-dependent strains. VWG elastic and creep strain measurements are comparable to Whittemore Gage measurements. VWG drying creep and shrinkage strains are significantly lower than Whittemore shrinkage strains because more drying occurs at the outside surface of a specimen.

For Standard Cure Applications

1. The total strain of the HSC standard cure mixture loaded to 20.7 MPa (3000 psi) was 1276 ± 38 microstrain at 98 days, at a 95 percent confidence level.

2. ACI 209 Modified by Huo is the best overall predictor and best predictor of total strain for the Bayshore HSC mixture loaded to 20.7 MPa (3000 psi).

3. AASHTO-LRFD is the best predictor of creep strain for the Bayshore HSC mixture loaded to 20.7 MPa (3000 psi).

4. B3 is the best predictor of cylinder shrinkage strain for the Bayshore HSC mixture, while GL2000 is the best predictor of prism shrinkage strain.

5. Meyerson reported 90-day total and shrinkage strains of 1560 ± 132 and 340 ± 57 microstrain, respectively, for the VDOT A5 Gravel GGBFS mixture.[6] The HSC 77-day total and shrinkage strains are 1246 ± 36 and 228 ± 4 microstrain, respectively.

   Both mixtures contain blast-furnace slag as a cementitious material. Meyerson's mixture had a w/cm ratio of 0.35 and 28-day compressive strength of 51.0 MPa (7400 psi). These specimens were loaded to 16.6 MPa (2400 psi).[6] The HSC mixture had a lower w/cm ratio (0.30), and higher 28-day strength of 91.0 MPa (13200 psi). Both factors tend to decrease time-dependent deformations. The HSC mixture had lower total strains even though the applied stress was 25 percent higher. Meyerson's specimens were loaded to a higher fraction of their 28-day compressive strength (32.4 percent vs. 22.7 percent), but this is not significant because in general the creep coefficient is constant up to an applied stress of 40 percent of the compressive strength.[3]

Recommendations

1. Creep and shrinkage models should contain modification factors for compressive strength. In this study, the models that contained such modification factors predicted much more accurately than those that did not consider compressive strength.

2. The AASHTO Standard Specification is used in Virginia, but it significantly over predicts prestress losses due to creep and shrinkage for high strength concrete. It should be updated by using a model that is applicable to high strength concrete.

3. Whenever possible, laboratory specimens should be cast in the field from the concrete batches being used in the test girders, so that the specimens are of identical material as the girders. This would eliminate significant discrepancies in material properties between the laboratory concrete and girder concrete.

4. Creep testing of sealed specimens could be useful in order to compare with creep strains inside a large bridge girder, where basic creep dominates.

References

1. ACI Committee 363, “State of the Art Report on High-Strength Concrete.” American Concrete Institute, Detroit, MI (1992) p. 3.

2. MacGregor, James G., “Reinforced Concrete: Mechanics and Design,” 3rd ed., Prentice Hall, 1997, p. 49,71.

3. Shah, S. P. and Ahmad, S. H., “High Performance Concrete: Properties and Applications,” McGraw-Hill, Inc., New York, 1994.

4. Tadros, et al. “Prestress Losses in Pretensioned High-Strength Concrete Bridge Girders,” Final Report (2002).

5. Vincent, Edward C., “Compressive Creep of a Lightweight, High Strength Concrete Mixture,” Master of Science Thesis in Civil Engineering, Virginia Tech, January 2003.

6. Meyerson, R., “Compressive creep of prestressed concrete mixtures with and without mineral admixtures.” Master of science thesis in Civil Engineering, Virginia Tech, February 2001.

7. ACI Committee 214, “Recommended Practice for Evaluation of Strength Test Results of Concrete, ACI 214-77, American Concrete Institute, Detroit, 1977, pg. 7.

8. Waldron, Chris, meeting in May 2003.

9. ACI Committee 209 (1990), “Prediction of creep, shrinkage and temperature effects in concrete structures.” *Manual of Concrete Practice*, Part 1, 209R 1-92.

10. Gardner, N. J. and Lockman, M. J., “Design Provisions for Drying Shrinkage and Creep of Normal-Strength Concrete,” ACI Materials Journal, v. 98, March-April 2001, pp. 159-167.

11. Huo, X. S., Al-Omaishi, N., and Tadros, M.K., Creep , Shrinkage, Modulus of Elasticity of High Performance Concrete., ACI Materials Journal, v. 98, n.6, November-December 2001.

12. CEB-FIP Model Code, "Evaluation of the Time Dependent Behavior of Concrete," September 1990.

13. Bazant, Z.P. and Baweja, S., "Creep and Shrinkage Prediction Model for Analysis and Design of Concrete Structures – Model B3," RILEM Recommendation, Materials and Structures, v. 28, 1995, pp. 357-365.

14. American Association of State Highway and Transportation Officials, "AASHTO-LRFD Bridge Design Specifications," Second Edition, Washington, DC, 1998.

15. ASTM C192 *Making and Curing Test Specimens in the Laboratory.* American Society of Testing and Materials, Philadelphia, PA.

16. ASTM C157 *Length Change of Hardened Hydraulic-Cement Mortar and Concrete.* American Society of Testing and Materials, Philadelphia, PA.

17. ASTM C39 *Compressive Strength of Cylindrical Concrete Specimens.* American Society of Testing and Materials, Philadelphia, PA.

18. ASTM C496 *Splitting Tensile Strength of Cylindrical Concrete Specimens.* American Society of Testing and Materials, Philadelphia, PA.

19. ASTM C512 *Creep of Concrete in Compression.* American Society of Testing and Materials, Philadelphia, PA.

20. ASTM C617 *Capping Cylindrical Concrete Specimens*. American Society of Testing and Materials, Philadelphia, PA.

21. ASTM C469 *Static Modulus of Elasticity and Poisson's Ratio of Concrete in Compression.* American Society of Testing and Materials, Philadelphia, PA.

22. American Association of State Highway and Transportation Officials, “AASHTO-Standard Specifications for Highway Bridges,” Fifteenth Edition, Washington DC (1993).

APPENDIX A

Literature Review and Prediction Models

TABLE OF CONTENTS

INTRODUCTION

The use of high strength concrete (HSC) has been steadily increasing, and today it is a very popular construction material. Common applications of HSC include high-rise buildings and precast prestressed bridge girders. High strength concrete offers significant economic advantages over conventional normal strength concrete (NSC) because HSC structures are more durable[9] and more slender members can be designed, resulting in reduced material and transportation costs. In fact, the strength-to-weight ratio of prestressed HSC structures is competitive with steel structures.[14]

All concretes undergo long-term deformations known as creep and shrinkage, and these phenomena must be carefully considered in design. Creep is defined as the deformation over time of a viscoelastic material, in excess of initial elastic strain, that results when a sustained stress is applied.[13] Shrinkage is also a time-dependent deformation, but it occurs in the absence of any applied load. Therefore, the total strain of a concrete specimen at any time is the sum of its initial elastic strain, creep strain, and shrinkage strain.

Creep and shrinkage have a significant effect on the performance of certain types of structures. One beneficial effect is that creep improves the distribution of stresses within a member. However, most effects are harmful. Prestress losses in a precast beam occur in part because of creep and shrinkage. In high-rise buildings, creep of column concrete can create problems with floor levelness and exterior skin movement.[4] Creep and shrinkage are especially important in designs using HSC because more slender members are possible, making deflection a more crucial issue.[12]

In general, as the strength of concrete increases, its other attributes improve as well, and HSC indeed performs better with respect to creep and shrinkage than NSC.[13] The following is a summary of the literature pertaining to creep and shrinkage, with an emphasis on high strength concrete. Included are explanations of creep and shrinkage behavior and means of quantifying the behavior, along with the factors that affect creep and shrinkage behavior.

CREEP BEHAVIOR

The processes of creep and shrinkage actually affect each other, but for analysis and testing purposes, they are treated as additive, independent processes.[11] In laboratory testing, companion shrinkage specimens are cast and stored in the same environment as the creep specimens being tested. Creep strain is calculated by subtracting the initial elastic strain of the loaded creep specimen and the shrinkage strain of the companion specimen from the total strain of the loaded creep specimen. Interaction between creep and shrinkage is neglected.

Creep of concrete may be separated into two components: basic creep and drying creep. Basic creep occurs in a sealed condition, without any exchange of water between the concrete and its surroundings. Drying creep involves water movement to the surrounding environment. The creep experienced by the innermost region of a large concrete member is predominantly basic creep, since very little water is lost to the outside environment.[13] Movement of water due to basic and drying creep brings about the formation of microcracks at the interface between the aggregate and cement paste, resulting in further deformation. Microcracking becomes more severe at stresses above normal working stress levels.[14]

Quantifying Creep

Creep is usually described by one of two quantities: creep coefficient or specific creep. Creep coefficient is defined as the ratio of ultimate creep strain to initial elastic strain. A typical value of creep coefficient is 2.35, which is the average value given by ACI 209 for standard conditions.[1] Specific creep is computed by dividing creep strain by the applied stress. This quantity is useful in comparing the creep behavior of concretes of different compressive strengths. Typical values of specific creep range from 2.5 microstrain/psi for small, low strength concrete members, to 0.15 microstrain/psi for large, high strength members.[11]

FACTORS AFFECTING CREEP BEHAVIOR

Creep of concrete is an extremely complex phenomenon, mostly because concrete is such a complex composite material.[5] Extensive testing has been performed on numerous varieties of concrete, but the creep mechanism is still not fully understood today. However, the effects of certain factors have been concluded based on trends observed in creep testing.

Cement

Cement plays a vital role because creep occurs chiefly in the hydrated cement paste that surrounds the aggregate. Rapid-hardening cements such as Type III tend to creep least. This is logical because if the cement hardens quickly, then the concrete matrix has more stiffness when the load is applied, making it more resistant to creep.[11]

In many concrete mixtures, Portland cement is partially replaced with ground blast furnace slag cement (BFSC). Chern and Chan[3] performed creep tests on specimens with varying amounts of BFSC. Some specimens were tested in a moist room and others in a drying room at 50% relative humidity. For the moist room specimens, an increase in slag content resulted in a slight decrease in specific creep, but the drying room specimens experienced more creep with increasing slag contents. Therefore, BFSC slightly decreased basic creep, but the specimens experienced more total creep strain under drying conditions with increasing slag proportions.

Silica fume is another supplementary cementing material that is used predominately in HSC mixes, especially those with compressive strengths of over 14,000 psi. Wiegrink, Marikunte, and Shah[15] reported decreasing specific creep values with increasing amounts of silica fume. There is an upper bound on the benefit of using silica fume. Shah and Ahmad[13] pointed out that if silica fume is included at a dosage of over 10 per cent by weight, it can actually increase creep.

Neville[11] pointed out that cements with high alumina content have a unique behavior. Whereas creep rate decreases over time and eventually approaches a near constant rate for most cements, high-alumina cement undergoes a linear period of creep beginning at around 6 months after loading, and the time for the creep rate to reach a near constant rate is longer.

Aggregate

Normal-weight aggregates themselves do not creep significantly, but they restrain water movement throughout the concrete. High strength concrete mixes tend to have a higher aggregate content, which amplifies its role in affecting long-term deformation. Aggregate characteristics that influence creep include stiffness, size, absorption, and surface roughness.[2]

The elastic modulus of aggregate has been shown to significantly affect creep behavior. As the cement paste begins to creep, load is transferred to the aggregate in proportion to the aggregate stiffness. The stiffer the aggregate, the lower the stress being applied to the cement paste, thereby reducing paste movement and creep.[2,11]

Collins[4] studied the effect of course aggregate size on creep behavior. Mixtures with a maximum aggregate size of 1 ½ in. experienced 15 per cent less creep after 90 days than those with a ¾ in. maximum size.

The aggregate-paste interface strongly affects the aggregate's ability to resist deformations. Aggregates with rough surfaces resist creep much more effectively than those with smooth surfaces. Mokhtarzadeh and French[9] studied creep of mixtures containing five different types of aggregate, and observed that the mixtures containing round river gravel had much higher specific creep values than the other mixtures.

It is thought that aggregate absorption affects creep by causing additional moisture movement in concrete. For example, if the aggregate is not fully saturated during mixing, it could absorb water from the paste, causing more creep caused by additional water movement into the empty aggregate void spaces. This factor is closely related to aggregate stiffness because aggregate having high stiffness also tends to exhibit less absorption.[11]

Admixtures

Chemical admixtures generally do not significantly affect creep behavior. Air entrainment agents are not considered a factor. However, it has been shown that admixtures containing lignosulfonic and hydorxylated carboxylic acid significantly increase creep.[11]

W/CM Ratio

The ratio of water to cementitious materials (w/cm ratio) is the most dominant parameter, with respect to mixture proportions, that determines the creep characteristics of concrete. In order to attain high compressive strengths in HSC mixtures, lower w/cm ratios are used. Values of 0.30 and below are common.[13] Neville[11] discussed the undisputed point that specific creep of concrete increases with increasing w/cm ratio. This is because with a lower w/cm ratio, the volume of hydrates is reduced along with the free water content, thereby reducing creep deformations. The low w/cm ratio of HSC concrete gives it more desirable creep characteristics.

Curing Conditions

Curing method can substantially impact the creep behavior of concrete. Steam curing, which is commonly done in the production of prestressed bridge girders, can reduce creep by 30 to 50 per cent. This reduction is due to accelerated hydration of the cement and the moisture loss that occurs when the specimens are transferred to a drier, cooler environment.[11]

Khan, Cook, and Mitchell[5] examined the effects of air-dried curing and moist curing on creep of normal, medium, and high strength concrete. The results were significantly higher creep strains in the air-dried specimens. Mokhtarzadeh and French[9] reported that for the specimens that were moist cured, the differences in creep behavior due to mixture characteristics were miniscule. Moist curing caused the different mixtures to have similar microstructures, resulting in similar creep behavior. Another conclusion from Mokhtarzadeh's research was that higher curing temperatures resulted in more creep. Their explanation was that higher temperatures increase porosity and internal cracking, which contribute to creep.

Ambient Conditions During Loading

The environment surrounding a concrete specimen can greatly affect creep deformations. High temperatures result in greater creep, as do low relative humidity conditions. Creep has been observed to be 2-3 times greater in 50 per cent humidity than in 100 per cent humidity.[11].

Stress Level

Creep of concrete is highly sensitive to the magnitude of sustained stress that is applied.[4] For example, a specimen loaded to 80 per cent of its ultimate strength experiences about three times as much creep as a similar specimen loaded to 40 per cent.[14] Microcracking at the aggregate-paste interface becomes more significant at high stresses, and delayed failure may occur at sustained stresses above 75 per cent of the compressive strength.[13] Smadi, Slate, and Nilson[14] performed creep tests on high-, medium-, and low-strength concretes and investigated the response to sustained stress levels between 40 and 80 per cent. They found that the creep strain was proportional to the stress level, up to a certain proportionality limit. The limit is about 65 per cent of ultimate for HSC, and 45 per cent of ultimate for NSC and LSC. These results imply that HSC can be safely loaded to a higher fraction of its ultimate strength without experiencing excessive time-dependent deformations.

Age of Loading

Another factor affecting creep is the concrete age when a sustained load is applied. Specimens loaded after one day of curing typically have twice the specific creep of specimens loaded after 28 days.[13] If the concrete has not been given adequate time to cure, then it will not have the stiffness needed to resist creep. In particular, Khan, Cook, and Mitchell[5] observed that HSC is much more sensitive to early-age loading than NSC.

SHRINKAGE BEHAVIOR

Unlike creep, shrinkage of concrete occurs in the absence of an applied load. It consists of three different mechanisms, known as drying shrinkage, autogenous shrinkage, and carbonation shrinkage. A typical concrete mixture contains more water than is needed for initial hydration, and this excess water is stored in the pores, or void spaces, in the concrete.[9] Drying shrinkage occurs when this excess water diffuses into the surrounding environment, resulting in a net volume loss.[14] Autogenous shrinkage, also known as “self-desiccation,” is the water loss due to continued hydration of the cement. This mechanism only results in shrinkage if there is not a supply of water to replenish the amount lost to hydration, such as in the interior of a large member.[9] Carbonation shrinkage is the process by which CO_2 in the atmosphere reacts with

$Ca(OH)_2$ in the cement paste, in the presence of moisture. For shrinkage to occur, the water produced in this reaction must be lost to the environment, similar to autogenous shrinkage. Shrinkage deformations are usually expressed in units of microstrain.

FACTORS AFFECTING SHRINKAGE BEHAVIOR

Many of the factors that affect creep behavior also influence shrinkage. As with creep, HSC tends to have more favorable shrinkage characteristics than NSC.

Cement

The effects of different cement types are generally negligible, except when they affect the rate of strength gain. Rapid hardening cement tends to shrink more due to its fineness and increased water demand.[13]

The amount of cement in a concrete mixture influences shrinkage during hydration. Higher cement content promotes a faster rate of hydration, and therefore more water loss early on. High strength concrete tends to contain more cement than NSC mixes, and therefore tends to experience more shrinkage during initial hydration.[14]

Partial replacement of cement with pozzolanic material such as fly ash and slag tends to increase shrinkage by refining the cement paste and decreasing the stiffness of the cement paste.[13] Chern and Chan[3] noted that the increase in shrinkage observed with increasing slag contents might be due to greater paste volume. If Portland cement is replaced by slag on an equal-weight basis, a higher cement content results because slag has a lower specific gravity than Portland cement.

Aggregate

Favorable aggregate characteristics for shrinkage control parallel those for creep. Aggregate restrains shrinkage of the surrounding cement paste, and hard, dense, low-absorption aggregates such as dolomitic limestone are ideal.[4] Higher aggregate content leads to lower shrinkage, and aggregates with rough surfaces are more effective in restraining shrinkage.[13]

Admixtures

Chemical admixtures tend to increase shrinkage unless they reduce the water content of the mix. Collins[4] investigated the effect of a high range water-reducing admixture on shrinkage, and concluded that it did not significantly affect shrinkage. Calcium chloride, which accelerates the hardening and setting of concrete, tends to increase shrinkage. Air entrainment agents have not been shown to affect shrinkage.[13]

W/CM Ratio

Lower w/cm ratios are imposed on HSC mixes in order to attain higher strengths, and this leads to a decrease in shrinkage. The water content of a mixture greatly impacts the paste rigidity. Lower water content results in fewer pores in the mature cement, which increases the rigidity of the solid matrix and decreases deformation.[14] The higher the w/cm ratio, the more excess water that remains in the concrete after hydration. More excess water means a potential for more drying shrinkage.[13]

Curing Conditions

Curing conditions greatly affect shrinkage behavior of concrete. Collins[4] found that shrinkage deformation is inversely proportional to moist-curing time. She observed that longer moist-curing times result in lower shrinkage deformation.

Heat-accelerated curing (HAC) significantly reduces drying shrinkage. Mak, Foster, Chirgwin, and Ho[7] observed that specimens subjected to HAC had 75 percent less shrinkage than specimens cured at standard temperature. Mokhtarzadeh and French[9] varied the temperature of heat-accelerated curing, and found that specimens cured at 120 F had more drying shrinkage than specimens cured at 150 F, which confirms the trend that drying shrinkage decreases with increasing curing temperature.

Ambient Conditions

The relative humidity (RH) of the surrounding environment has a significant influence on shrinkage deformation. Drying shrinkage only occurs if the ambient RH is less than the internal

RH, which is usually about 80 per cent. Therefore, far less drying shrinkage occurs when the ambient RH is high.[13]

Member Size

The size of a concrete member also influences its shrinkage behavior. For larger members, it takes much more time for shrinkage effects to reach the interior regions. Thus, larger members have a lower rate and total magnitude of shrinkage.[13]

CREEP AND SHRINKAGE OF HSC

As stated before, HSC generally performs better than conventional concretes under long-term loading. Mokhtarzadeh[9] reported that his creep tests on HSC yielded ultimate creep coefficients ranging from 0.92 to 2.46, while the usual range for NSC is from 1.30 to 4.15. Likewise, Smadi, Slate and Nilson[14] found that HSC had lower specific creep than NSC at all stress/strength ratios. The primary explanation for this superior performance is that HSC mixtures contain a lower volume of hydrates and free water, resulting in a more rigid internal structure.[13]

High strength concrete is subject to faster early shrinkage than conventional concretes. This is likely due to a greater cement content, which increases the heat and rate of hydration.[14] However, the long-term drying shrinkage is reduced in HSC because of its finer pore structure and reduced supply of evaporable water. The refined pore structure has a lower gas permeability, which slows down the drying process.[13]

SUMMARY

Creep and shrinkage of concrete are complicated processes that are difficult to model, but understanding of these processes is vital in designing safe and economical structures. Creep and shrinkage are sensitive to several factors, which include mixture composition, curing methods, ambient conditions, loading age and intensity, and member size.

The following characteristics have been found to decrease creep deformation:

- Rapid-hardening cements.
- Blast furnace slag (decreases basic creep but increases drying creep).
- Silica Fume (up to 10 per cent dosage by weight).
- High aggregate content, stiffness, size, and surface roughness.
- Low w/c ratio.
- Steam curing and moist curing.
- Low ambient temperature.
- High ambient relative humidity.
- Low stress level.
- Higher concrete age at loading.

The following characteristics have been found to decrease shrinkage:

- Low cement content.
- High aggregate content, stiffness, size, and surface roughness.
- Low w/c ratio.
- Longer moist-curing time.
- Heat-accelerated curing.
- High ambient relative humidity.
- Large member size.

MODEL EQUATIONS

ACI 209 Model

Creep strain at time t (days)

$$v_t = \frac{t^{0.6}}{10 + t^{0.6}} v_u \qquad \text{(Eq. 2-8)}$$

where v_u = ultimate creep coefficient

recommended value = $2.35\gamma_c$

where γ_c = product of all applicable correction factors

Shrinkage strain at time t

$$(e_{sh})_t = \frac{t}{35 + t}(e_{sh})_u \quad \text{for moist cured concrete} \qquad \text{(Eq. 2-9)}$$

$$(e_{sh})_t = \frac{t}{55 + t}(e_{sh})_u \quad \text{for steam cured concrete} \qquad \text{(Eq. 2-10)}$$

where v_u = ultimate shrinkage strain

recommended value = 780 γ_{sh} x 10^{-6}

where γ_{sh} = product of all applicable correction factors

Correction factors

-Loading Age:

creep $g_{la} = 1.25(t_{la})^{-0.118}$ for moist cured concrete (Eq. 2-11)

creep $g_{la} = 1.13(t_{la})^{-0.094}$ for steam cured concrete (Eq. 2-12)

where t_{la} = loading age in days

-Relative Humidity:

creep $\gamma_1 = 1.27\text{-}0.0067\gamma$, for $\gamma > 40$ (Eq. 2-14)

shrinkage $\gamma_1 = 1.40 - 0.010\gamma$, for $40<\gamma<80$ (Eq. 2-15)

$= 3.00 - 0.030\gamma$, for $80<\gamma<100$ (Eq. 2-16)

where γ = relative humidity in percent.

-Volume-surface ratio:

creep $\gamma_{vs} = 2/3[1+1.13 \exp(-0.54\ v/s)]$ (Eq. 2-22)

shrinkage $\gamma_{vs} = 1.2 \exp(-0.12\ v/s)$ (Eq. 2-22)

where v/s = volume to surface ratio of member in inches

-Slump:

creep $\gamma_s = 0.82 + 0.067s$ (Eq. 2-23)

shrinkage $\gamma_s = 0.89 + 0.041s$ (Eq. 2-24)

where s = observed slump in inches

-Fine aggregate percentage:

creep $\gamma_\psi = 0.88 + 0.0024\psi$ (Eq. 2-25)

shrinkage $\gamma_\psi = 0.30 + 0.014\psi$, for $\psi<50$ percent (Eq. 2-26)

$= 0.90 + 0.002\psi$, for $\psi>50$ percent (Eq. 2-27)

where ψ = percent ratio of fine aggregate to total aggregate by weight

-Cement content::

shrinkage $\gamma_c = 0.75 + 0.00036c$ (Eq. 2-28)

where c = cement content in pounds per cubic yard.

-Air content:

creep $\gamma_\alpha = 0.46 + 0.09\alpha$, but not less than 1.0 (Eq. 2-29)

shrinkage $\gamma_\alpha = 0.95 + 0.008\alpha$ (Eq. 2-30)

where α = air content in percent.

ACI 209 Modified by Huo

-Same as ACI 209, with additional modification factors for compressive strength.

Creep

$\gamma_{st,c} = 1.18 - 0.045*f'_c$

where f'_c = 28-day compressive strength in ksi

$$v_t = \frac{t^{0.6}}{K_C + t^{0.6}} v_u$$

where $K_C = 12 - 0.50*f'_c$

Shrinkage

$\gamma_{st,s} = 1.20 - 0.05*f'_c$

$$(e_{sh})_t = \frac{t}{K_s + t} (e_{sh})_u$$

where $K_s = 45 - 2.5*f'_c$

CEB-MC90 Model

Calculate creep compliance function:

$$\text{Compliance function } (\mu\varepsilon/\text{psi}) = \frac{j\,(t,t_o)}{E_c} + \frac{1}{E_c(t_o)}$$

where:

t = age of concrete after casting

t_o = age of concrete at loading

$$j\,(t,t_o) = f_o\, b_c(t-t_o)$$

$$f_o = f_{RH}\, b\,(f_{cm})\, b\,(t_o)$$

$$f_{RH} = 1 + \frac{(1-RH/100)}{0.46(h_o/4)^{1/3}}$$

RH = ambient relative humidity expressed as a percent

$$b\,(f_{cm}) = 5.3/(f_{cm}/1450)^{1/2}$$

$$b_c(t-t_o) = \frac{(t-t_o)^{0.3}}{[b_H + (t-t_o)]^{0.3}}$$

$$b_H = 150[1+(0.012RH)^{18}](h_o/4) + 250 \le 1500$$

$E_c = (E_{co})(f_{cm}/1450)^{1/3}$

E_{co} = 3,117,500 psi

$E_c(t_o) = (E_c)\{\exp[0.5S(1-(28/t_o)^{0.5})]\}$

S = 0.38 for slow hardening cement
0.25 for normal and rapid hardening cement
0.2 for rapid hardening high strength

Shrinkage Strain:

$$e_{cs}(t-t_s) = (e_{cso})b_s(t-t_s)$$

$$e_{cso} = e_s(f_{cm})b_{RH}$$

$$e_s(f_{cm}) = [160+10b_{sc}(9-f_{cm}/1450)]*10^{-6}$$

β_{sc} = 4 for slow hardening cement
5 for normal and rapid hardening cement
8 for rapid hardening high strength

β_{RH} = -1.55 [1-(RH/100)^3] for 40%<RH<99%, stored in air
= 0.25 for RH>99%, immersed in water

$$b_s(t-t_s) = \sqrt{\frac{(t-t_s)}{\left[350\left(\frac{h_o}{4}\right)^2+(t-t_s)\right]}}$$

Total strain:

$$e(t) = e_{cs}(t-t_s)+\left[\frac{f(t,t_o)}{E_c}+\frac{1}{E_c(t_o)}\right]s$$

where σ = sustained stress

GL2000 Model

Mean compressive strength:

Use experimental mean compressive strength, otherwise:

$f_{cm28} = 1.1*f_{ck28} + 700$ (in psi)

Mean compressive strength over time:

Use experimental compressive strength at loading, otherwise:

$$f_{cmto} = f_{cm28}\frac{t_o^{3/4}}{(a+b(t_o)^{3/4})}$$

Cement Type	a	b	k
I	2.8	0.77	1.0
II	3.4	0.72	0.7
III	1.0	0.92	1.33

Mean modulus of elasticity:

Use experimental modulus, otherwise:

$E_{cmto} = 500{,}000 + 52{,}000(f_{cmto})^{1/2}$ (in psi)

Creep strain:

Creep strain = $(\sigma/E_{cmto})(1 + \text{Creep Coefficient})$

If Experimental E_{c28} and E_{cmto} is available then:

Creep strain = $\sigma[(1/E_{cmto(experimental)}) + (\text{creep coefficient}/E_{cmto(average)})]$

Creep coefficient Φ_{28} =

$$\Phi(t_c)\left[2\left(\frac{(t-t_c)^{0.3}}{(t-t_c)^{0.3}+14}\right)+\left(\frac{7}{t_0}\right)^{0.5}\left(\frac{t-t_c}{t-t_c+7}\right)^{0.5}+2.5\left(1-1.086h^2\right)\left(\frac{t-t_0}{t-t_0+97(V/S)^2}\right)^{0.5}\right]$$

If $t_0 = t_c$,

$$\Phi(t_c) = 1$$

If $t_0 > t_c$,

$$\Phi(t_c) = \left[1-\left(\frac{t_o-t_c}{t_0-t_c+97(V/S)^2}\right)^{0.5}\right]^{0.5}$$

<u>Without experimental data</u>

$$\text{Specific Creep} = \frac{\Phi_{28}}{E_{cmto}}$$

$$J(t,t_0) = \frac{1+\Phi_{28}}{E_{cmto}}$$

$$\text{Creep Strain} = s * \frac{\Phi_{28}}{E_{cmto}}$$

<u>With experimental data</u>

$$\text{Specific Creep} = \frac{\Phi_{28}}{E_{cm28(average)}}$$

$$J(t,t_0) = \frac{1}{E_{cmto}} + \frac{1+\Phi_{28}}{E_{cm28(average)}}$$

$$\text{Creep Strain} = s * \frac{\Phi_{28}}{E_{cm28(average)}}$$

Shrinkage strain:

$\varepsilon_{sh} = (\varepsilon_{shu})\beta(h)\beta(t)$

$\beta(h) = 1\text{-}1.18h^4$, for $h<0.96$

$= 0.0$, for sealed specimens $h = 0.96$

where h = relative humidity (decimal)

$$\beta(t) = \sqrt{\left(\frac{t - t_c}{t - t_c + 97(V/S)^2}\right)}$$

$$\varepsilon_{shu} = 1000 * K * \sqrt{\left(\frac{4350}{f_{cm}}\right)} \times 10^{-6}$$

Total strain:

$\varepsilon(t) = \varepsilon_{sh} + [(\sigma/E_{cmto})(1 + \text{creep coefficient})]$

If experimental E_{c28} and E_{cmto} are available use:

$\varepsilon(t) = \varepsilon_{sh} + \sigma[(1/E_{cmto(experimental)}) + (\text{creep coefficient}/E_{cmto(average)})]$

B3 Model

Creep compliance function:

$$j(t,t') \left[\mu\varepsilon/psi\right] = q_1 + C_o(t,t') + C_d(t,t',t_o)$$

Total strain:

$$\varepsilon(t) = j(t,t')\sigma + \varepsilon_{sh}(t)$$

$$C_o(t,t') = q_2 Q(t,t') + q_3 \ln(1 + (t - t')^n) + q_4 \ln(t/t')$$

where: t = age of concrete after casting

t' = age of concrete at loading

t_o = age of concrete at the beginning of shrinkage

$$Q(t,t') = Q_f(t')\left[1 + \frac{(Q_f(t'))^{r(t')}}{Z(t,t')^{r(t')}}\right]^{-1/r(t')}$$

$$Q_f(t') = [0.086(t')^{2/9} + 1.21\,(t')^{4/9}]^{-1}$$

$$Z(t,t') = (t')^{-m} \ln(1 + (t - t')^n)$$

where m = 0.5, n = 0.1

$$r(t') = 1.7\,(t')^{0.12} + 8$$

$$q_2 = 451.1\,(c)^{0.5}\,(f'_c)^{-0.9}$$

where c = cement content (lb/ft^3)

$$q_3 = 0.29(w/c)^4\, q_2$$

$q_4 = 0.14\ (a/c)^{-0.7}$

where a/c = aggregate to cement ratio by weight

$C_d(t,t',t_o) = q_5\ \{\exp[-8H(t)] - \exp[-8H(t')]\}^{1/2}$

$H(t) = 1 - (1 - h)\ S(t)$

$H(t') = 1 - (1 - h)\ S(t')$

$q_5 = 7.57 \times 10^5\ (f'_c)^{-1}\ ABS(\varepsilon_{sh\infty})^{-0.6}$

$\varepsilon_{sh\infty} = -\alpha_1\alpha_2(26(w)^{2.1}\ (f'_c)^{-0.28} + 270) \times 10^{-6}$

α_1 = 1.0 for type I cement
0.85 for type II cement
1.1 for type III cement

α_2 = 0.75 if steam cured
1.0 if water cured or h = 100%
1.2 if sealed during curing

$$S(t) = \tanh\sqrt{\frac{t - t_o}{T_{sh}}}$$

$$S(t') = \tanh\sqrt{\frac{t' - t_o}{T_{sh}}}$$

$T_{sh} = K_t(K_sD)^2$

$K_t = 190.8\ (t_o)^{-0.08}\ (f'_c)^{-0.25}$

Type of Member or Structure	**K_s**
Infinite slab	1.00
Infinite cylinder	1.15
Infinite square prism	1.25
Sphere	1.30
Cube	1.55
Undefined member	1.00

Relative Humidity	**K_h**
for $h < 0.98$	$1-h^3$
for $h = 1$	-0.2
for $0.98<h<1$	use linear interpolation

AASHTO-LRFD Model

Creep Coefficient

$$\varphi(t,t_i) = 3.5 k_c k_f \left(1.58 - \frac{H}{120}\right) t_i^{-0.118} \frac{(t - t_i)^{0.6}}{10.0 + (t - t_i)^{0.6}}$$

where:

$$k_f = \frac{1}{0.67 + \left(\frac{f'_c}{9}\right)}$$

H = relative humidity (%)

$$k_c = \left[\frac{\frac{t}{26e^{0.36(V/S)} + t}}{\frac{t}{45 + t}}\right]\left[\frac{1.80 + 1.77e^{-.54(V/S)}}{2.587}\right]$$

f'_c = specified 28-day concrete strength (ksi)

t = maturity of concrete (days)

t_i = age of concrete when load is initially applied (days)

Shrinkage

For moist-cured concretes:

$$\varepsilon_{sh} = -k_s k_h \left(\frac{t}{35.0 + t}\right) 0.51x10^{-3}$$

For steam-cured concretes:

$$\varepsilon_{sh} = -k_s k_h \left(\frac{t}{55.0 + t}\right) 0.51x10^{-3}$$

where:

$$k_s = \left[\frac{\frac{t}{26e^{0.36(V/S)} + t}}{\frac{t}{45 + t}}\right]\left[\frac{1064 - 94(V/S)}{923}\right]$$

$k_h = (140 - H)/70$ for H<80%

$k_h = 3(100 - H)/70$ for H>80%

t = drying time (days)

Tadros Model

Creep Coefficient

$\varphi(t,t_i) = 1.90\ \gamma_{cr}$

$\gamma_{cr} = k_{td}\, k_{la}\, k_s\, k_{bc}\, k_f$

$k_{td} = \dfrac{t}{61 - 4f'_{ci} + t}$ f'_{ci} = compressive strength at release

$k_{la} = t_i^{-0.118}$ t_i = loading age (days)

$k_{hc} = 1.56 - 0.008H$ H = relative humidity (%)

$k_s = \dfrac{1064 - 94V/S}{735}$ V/S = volume-to-surface ratio (in.)

$k_f = 5/(1+f'_{ci})$

Shrinkage Strain

$\varepsilon_{sh} = 480*10^{-6}\ \gamma_{sh}$

$\gamma_{sh} = k_{td}\, k_s\, k_{hs}\, k_f$

$k_{td} = \dfrac{t}{61 - 4f'_{ci} + t}$

$k_{hs} = 2.00 - 0.0143H$

$k_s = \dfrac{1064 - 94V/S}{735}$

$k_f = 5/(1+f'_{ci})$

REFERENCES

1. ACI Committee 209 (1990), "Prediction of creep, shrinkage and temperature effects in concrete structures." *Manual of Concrete Practice*, Part 1, 209R 1-92.

2. Alexander, Mark G., "Aggregates and the deformation properties of concrete." *ACI Materials Journal*, November1996 – December 1996, v.93, n. 6, pp. 569-577.

3. Chern, Jenn Chuan and Chan, Yin Wen, "Deformations of concretes made with blast furnace slag cement and ordinary Portland cement." *ACI Materials Journal*, July 1989 – August 1989, v. 86, n. 4, pp. 372-382.

4. Collins, Therese M., "Proportioning high strength concrete to control creep and shrinkage." *ACI Materials Journal*, November 1989 – December 1989, v. 86, n. 6, pp. 567-580.

5. Khan, Arshad A., Cook, William D. and Mitchell, Denis, "Creep, shrinkage, and thermal strains in normal, medium, and high strength concretes during hydration." *ACI Materials Journal*, March 1997 – April 1997, v. 94, n. 2, pp. 156-163.

6. Khatri, R. P., Sirivivatnanon, V. and Gross, W., "Effect of different supplementary cementitious materials on mechanical properties of high performance concrete." *Cement and Concrete Research*, January 1995, v. 25, n. 1, pp. 209-220.

7. Mak, S. L., Foster, G., Chirgwin, G. and Ho, D. W. S., "Properties of high-performance, heat-cured slag cement concrete for bridge structures." Proc. 3rd CANMET/ACI International Conference, Kuala Lumpur, Malaysia, 1997, pp. 821-830.

8. Meyerson, R., "Compressive creep of prestressed concrete mixtures with and without mineral admixtures." Master of science thesis in Civil Engineering, Virginia Tech, February 2001.

9. Mokhtarzadeh, A. and French, C., “Time-dependent properties of high-strength concrete with consideration for precast applications.” *ACI Materials Journal*, March 2000 - June 2000, v. 97, n. 3, pp. 263-271.

10. Nawy, Edward G., “Fundamentals of high strength high performance concrete.”

11. Neville, A. M., “Creep of concrete: plain, reinforced, and prestressed.”

12. Paulson, Kent A., Nilson, Arthur H. and Hover, Kenneth C., “Long term deflection of high strength concrete beams.” *ACI Materials Journal*, March 1991 – April 1991, v. 88, n. 2, pp. 197-206.

13. Shah, S. P. and Ahmad, S. H., “High performance concrete: properties and applications.”

14. Smadi, Mohammed M., Slate, Floyd O. and Nilson, Arthur H., “Shrinkage and creep of high, medium, and low strength concretes, including overloads.” *ACI Materials Journal*, May 1987 – June 1987, v. 84, n. 3, pp. 224-234.

15. Wiegrink, Karl; Marikunte, Shashidhara; and Shah, Surendra P., “Shrinkage cracking of high strength concrete.” *ACI Materials Journal*, September 1996 – October 1996, v. 93, n. 5, pp. 409-415.

16. Gardner, N. J. and Lockman, M. J., “Design Provisions for Drying Shrinkage and Creep of Normal-Strength Concrete,” ACI Materials Journal, v. 98, March-April 2001, pp. 159-167.

17. Huo, X. S., Al-Omaishi, N., and Tadros, M.K., Creep , Shrinkage, Modulus of Elasticity of High Performance Concrete., ACI Materials Journal, v. 98, n.6, November-December 2001.

18. CEB-FIP Model Code, “Evaluation of the Time Dependent Behavior of Concrete,” September 1990.

19. American Association of State Highway and Transportation Officials, “AASHTO-LRFD Bridge Design Specifications,” Second Edition, Washington, DC, 1998.

20. Bazant, Z.P. and Baweja, S., “Creep and Shrinkage Prediction Model for Analysis and Design of Concrete Structures – Model B3,” RILEM Recommendation, Materials and Structures, v. 28, 1995, pp. 357-365.

21. Tadros, et al. “Prestress Losses in Pretensioned High-Strength Concrete Bridge Girders,” Final Report (2002).

APPENDIX B

Batch Weights and Aggregate Properties

Batch Weights

Table 15 presents the batch weights that were used in producing the laboratory concrete mixtures. Extra amounts of Adva were added to the standard cure mixtures to achieve higher slumps. Batches 3A and 4A contained 98 ml and 67 ml of additional Adva, respectively.

cement, kg (lbs)	20.8 (45.89)
slag, kg (lbs)	13.9 (30.6)
sand, kg (lbs)	40.4 (88.92)
aggregate, kg (lbs)	79.7 (175.46)
water, kg (lbs)	10.3 (22.68)
total mix, kg (lbs)	166 (365)
Daravair1000, ml	29
Adva, ml	112
Hycol, ml	67
DCI, ml	1364
Batch size, m^3 (ft^3)	0.068 (2.40)

Table 15 Batch Weights for the Laboratory Specimens

Aggregate Properties

Coarse Aggregate:

Absorption	0.6
Specific gravity	2.98
Unit Wt.	108.4 pcf

Fine Aggregate:

Absorption	1.4
Fineness modulus	2.60
Specific gravity	2.61

APPENDIX C

Photographs

Figure 72 Creep Room Photograph

Figure 73 Sure Cure System Photograph

Figure 74 Whittemore Gage Top View Photograph

Figure 75 Whittemore Gage Side View Photograph

APPENDIX D

Creep Frame Calibration

Creep Frame Calibration

The creep frames were originally built and calibrated by Richard Meyerson and David Mokarem. Table 16 presents the calibration values that were used in this study to apply the desired loads on the creep specimens. Details of the calibration procedure can be found in Meyerson's thesis

	Calibration Value
Frame 1	19.998
Frame 2	19.836
Frame 3	19.805
Frame 4	20.242

Table 16 Creep Frame Calibration Values (psi/kip)

APPENDIX E

Accelerated Curing

Accelerated Curing

Figures 75 and 76 present sample curing temperature profiles for a test girder and a batch of laboratory specimens. The Bayshore temperature curves represent readings from thermocouples embedded at various heights in the girder. The laboratory curves represent temperatures of the Sure Cure cylinders. Most of the cylinders followed the specified temperature profile closely. Any cylinders that departed significantly from the specified temperature profile were used for tensile strength tests so that the creep, shrinkage, compressive strength, and modulus cylinders would have similar maturities.

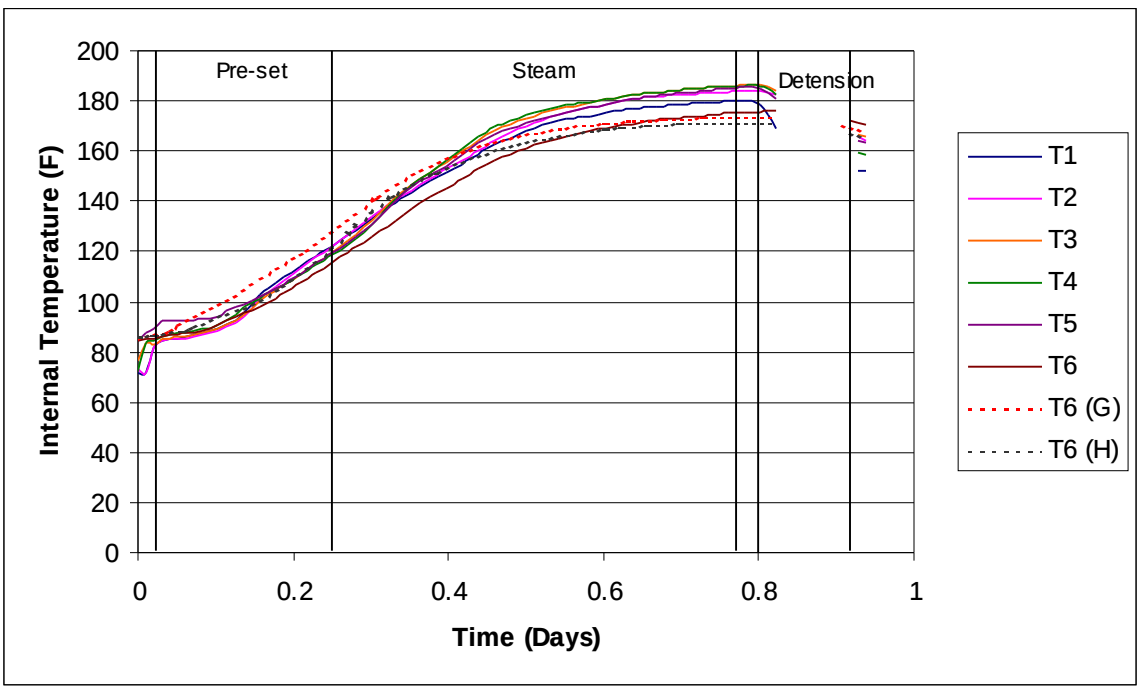

Figure 76 Curing Temperature Profile of a Bayshore Test Girder

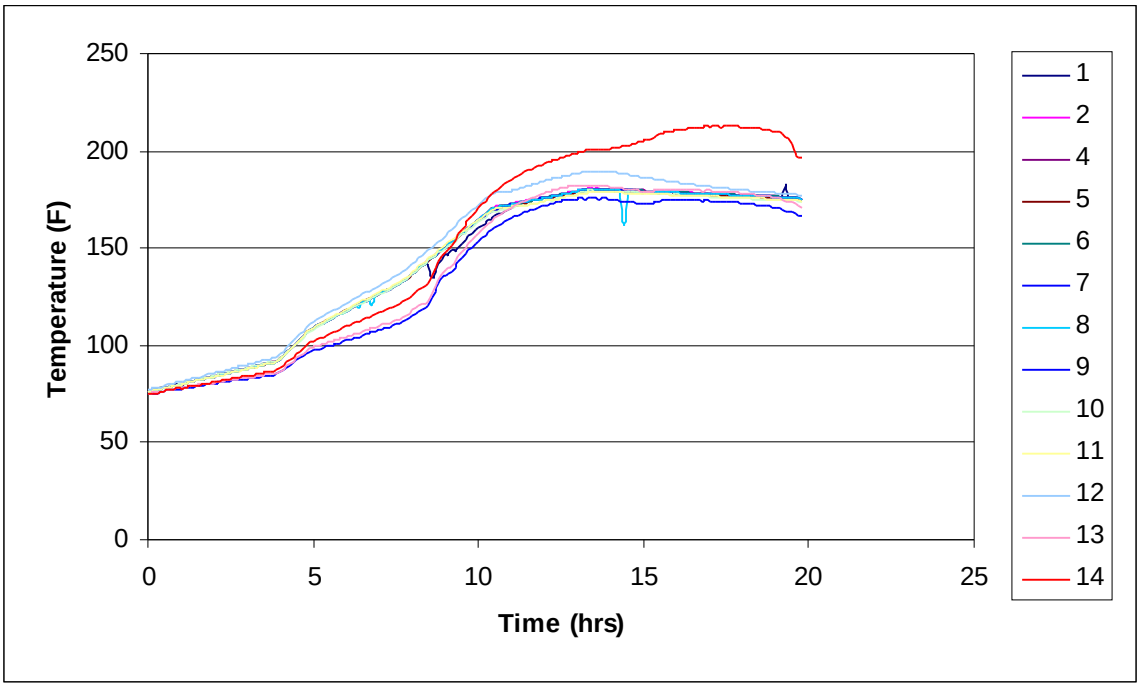

Figure 77 Sample Laboratory Curing Temperature Profile

APPENDIX F

Strain Measurements

	Total Strain			Elastic Strain			Shrinkage Strain			Creep Strain		
Time after loading	Mean	Std Dev	95% CI	Mean	Std Dev	95% CI	Mean	Std Dev	95% CI	Mean	Std Dev	95% CI
1	727	45	44	561	24	23	49	20	19	116	34	33
2	790	54	53	561	24	23	90	15	15	139	27	26
3	841	54	53	561	24	23	106	17	16	173	22	21
4	857	56	55	561	24	23	112	19	19	184	30	29
5	919	58	57	561	24	23	135	30	30	223	17	16
6	947	46	45	561	24	23	120	24	24	265	26	25
13	1080	104	102	561	24	23	198	26	25	320	60	59
20	1151	100	98	561	24	23	210	29	29	379	61	59
27	1194	95	93	561	24	23	198	34	33	435	54	53
34	1263	112	109	561	24	23	212	29	29	489	67	65
41	1243	89	87	561	24	23	198	45	44	484	50	49
48	1306	94	92	561	24	23	229	36	35	516	46	45
55	1321	95	93	561	24	23	243	40	39	516	50	49
62	1355	92	90	561	24	23	241	38	37	553	47	47
69	1357	91	89	561	24	23	249	44	43	547	42	41
76	1370	93	91	561	24	23	266	43	42	543	31	30
83	1353	76	75	561	24	23	259	39	39	533	30	29
90	1357	73	72	561	24	23	249	48	47	547	24	23
97	1374	94	93	561	24	23	268	42	41	545	43	42
104	1386	91	89	561	24	23	268	42	41	557	44	43

Table 17 Accelerated Cure Batch 1A Measurements (microstrain)

	Total Strain			Elastic Strain			Shrinkage Strain			Creep Strain		
Time after loading	Mean	Std Dev	95% CI	Mean	Std Dev	95% CI	Mean	Std Dev	95% CI	Mean	Std Dev	95% CI
1	707	23	23	521	26	26	97	21	21	89	40	39
2	785	15	15	521	26	26	132	20	19	133	37	37
3	816	31	31	521	26	26	130	36	35	166	63	61
4	856	30	30	521	26	26	161	45	44	174	67	65
5	891	39	38	521	26	26	150	39	38	220	79	78
13	1011	38	37	521	26	26	202	41	40	288	78	77
20	1075	36	35	521	26	26	202	41	40	352	72	71
27	1132	47	46	521	26	26	204	37	37	408	77	76
34	1163	40	39	521	26	26	243	43	42	400	68	66
41	1201	42	41	521	26	26	237	38	37	443	64	63
48	1213	39	39	521	26	26	247	31	31	445	57	56
55	1225	47	46	521	26	26	255	33	32	449	55	54
62	1244	38	37	521	26	26	253	32	32	470	58	57
69	1256	47	46	521	26	26	264	34	33	472	53	52
76	1250	49	48	521	26	26	270	36	35	460	45	44
83	1296	60	59	521	26	26	274	34	33	501	39	38
90	1298	39	39	521	26	26	280	30	29	497	46	45
97	1310	44	43	521	26	26	284	33	32	505	40	39

Table 18 Accelerated Cure Batch 2A Measurements (microstrain)

Time after loading	Total Strain			Elastic Strain			Shrinkage Strain			Creep Strain		
	Mean	Std Dev	95% CI	Mean	Std Dev	95% CI	Mean	Std Dev	95% CI	Mean	Std Dev	95% CI
1	709	13	15	553	20	22	42	7	8	115	16	18
2	765	7	8	553	20	22	65	4	4	148	16	18
3	803	13	15	553	20	22	65	4	4	186	13	15
4	849	16	18	553	20	22	77	10	11	219	6	7
5	872	13	15	553	20	22	92	4	4	227	16	18
6	905	10	11	553	20	22	108	10	11	244	11	12
7	919	11	12	553	20	22	113	6	7	254	16	18
14	984	13	15	553	20	22	138	0	0	294	17	19
21	1032	17	19	553	20	22	158	10	11	321	10	11
28	1076	12	14	553	20	22	160	10	11	363	17	19
35	1090	24	27	553	20	22	179	10	11	359	21	23
42	1109	24	27	553	20	22	188	11	12	369	17	19
49	1149	28	32	553	20	22	215	13	15	382	7	7
56	1170	25	28	553	20	22	227	7	8	390	10	11
63	1170	25	28	553	20	22	227	7	8	390	10	11
70	1176	23	26	553	20	22	231	0	0	392	20	22
77	1205	28	32	553	20	22	231	0	0	421	19	22
84	1224	28	32	553	20	22	240	7	8	432	13	15
91	1216	25	29	553	20	22	231	0	0	432	19	22
98	1232	29	32	553	20	22	252	7	8	428	16	18

Table 19 Standard Cure Batch 3A Measurements (microstrain)

Time after loading	Total Strain			Elastic Strain			Shrinkage Strain			Creep Strain		
	Mean	Std Dev	95% CI	Mean	Std Dev	95% CI	Mean	Std Dev	95% CI	Mean	Std Dev	95% CI
1	758	14	16	621	14	15	23	10	11	115	10	11
2	827	14	16	621	14	15	35	4	4	171	4	4
3	863	17	19	621	14	15	48	4	4	194	6	7
4	894	11	13	621	14	15	54	4	4	219	0	0
5	921	20	23	621	14	15	63	6	7	237	7	7
6	940	13	15	621	14	15	73	7	8	246	3	4
7	952	19	21	621	14	15	73	7	8	258	4	5
14	1058	13	15	621	14	15	121	10	11	317	7	8
21	1092	16	18	621	14	15	125	11	12	346	3	4
28	1144	29	33	621	14	15	158	14	16	365	7	8
35	1177	28	32	621	14	15	167	19	22	390	7	7
42	1196	16	18	621	14	15	175	17	19	400	18	21
49	1231	22	25	621	14	15	185	16	18	425	16	18
56	1242	19	21	621	14	15	196	16	18	425	12	14
63	1242	19	21	621	14	15	202	10	11	419	10	11
70	1265	16	18	621	14	15	215	4	4	429	9	10
77	1288	16	18	621	14	15	225	6	7	442	14	16
84	1294	13	14	621	14	15	225	6	7	448	9	10
91	1294	13	14	621	14	15	225	6	7	448	9	10
98	1319	13	14	621	14	15	244	11	12	454	7	8

Table 20 Standard Cure Batch 4A Measurements (microstrain)

VITA

Bradley Donald Townsend was born in Louisville, Kentucky on April 28, 1979 to Doug and Angie Townsend. He lived in Indiana, Kentucky, and Maryland before arriving in Roanoke, Virginia in the 5th grade. He graduated with honors from William Byrd High School in 1997. He earned an Associates Degree in Engineering from Virginia Western Community College in 1999 and a Bachelor of Science Degree in Civil Engineering from Virginia Tech in 2001, and then began graduate studies at Virginia Tech. Upon completion of his degree in May 2003, Brad will begin a career in structural design.